Single Molecule Studies of Dynamic Heterogeneities in Supercooled Liquids

Lindsay Marie Leone

Submitted in partial fulfillment of the
requirements for the degree of
Doctor of Philosophy
in the Graduate School of Arts and Sciences

COLUMBIA UNIVERSITY

2015

© 2015
Lindsay Marie Leone
All Rights Reserved

Abstract

Single Molecule Studies of Dynamic Heterogeneities in Supercooled Liquids

Lindsay Marie Leone

We describe a set of single molecule fluorescence experiments that directly demonstrate the existence of spatial and temporal heterogeneity in two different small molecule glass former, glycerol and ortho-terphenyl (OTP) as well as the polymeric glass former polystyrene near their glass transition temperatures. The rotational dynamics of a set of perylene diimide probes are investigated in each small molecule glass former in a temperature range near their glass transition temperature. For all probes, the temperature dependence of their median rotational relaxation times (τ_c) reflect that of the structural relaxation of glycerol and OTP. The distribution of relaxation times for each probe at each temperature span around one decade and remain constant across all temperatures probed. In both glass formers, a trend as a function of probe rate of rotation occurs, where the fastest rotating probes exhibit the broadest τ_c distributions. Unexpectedly, a correlation between the rotational dynamics and the strength of the probe's intermolecular interactions with the host is seen. In OTP, the fastest rotating probe is the smallest probe, with the lowest molecular weight, as expected. But in glycerol, the *largest* probe exhibits the fastest rotational dynamics. This counterintuitive result arises from the apparent inhibition of hydrogen bonding between the probe and host due to bulky non-polar groups sterically hindering the polar carbonyl groups on the probe. Analysis of dynamic exchange of probes on long time scales in glycerol (10^2 – 10^6 times the structural relaxation)

does not reveal the presence of temporal heterogeneity on this time scale. Another technique employed to assess exchange on a shorter time scale reveals that ~30 % of molecules exhibit temporally heterogeneous behavior.

Single molecule experiments on polystyrene (PS) near its glass transition temperature are also presented. Here, the rotational and translational dynamics of perlyene diimide probes in 100 nm PS films near its glass transition are studied. As in glycerol and OTP, average rotational relaxation times are found to mimic the temperature dependence of the host structural relaxation. These studies, intended as control experiments for confined film SM studies, reveal spatial and temporal heterogeneity in PS dynamics. The measured distribution of rotational relaxation times spans 1.5 decades and remains constant across all temperature probed. These distributions fall between the expected distribution width for the purely spatially and temporally heterogeneous cases, suggesting the distributions are comprised of combination of spatial and temporal components. The median stretching exponent (β) from fitting SM trajectories results in $\beta = 0.63$ and a "quasi-ensemble" result of $\beta = 0.58$ found from combining SM linear dichroism autocorrelation functions. These represent the smallest stretching exponents reported for single molecule studies in supercooled liquids to date, indicating that the probe employed truly mirrors the dynamic heterogeneity of the host. The SM rotational relaxation rates are found to be correlated to their stretching exponents i.e. the lowest relaxation rates also have, on average, the lowest β values. Additionally, small stretching exponents are correlated with long trajectories, suggesting that the rate of rotation together with the length of the trajectory dictate the degree of heterogeneity the probe is able to sample. Surprisingly, a mobile layer is observed in the films at temperatures near the glass transition. Translating molecules in this region are tracked and represent ~10% of the total molecules evaluated in this film. Molecules in the mobile region

appear to be diffusing at rates that are magnitudes greater than the molecules rotating in the bulk region of the film.

Contents

Acknowledgements

It is difficult to put into words how grateful I truly am to all of the people that have supported and helped me complete my journey through graduate school. I want to start by thanking my advisory committee, Dr. Ruben Gonzalez and Dr. Louis Brus. Ruben has provided

advice during my second year defense and ORP defense, has been great to work with as a teaching assistant while teaching General Chemistry II, and has graciously welcomed me into his lab space, as my office space was literally *in* his laboratory space. Louis has been a source of inspiration during my graduate career and always has scientific great insight to offer during my past oral defenses. I also want to thank my additional committee members, Dr. Wei Min and Dr. Andrew Crowther, who have agreed to attend my defense as well as read and critique my written dissertation. Your advice is greatly appreciated. Most importantly, I want to thank my advisor, Laura Kaufman, from the bottom of my heart for all that she has done during my graduate career. She has served as my academic advisor, my mentor, my confidant, my second mother, and last but not least, my friend. She has molded me into the critically thinking scientist I have become, and for that I cannot show enough thanks. She has a way of understanding the individual needs of each of her graduate students which has allowed all of us to take our own unique path to become a successful Ph.D. scientists.

The members of the Kaufman lab have become a second family to me. Having a pleasant work environment with supportive coworkers is so valuable. I first and foremost want to thank Dr. Stephan Mackowiak for being my mentor and my very good friend when I first joined the Kaufman Lab. His guidance and expertise propelled me into my graduate career as I attacked the steep learning curve during my first year of graduate school. He set the stage for my thesis work, and I will always want to emulate his work ethic. Dr. Keewook Paeng has also served as somewhat of a second advisor to me during my graduate career. His expertise in *so* many different fields has helped me make crucial decisions during experiments and analysis. Keewook is always there to remind me that when experiments yield an unexpected result, this is not a *bad* thing but instead an *interesting* finding. I want to thank Dat Tien Hoang for being a colleague

who is always there to help me out with coding of analysis, science talk, and planning out experiments. He is the graduate student that all graduates students should try to emulate. Jieling Zhu and Michelle Ziperstein have become my best friends throughout graduate school. They have always been there for great conversations about science and non-science, advice, and of course a shoulder to cry on.

Thank you to my fellow graduate school friends, Dr. Jeffrey Bandar, Allison Griffith, Dr. Neena Chakrabarti, Dr. Corinne Foley, Dr. Glen Hocky, Dr. Nicholas Anderson, Dr. Timothy Berkelbach, and Dr. James Eagan for supporting me and one another through the very interesting time that is graduate school. I couldn't have asked for a better crew during this time and after all of the times we have shared together, whether it be the celebration of a manuscript, a picnic in the park, or a wedding celebration, I know that we will remain lifelong friends. I want to say thank you to all of my family and friends outside of the department for being supportive and always asking about my work even though they probably have no idea what I am talking about! Thank you to Mom and Dad for always supporting in whatever I wanted to pursue. They have always been the most selfless, encouraging, supportive parents. They are my biggest fans even though I don't let them tell other people that they are proud of me. Thank you to my brothers, Michael and Matthew, who have always been by my side through all that life has thrown at us. Last but not least, I want to thank my partner in life, Chris, who has always been there for me through my graduate experience. He supports all of my endeavors and truly is a partner to me, and for that I can never be thankful enough.

Chapter 1. Introduction

1.1 Supercooled Liquids and Glasses

1.1.1 The Glass Transition

If a liquid is cooled below its melting temperature (T_m) fast enough to avoid the first order phase transition to a crystal, it will remain in a disordered liquid-like state even as it is

cooled to temperatures far below T_m (Figure 1.1, liquid schematic inset). As the temperature of this ergodic system is further decreased, its viscosity will increase quickly, often in a non-Arrhenius manner. At a characteristic temperature below T_m, known as the glass transition temperature (T_g), the system falls out of equilibrium and transitions into a solid-like, non-ergodic state called a glass. The layman's definition of "glass" refers to SiO_2 in its glassy state, though many vastly different types of materials including small organic molecules, metals, inorganic complexes, and polymers all are able to form glasses.

Glasses behave as solids and appear structurally homogeneous and yet they are not thermodynamically stable, as the crystalline state is lower in free energy. While in this non-equilibrium state, the glass can relax or "age" over time to a more stable glassy state. The fact that the glass is i makes it difficult to define a single T_g. Indeed, different cooling rates can yield different T_g values, as a slower cooling rate allows the liquid to obtain a more kinetically stable arrangement before it crosses over into the glassy regime (Figure 1.1). Given enough time, the less stable glass will age to the same stable state as the more slowly cooled glass.[1]

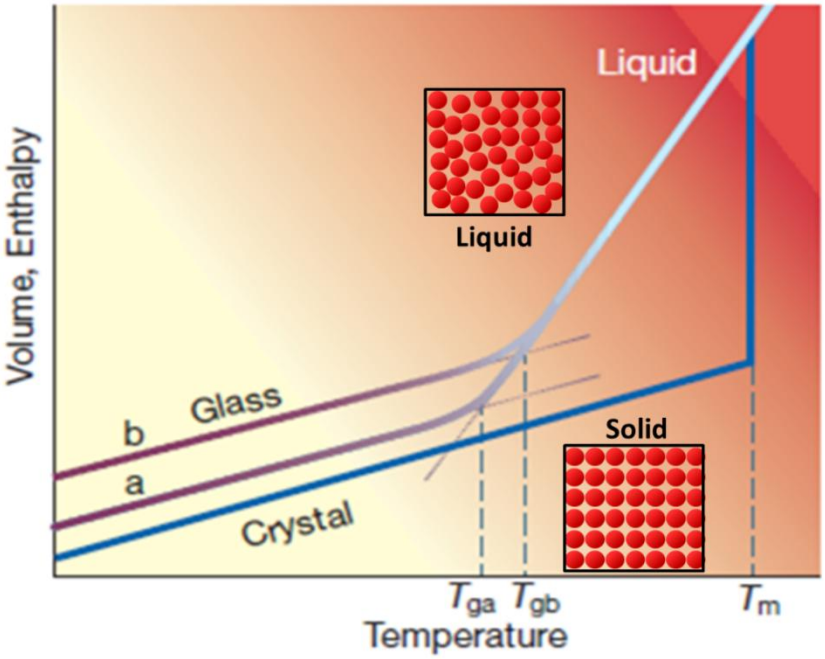

Figure 1.1 A schematic representation of changes in volume and enthalpy of a system with respect to temperature. If a liquid is cooled, it can crystallize to a solid (dark blue line, schematic of solid, inset) or instead remain in the liquid state, eventually forming a glass (light blue line/purple line). Glass a is associated with a slower cooling rate than glass b. Figure 1.1 is reproduced from Reference 1 with permission from the publisher.

Because the glass transition temperature is difficult to define, in practice many definitions have been employed. Among the definitions are the temperature at which: (1) a dramatic drop in heat capacity is measured during differential scanning calorimetry, (2) the average structural relaxation time is 100 seconds, or (3) the viscosity of the system reaches 10^{13} poise.[2] While these definitions do not necessarily converge on exactly the same temperature, they are often within 1-2 K and thus any of these definitions serve as a reasonable benchmark for experimental measurements.

Understanding the underlying cause of the glass transition and properties of glassy systems has been an area of active research for many decades. While many interesting

phenomenon about glasses have been uncovered, molecular motions of glasses are still poorly understood. By understanding these molecular motions, we will be able to uncover the origin of the glass transition. Since the contributions from the heterogeneity inherent in liquids near the glass transition temperature are poorly understood, understanding the molecular motions will provide clues as to the role heterogeneity plays in the glass trasition. Since systems in the glassy regime are non-ergodic, their dynamics are extremely difficult to study in the lab and through simulations. Experimentalists often turn to supercooled liquids, amorphous systems in the temperature range between T_m and T_g, to study molecular motions of this type of condensed matter, since the time scales of molecular motion in these systems are more easily observed.

1.1.2 Supercooled Liquids

The term supercooled liquid simply refers to a system between T_m and T_g that lacks long range order. When supercooled liquids are cooled below T_m, their viscosity increases as they approach T_g. Some glass formers have a temperature dependence that follows Arrhenius behavior given by the equation, $(T) = e^{\frac{E_a}{k_B T}}$, where *η(T)* is the viscosity as a function of temperature, E_a is the activation energy and k_B is the Boltzmann constant. These are referred to as "strong" glass formers (Figure 1.2). Many glass formers deviate from this relationship and have a more dramatic increase in viscosity as temperatures approach T_g.[1,3,4] These glass formers are referred to as "fragile" glass formers and are the main focus of this thesis work. The non-Arrhenius behavior of the viscosity as a function of temperature is well-described by the Vogel-Tamman-Fulcher equation, $\eta(T) = e^{A+\frac{B}{(T-T_0)}}$, where T_0 is the Vogel temperature and A and B are constants specific to a given glass former.

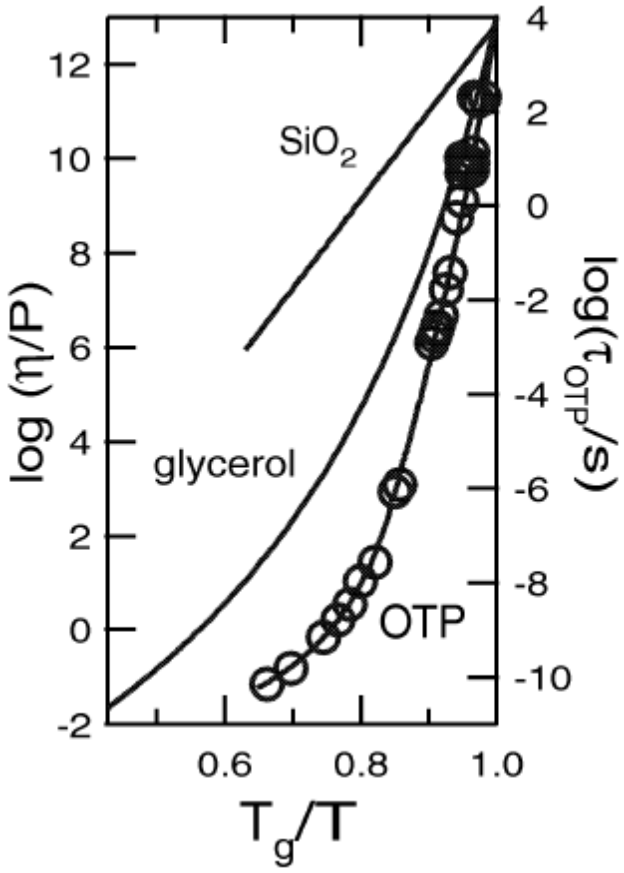

Figure 1.2 A log plot of viscosity with respect to temperature normalized by T_g for different glass formers. As shown in this plot, strong glass formers, like SiO_2, exhibit Arrhenius behavior whereas fragile glass formers exhibit non-Arrhenius behavior. The work presented in this thesis focuses exclusively on fragile glass forming liquids. Figure 1.2 is reproduced from Reference 2 with permission from the publisher.

The quickly increasing viscosity in the supercooled regime is accompanied by microscopic changes to the system as temperature is lowered from above T_m towards T_g. These changes are not overtly structural but do affect system dynamics. Indeed, the dynamical behavior of supercooled liquids near T_g differs from that of normal liquids. When a normal liquid above its T_m is perturbed, by – for example – an electric current, the relaxation of the system back to equilibrium as assessed by the decay of the autocorrelation of a monitored property, can be described very nicely by an exponential function, $C(t) = e^{-\left(\frac{t}{\tau_c}\right)}$, where τ_c is a single relaxation

time. If the same perturbation is performed on a supercooled liquid, the relaxation will typically be more accurately described by a stretched exponential decay or Kohlrausch-Willams-Watt function (KWW), $C(t) = e^{-\left(\frac{t}{\tau_c}\right)^{\beta}}$, where $\beta < 1$. The β value of the KWW function is a measure of the degree of non-exponentiality of a system's relaxation, with the more β deviates below 1, the more "stretched" the relaxation process. Relaxation processes measured in ensemble experiments performed on fragile glass formers at temperatures approaching T_g generally return $\beta < 1$.[2]

Non-exponential relaxation of glass formers can arise from two extreme scenarios. A "heterogeneous" case where the system is broken up into distinct spatial domains that all relax independently, each in an exponential fashion with a distinct relaxation time (Figure 1.3).[5] This scenario is sometimes called the "spatial heterogeneity" case. A "homogenous" scenario is also possible: in this case each spatial domain is indistinguishable in that they all relax in tandem as in a normal liquid; however, here they do so in a non-exponential fashion. One way for this scenario to manifest is for environments within the system to change in time on a timescale similar to the average relaxation time of the system. This scenario may be termed the "temporal heterogeneity" case. Each of these extreme scenarios may yield the same ensemble stretched exponential decays, leaving two different pictures that are indistinguishable in an ensemble measurement.

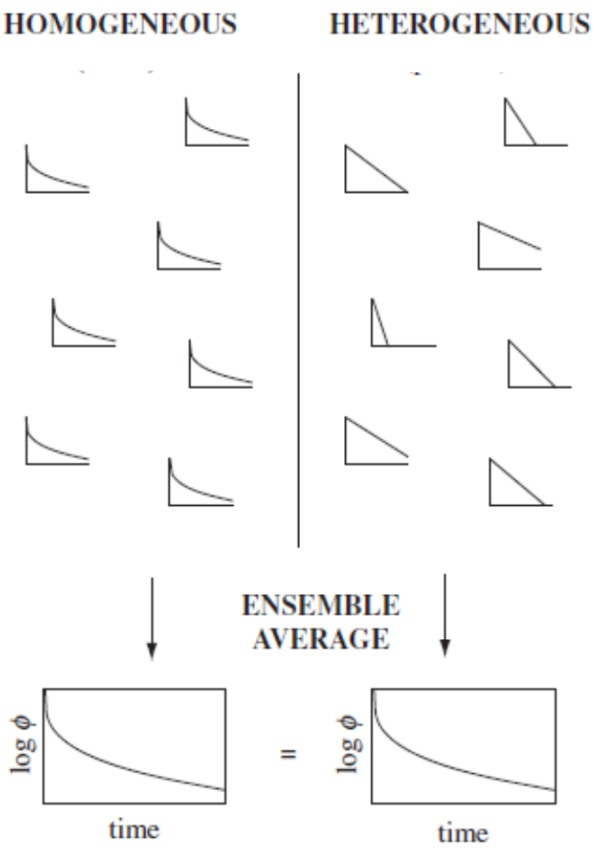

Figure 1.3 A schematic depiction of two extreme scenarios that yield an identical ensemble non-exponential relaxation as is typically measured in supercooled liquids. On the left, the homogeneous case reflects a scenario where all domains relax in the same, non-exponential manner. On the right, the heterogeneous scenario illustrates the case where each spatial domain relaxes exponentially, with a distinct time constant. Figure 1.3 is reproduced from Reference 5 with permission from the publisher.

The most common interpretation of the non-exponential behavior of glass formers meshes the homogeneous and heterogeneous scenarios. Although supercooled liquids appear to lack static structural heterogeneity, they may consist of a mosaic of spatial regions, each having distinct relaxation time scales. These regions are likely related to "cooperatively rearranging regions" (CRRs) that are slowly but constantly interchanging over time. [2,6–9] The slowing dynamics as a system approaches the glass transition can be explained by the emergence of CRRs. However, there remains ongoing debate over the length and time that characterize the

spatially heterogeneous dynamics as well as whether the growing length scales of CRRs govern dynamics of supercooled systems as they approach T_g. Given the non-exponential relaxations measured in ensemble experiments on supercooled liquids as well as the putative existence of CRRs, the non-exponential dynamics are thought to be predicated on the existence of spatial heterogeneity, but spatial heterogeneity that is evolving such that the same regions display different dynamics over time. Since bulk measurements cannot discern whether the non-exponential decay arises from spatial, temporal or some combination of both forms of heterogeneity, experimental techniques with the ability and resolution to probe these cases independently are critical.

1.2 Small Molecule Glass Formers: Single Molecule Studies

1.2.1 Previous Work

Novel methods to avoid full ensemble averaging and interrogate sub-ensembles of molecules have been developed and employed to provide insight into the degree of each type of heterogeneity in small molecule supercooled liquids. [2,6,10–12] To limit spatial averaging as much as possible and interrogate molecular length scales in these systems, single molecule (SM) approaches have been employed.[13–16] The SM technique that has been most commonly applied to the study of supercooled liquids involves embedding fluorescent probes very dilutely in the host under study and monitoring SM probe rotations over time through measurement of probe linear dichroism (LD). In theory, these experiments can identify both spatial and temporal heterogeneity in supercooled liquids through analysis of differences between individual SM

probe behavior (spatial heterogeneity) and differences in behavior that occur for a given SM over time (temporal heterogeneity) (Figure 1.4). In practice, one must ensure that the probes are indeed mirroring the host's dynamics and not perturbing the host if such an approach is to reveal the details of spatial and temporal heterogeneity in these systems.

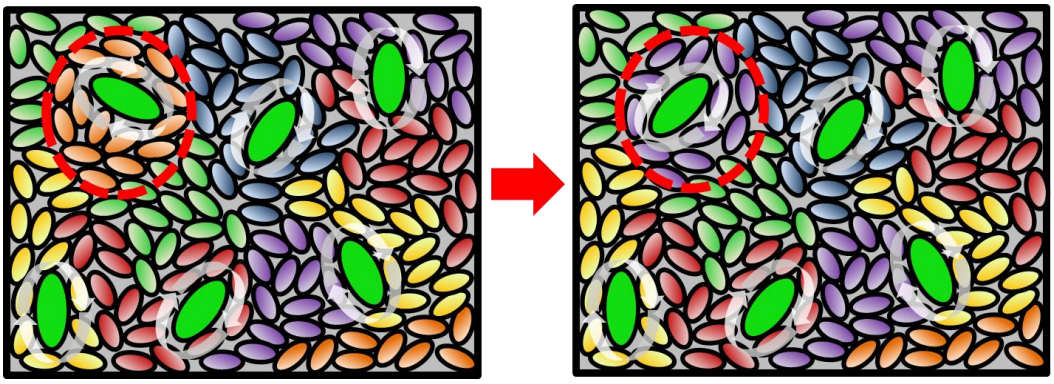

Figure 1.4 A schematic of single molecule probes dispersed in a supercooled liquid. Large green ellipsoids represent probe molecules and smaller ellipsoids represent host glass former molecules with varying colors indicating distinct relaxation rates, i.e. spatial heterogeneity, within the system. The red arrow indicates some elapsed time t and the red dashed circle highlights a region with a change in dynamics over that time period, i.e. temporal heterogeneity.

1.2.2 Experimental Shortcomings

Identifying temporal heterogeneity and distinguishing spatial and temporal heterogeneity have proven difficult in practice, due in large measure to typical SM probe characteristics.[12,17,18] First, SM probes are usually large, and their rotations are slow compared to molecular motion of the host molecules. It is possible that dynamic exchange -- the changes in dynamics of particular regions of the supercooled liquid over time -- occurs on time scales that are faster than and/or not well separated from probe rotational time scales, thus limiting probe ability to report these dynamics. Moreover, typical SM probes photobleach on time scales that limit trajectory length,

which affects the accuracy of variables obtained from fitting correlation functions derived from these trajectories. It may be expected that an SM LD trace analyzed via an autocorrelation function (ACF) would yield a single exponential decay if the probe were experiencing an environment of given dynamics but would yield a stretched exponential decay for an SM that explored multiple such environments. Unfortunately, typical SM LD trajectories are short enough and therefore display an erroneous decay that would be best fit by stretched exponential decays even in the presence of homogeneous dynamics.[19–22] This complication requires that temporal heterogeneity be identified with other approaches, and several such approaches have been developed.[14,15,17,23,24] One approach, investigated in the Kaufman lab, involved simulating probes within systems with varying breadth of spatial heterogeneity and varying trajectory length to set a threshold for determining when SM probe reports of seeming heterogeneity can be taken as valid reports on the heterogeneous character of the host.[20] Unfortunately, this approach can only yield information on time scales much longer than the structural, or α-relaxation time, τ_α, of the host, a time scale that has been suggested to be similar to that of dynamic exchange at temperatures near T_g.[25–27]

1.2.3 Thesis Contribution: Probe Dependent Studies

The first stage of this thesis work was carried out to potentially identify temporal heterogeneity and quantify dynamic exchange on shorter time scales by monitoring the rotational dynamics of a set of three SM probes.[16] By systematically employing probes with the same core but differing side chains, the effects of the probe size, speed, and lifetime until photobleaching could be more fully investigated. These SM studies in supercooled glycerol revealed that the largest probe employed unexpectedly displayed the shortest rotational correlation time, likely

because steric hindrance prevented it from participating in glycerol's hydrogen-bonding network. A key observation of this study was the faster the probe's average rotational correlation time, regardless of probe size, the broader the distribution of individual SM probe rotational correlation times. We hypothesized that the most quickly rotating probe reported the greatest breadth of heterogeneity in the host because it did less averaging over dynamic exchange in the system, allowing it to more accurately report the spatially heterogeneous dynamics of the surrounding supercooled glycerol than could the slower probes.

The results of the study of SM probes in supercooled glycerol led to predictions for how these probes would behave in other supercooled liquids, and we undertook such a probe-dependent study in a non-polar glass former, ortho-terphenyl (OTP). Here the molecular interactions between all employed probes and the host were expected to be very similar and thus probe relaxation time would decrease with decreasing probe size monotonically. As in glycerol, we expected the probes in OTP to show an increase in breadth of rotational relaxation time distribution with decreasing average probe rotational correlation time, consistent with fast probes doing less averaging over and better reporting of dynamic exchange occurring in the host. Because OTP is a more fragile glass former than glycerol, and fragility may be correlated with the degree of heterogeneous dynamics in a glass former[2, 29], we examined whether results from these studies suggest differences in the relative heterogeneity of glycerol and OTP.

1.3 Confined Polymers

1.3.1 Background

Polymers are another type of glass former that are used for a wide range of technological applications. Polymeric materials have much more desirable viscoelastic and transport properties than organic glass formers and therefore are utilized frequently in building materials, consumer products, and functional electronic materials such as solar cells and personal electronic devices. Polymers are easily manipulated, inexpensive to produce, and resilient to external factors including large temperature fluctuations, corrosive environments and light exposure. As with other technologies, applications utilizing polymers are moving towards miniaturization, down to the nanoscale level. At this length scale properties distinct from the bulk properties of the system may dominate system behavior. By determining the non-exponential nature of the will help determine the heterogeneity and therefore the limitations of these applications in more detail for commercialization purposes.

An interesting phenomenon that occurs when polymers are confined to geometries or thin films on the nanoscale is a shift from the bulk glass transition temperature. [30–40] When a polymeric system is confined to < 100 nm, for instance in a thin film, the system size may be smaller than the end to end distance of the polymer chain itself. In this situation, the polymer will exist in a conformation distinct from that in a bulk system. Presumably, the change in the glass transition temperature in such systems is a consequence of these conformational differences that result in altered relaxation dynamics of the system. In some instances, confinement of a polymeric system results in a depressed glass transition temperature [30,31,34–36,39,41–45]. On the other hand, experiments on polymers in thin films supported by substrates have seen an elevation of

T_g.[46–50] Given this diversity of findings, a fuller understanding of the underlying details of the change in T_g and the associated changes in dynamics is needed. [51–54]

1.3.2 Existence of a Mobile Layer Affects T_g

Many experiments have suggested that a depression in the glass transition temperature in confined thin film polymers is a result of increased mobility of the surface layer (Figure 1.5). Several physical pictures of thin film polymer systems have been proposed to explain the variety of observed phenomena. First, the depression of the glass transition temperature has been seen in thin film polymers as the films become thinner, [31,34,55–57] which is believed to be at least in part due to increased molecular mobility near the free surface dynamics. The free surface layer, i.e. the top layer of a polymer film sharing an interface with air, can be thought of acting as a liquid-like layer atop a much less mobile, supercooled system. On the other hand, a variety of studies have found an increase in T_g; This is thought to be due to polymer-substrate interactions slowing the system's dynamics.[41,47,58–60] These two physical situations do not have to be mutually exclusive, and the resultant T_g upon confinement can dependon which effect dominates in the competition of the increased mobility from surface dynamics or slowed dynamics from substrate-system interactions. The work presented in this thesis focuses on systems that consistently have been found to have reduced T_g under confinement, presumedly as a result of a mobile free surface layer. Specifically, we study confined polystyrene films supported by SiO_2 substrates (experimental details will be discussed below).[31,34,35,41,43,55,61,62]

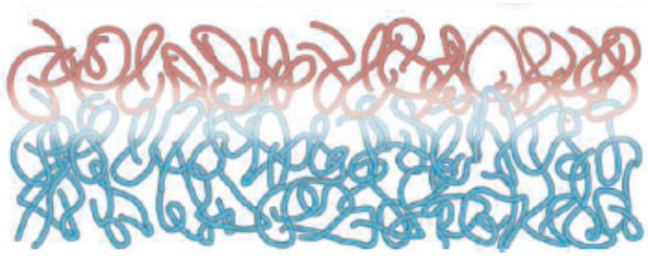

Figure 1.5 A schematic of a confined polymer system where the mobile species are in red and the bulk-like species are in blue. Figure 1.5 is reproduced from Reference 63 with permission from the publisher.

1.3.3 Ensemble Studies Attempt to Probe Mobile Layer Dynamics

Results of studies exclusively investigating the mobile surface layer thin polymer films do not completely coincide. Some experiments of PS thin films, free-standing and supported, have yielded results that suggest a mobile region at the surface of the film that penetrates tens of nanometers into the film.[32,63,64] The remaining "bulk" interior of the film exhibits bulk-like dynamics and a small layer near the substrate exhibits either bulk or simply arrested dynamics.[65] Alternatively, an experiment exploiting fluorescence anisotropy measurements in free standing PS thin films, found the mobile layer is at most 7 nm in thickness at T_g and is independent of total film thickness. [66,67]

Directly probing the mobility of segmental and terminal end chain dynamics at the surface and within the confined film will help elucidate experimental discrepancies and create a deeper understanding of the origin of the change in T_g upon confinement. Segmental dynamics, the torsional dynamics of the inter-chain of the polymer, have been found to be the main contributor of the change in T_g upon confinement.[7] Probing these dynamics via techniques including dielectric spectroscopy and fluorescence anisotropy have been the focus of many recent studies. [68,69] Unfortunately, such measurements are not height resolved and measurements at a particular

depth from the surface are not possible. Additionally, such measurements of thin polymeric films are ensemble averages thus preventing differentiation of spatial and temporal heterogeneities within the system.

Some recent experiments have attempted to combat averaging over the unique layers of the film, i.e. mobile vs. bulk portions, by exclusively probing the mobile surface. Experiments using atomic force microscopy (AFM) have been used to probe the first ~3 nanometers of a polymeric thin film .[62,70] These experiments can only probe the surface, losing any information about the thickness and mobility of interior regions. Other experiments create multilayer films, containing layers with labeled components and with unlabeled components. The thickness and position of the labeled layer can be varied and the mixing of the labeled and unlabeled layers can be monitored. This method's resolution is limited by the labeled layer's thickness. [32,63,64]

1.3.4 Thesis Contribution: Single Molecule Studies of Bulk and Confined Polymer Films

In preliminary work, we attempt to elucidate experimental discrepancies described above through single molecule studies of confined polymer films. These measurements also provide a more detailed and extensive study of the spatial and temporal heterogeneities of these films. In advance of investigating confined films via single molecule measurements, experiments investigating bulk films of polystyrene were carried out to detail the spatial and dynamic heterogeneities in these systems. Much like the small molecule glass former studies, polystyrene was doped with single molecule perylene diimide type probes and spincoated to be of bulk-regime thickness. As expected, SM results from PS films follow the same temperature dependence of PS, indicating the probes are following the dynamics of the host. The dynamics of the probe molecules were shifted by ~0.4 decades in rotational relaxation time, as expected

given the size of the probe relative to that of the monomers comprising the PS. These measurements revealed a wider breadth of relaxation times than have been seen in any molecular supercooled liquids using similar probes. Similarly, the median stretching exponent of the single molecule trajectories approaches those reported in dielectric studies. Taken together, these findings indicate that the PDI probe employed may be a more appropriate reporter of dynamics of high molecular weight polystyrene than of small molecule glass formers.

In the measurements described above, unexpectedly, a subset of probe molecules appeared to be exhibiting dynamics much faster than the majority of the probes. We believe this may be an indication that a mobile layer was present and probed. This observation further motivates planned single molecule experiments in confined films to be carried out using the same probes. Taking previous single molecule studies of confined films into consideration [71–73], the motivation to carry out new single molecule studies in confined films is multifaceted: to help uncover the details of the heterogeneous nature of the bulk and confined portions of the film; to investigate a temperature range, spanning well below and above T_g to investigate dynamics of the dynamics of mobile and bulk layers at these temperatures and understand the temperature dependence of the mobile region; and to assign a length scale to the mobile region and examine the dependence of thickness of the film of the mobile region.

1.4 Outline of Thesis

The work in this thesis exploits single molecule microscopy in an effort to gain a deeper understanding of different aspects of the dynamics of the supercooled regime of glass forming systems. Chapters 2 and 3 focus on probe-dependent rotational measurements in glycerol and

OTP that assist in understanding the breadth and degree of heterogeneity found in glass forming systems. In Chapter 4, results of SM rotational studies in supercooled polystryrene are reported to both gain deeper insight into spatial and temporal heterogeneity in polystyrene and as a control for planned thin film experiments.

Chapter 2. Probe Dependent Studies in Supercooled Glycerol

This chapter is adapted from Reference 16.

In this chapter, results of SM experiments in supercooled glycerol in a temperature range near T_g using three different perylene diimide probes are presented. These probes were used to investigate whether *probe size* and *probe–host interactions* affect breadth of heterogeneity reported in the glassy host by such SM experiments. Through the use of widefield (WF) SM microscopy, heterogeneous dynamics are identified by following rotational dynamics of many single molecule probes in the same sample simultaneously. Breadth of rotational relaxation times of such probes are monitored and report on spatial heterogeneity. Temporal heterogeneity i.e. explicit changes in particular molecules' dynamics over time are quantified by exchange time,

the average time over which an environment is characterized by a single relaxation time, on short and long time scales using methods proposed previously.[14,17] Measurements across probes are compared to more fully understand probe ability to report spatially heterogeneous dynamics.

2.1 Motivation for Probe Dependent Studies

Results from SM experiments on small organic molecule supercooled liquids to date have been largely consistent with each other in terms of reported spatial heterogeneity.[13–15] Most recently, two studies following probe molecule rotation in supercooled glycerol reached similar conclusions regarding the breadth of spatial heterogeneity present in the system. However, the two studies reached different conclusions regarding temporal heterogeneity.[14,15] In particular, in WF SM microscopy using rubrene as a probe in glycerol at 1.07 T_g, we reported that ≈ 15% of the molecules assessed experienced detectable changes in dynamics over the course of the experiment.[15] Of the molecules experiencing detected exchange, the average time until first exchange (τ_{pers}) and the average time between exchanges (τ_{ex}) were, respectively, ≈ 60 and 30 times the rotational correlation time of the rubrene probe, τ_c. Given the rotational correlation time of rubrene relative to glycerol's structural or α- relaxation time (τ_α), these values translate to $\tau_{pers} \approx 400\ \tau_\alpha$ and $\tau_{ex} \approx 200\ \tau_\alpha$. In contrast, Zondervan et al. measured rotations of a perylene dicarboximide probe (*N*,*N*′-bis(2,5-di-*tert*-butylphenyl)-3,4,9,10-perylenedicarboximide, tbPDI) in glycerol and, over the temperature range of $1.08T_g$ – $1.12T_g$, found evidence for very long-lived spatial heterogeneities, with almost all molecules exhibiting persistent rotational relaxation times and no dynamic exchange for 10^5 – $10^6\ \tau_\alpha$.[14] This finding suggested a picture of supercooled glycerol as a mosaic of liquid-like regions separated by a nearly static network. The

presence of such a network is not consistent with the picture of supercooled liquids as *ergodic*, *interchanging* mosaics of local environments[7–9] but was further supported by rheological findings and a study indicating fluorescent probes in supercooled glycerol are excluded from micron-size regions that may delineate the solid-like network.[74,75]

The discrepancy in measured exchange time relative to τ_α in supercooled glycerol as revealed by the two SM microscopy experiments may emerge from a combination of factors. These include differences in probe size, probe-host interactions, sample preparation, and analysis methods. The probes used in the two studies were quite different in size and somewhat different in interactions with the host. The tbPDI used by Zondervan et al. is significantly larger (767 g/mol) and more structurally anisotropic than rubrene (532.7 g/mol), though both are significantly larger than glycerol (92 g/mol). Probes approaching the size of a region characterized by a single relaxation time in a system with spatial heterogeneity may sample and average over several distinct environments and thus fail to report the presence or full breadth of spatial heterogeneity in the system (Fig 2.1a). Just as large probe molecules may average over heterogeneities in space, they may also do so in time. Even in the presence of heterogeneous regions much larger than the probe, if the time scale for probe rotation is similar to or slower than the typical time over which a fast region of the supercooled liquid becomes slow or vice-versa, the probe dynamics will not mirror the exchanges occurring in the environment (Fig 2.1b). Both types of averaging over spatially heterogeneous dynamics in molecular glass formers have been considered previously[27,76–87], though probe dependence studies have not yet been undertaken for single molecule approaches. Just as probe size may affect probe ability to report spatially heterogeneous dynamics in the host, interactions between probe and host molecules may do so as well. For example, a probe with strong interactions with the host may rotate with a

shell or partial shell of host molecules, increasing the effective size of the probe. Another possibility is that probes may segregate into non-representative regions of a polar host or vice-versa and in turn report preferentially on these regions of the supercooled host.

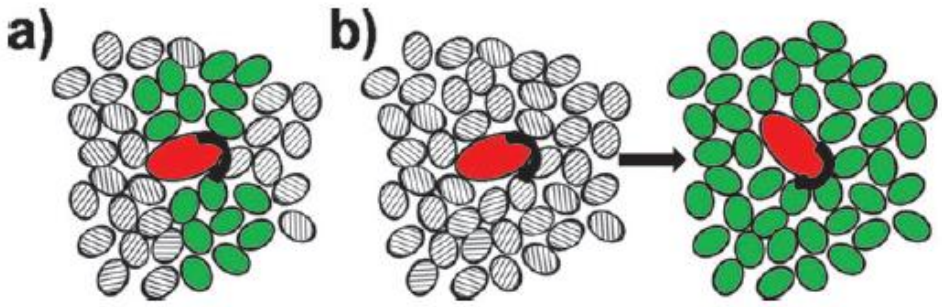

Figure 2.1 Schematic of a probe (red solid ellipsoid) in two different types of heterogeneous environments. (a) The probe is surrounded by two regions exhibiting different dynamics. Assuming the filled ellipsoids represent slow molecules and the striped ellipsoids represent fast molecules, if these regions maintain their dynamics for infinite time (i.e. there is spatial but not temporal heterogeneity in the system), a large probe will rotate through both types of regions, reporting an average dynamics. (b) If all molecules surrounding the probe are fast but become slow during the probe rotation (i.e. there is temporal heterogeneity but no spatial heterogeneity in the microenvironment of the probe), the probe will also only report an average dynamics. In the presence of both spatial and temporal heterogeneity, the probe may average over spatially heterogeneous dynamics both in space and time and may not report the full breadth of spatially heterogeneous dynamics in the system.

In addition to differences in probe size and probe-host interactions, differences in sample preparation could contribute to the differences seen in exchange time in the two SM studies in supercooled glycerol. Mackowiak et al. used a cooling rate of ≈ 5 K/min while Zondervan et al. cooled approximately two orders of magnitude more slowly.[14,15] In the generally accepted view of the supercooled liquid as ergodic, cooling rate and time in the supercooled regime should not affect behavior of the system so long as a crystalline transition is avoided. However, Xia et al.

found patterns of micron length scale fluorophore density variations in supercooled glycerol, with the patterns differing with sample cooling rate.[75] A final factor that may have strongly influenced the different findings on temporal heterogeneity in the two SM experiments in glycerol relates to the manner in which temporal heterogeneity was assessed. The sliding window autocorrelation used by Mackowiak et al. reports on probe molecules, and presumably the surrounding host environments, that alter their dynamics from average to slower than average. This approach examines a portion of the "dynamic exchange phase space" between ≈ 10 and 300 τ_c, or, for a rubrene probe, ≈ 100 - 3000 τ_α. On the other hand, the approach described in Ref. 14 investigated changes over much longer time scales, and was directly sensitive to exchanges on time scales of 10^5 – 10^6 τ_α. In this approach, molecules that do not exhibit exchange during the experiment can also be assumed not to have experienced exchange on time scales shorter than those probed directly (down to those timescales associated with accurate rate determination of rotational correlation times of the probe [≈ 400 τ_α for tbPDI]).

In this work, we use SM microscopy to monitor the rotations of three perylene probes, including the one used by Zondervan et al., in supercooled glycerol over the temperature range of 1.04 – 1.12 T_g. This work aims to reconcile the findings of Mackowiak[15] and Zondervan[14], investigate the temperature dependence of spatial and temporal heterogeneity as reported by perylene probes in glycerol, and more broadly investigate sensitivity of SM microscopy findings in supercooled liquids to probe size and interactions.

2.2 Detailed Sample Preparation

Solid N,N'-Bis(2,6-dimethylphenyl) -3,4,9,10-perylene dicarboximide (dpPDI), N,N'-Bis[(3-dimethylamino)propyl]-3,4,9,10-perylenedicarboximide (dapPDI), and N,N'-Bis(2,5-*tert*-butylphenyl)-3,4,9,10-perylenedicarboximide (tbPDI) are obtained from Sigma Aldrich (Fig. 2.2). dpPDI and tbPDI are provided as solids and are dissolved in ethanol (Sigma Aldrich, spectrophotometric grade) to obtain $\approx 1.0 \times 10^{-4}$ M concentration solutions. dapPDI is provided as a 1 mM solution in [2-N-morpholino]-ethanesulfonic acid and is diluted to 1×10^{-6} M in ethanol. For dpPDI, 1.6 μl of 1.0×10^{-7} M solution is added to 200 μl of glycerol giving a 8×10^{-10} M dye concentration. For tbPDI, 2.0 μL of 1.0×10^{-7} M is added to 100 μL of glycerol giving a 2×10^{-9} M dye concentration. For dapPDI, a somewhat higher concentration is required for optimum number of visualized probe molecules per typical field of view. 2.0 μL of 1×10^{-6} M dapPDI solution is added to 100 μL of glycerol to produce a 2×10^{-8} M solution. The number of visualized molecules per typical field of view is comparable for all three probes, and the discrepancy in final concentration between the dapPDI and the other probes employed is assumed to be related to inaccuracy in the reported concentration of the purchased solution.

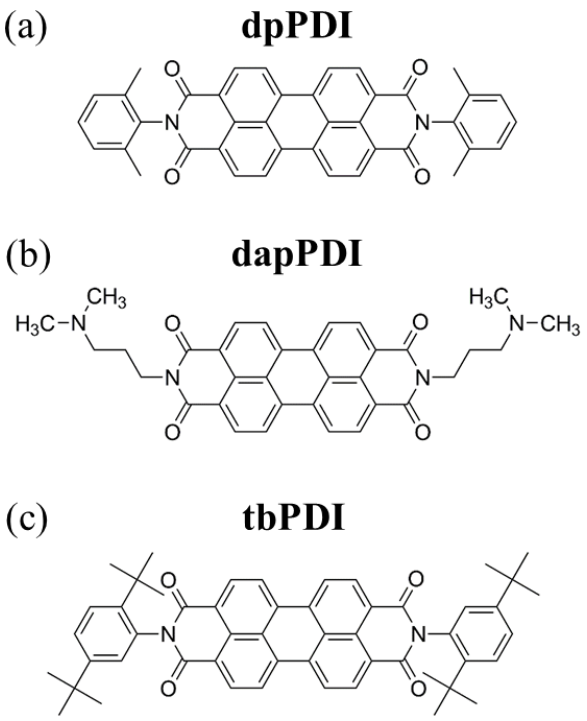

Figure 2.2 Perylene derivatives used in this study. (a) N,N'-Bis(2,6-dimethylphenyl)-3,4,9,10-perylenedicarboximide (dpPDI), molecular weight (MW) = 598.65 g/mol (b) N,N'-Bis[3-(dimethlyamino)propyl]-3,4,9,10-perylenedicarboximide (dapPDI), MW = 560.64 g/mol (c) N,N'-Bis(2,5-*tert*-butylphenyl)-3,4,9,10-perylenedicarboximide (tbPDI), MW = 766.96 g/mol.

In all cases, the dye solutions are added to glycerol that is photobleached for 2 weeks in a bleaching setup[11]. To ensure mixing, the PDI/glycerol mixtures are heated for 20 – 60 minutes at 120^{o}C and shaken occasionally under exclusion of light to avoid photobleaching. The PDI/glycerol solutions are spin coat (Specialty Coating Systems, Model P6204) at 8000 rpm from a 120 ^{o}C solution onto a silicon wafer (University Wafer). Just prior to spin coating, each wafer is sonicated in acetone (Sigma Aldrich, spectrophotometric grade), rinsed with Millipore water, and heated briefly in an open flame to pyrolyze any remaining impurities and oxidize the surface to improve the wetting of the glycerol. The spin-coating procedure produces a glycerol

film of several hundred nanometer thickness in the center of the wafer, as judged by the color of the film and the interference fringes.

The sample is placed into a microscopy cryostat (Janis Research Company Inc, Model ST-500-LN) using vacuum grease (Apiezon N) to optimize thermal contact between the sample stage and silicon wafer. The cryostat is evacuated and flushed with dry nitrogen five times at room temperature (at pressures no lower than 1 mTorr to prevent evaporation of glycerol) and subsequently cooled at ≈ 5 K/min to the desired temperature (T = 198-212 K). Upon reaching the measurement temperature, the cryostat is evacuated for 1-2 hours to a pressure of 0.3 mTorr. The evacuation procedure is required to remove water, which can be absorbed during spin coating. The water content of glycerol was confirmed to be reproducibly < 0.5% both when removed from the bottle and after 15 minutes at atmospheric conditions by viscosity measurements. The time required for spin coating and transfer of the sample to the cryostat is ≈ 5 minutes, after which the evacuation procedure is performed: we thus expect 0.5% water to be an upper bound on the water content.

2.3 Optical Setup

Data is acquired using a home built microscope in an epi-fluorescence configuration (Figure 2.3). The 514 nm line of an Argon ion laser (Melles Griot 43 series, 543-APAO1) is the excitation source. The emitted light is directed through a laser line filter (Semrock, LL01-514), a $\lambda/2$ waveplate (Karl Lambrecht), and an electro-optic modulator (EOM; Conoptics, modulator M370 and amplifier 302RM). The waveplate aligns the polarization of the incoming laser light with the crystal axis of the EOM. The EOM switches the light between *s* and *p* polarization at a

frequency of 1 kHz. A second λ/2 waveplate (Karl Lambrecht) after the EOM is used to align the incoming polarization to ensure a polarization ratio of at least 50:1 after the objective. The excitation beam is reflected towards the objective lens by a dichroic mirror (Semrock, FF520-Di01-25x36). The light is focused onto the rear focal plane of a long working distance objective with correction collar (Zeiss, LD Plan - Neofluar, air 63x, NA=0.75, WD = 1.5 mm), resulting in a collimated excitation beam. This objective lens allows imaging through the 0.5 mm thick cryostat window with an additional separation of 0.25 mm between the cryostat window and sample. The illumination area is a circle of ≈ 70 μm diameter. The fluorescence signal is collected by the objective in the epi-direction, passed through the dichroic mirror, and further filtered by a long pass filter (Semrock, LP02-514RS-25). Fluorescence is directed through a Wollaston prism (Karl Lambrecht) and another bandpass filter (Chroma, 600/150m) onto an EMCCD camera (Andor, iXon DV887). The Wollaston prism splits the signal into two orthogonal polarizations, resulting in two images on the CCD chip. 14-bit movies are recorded using LABView.

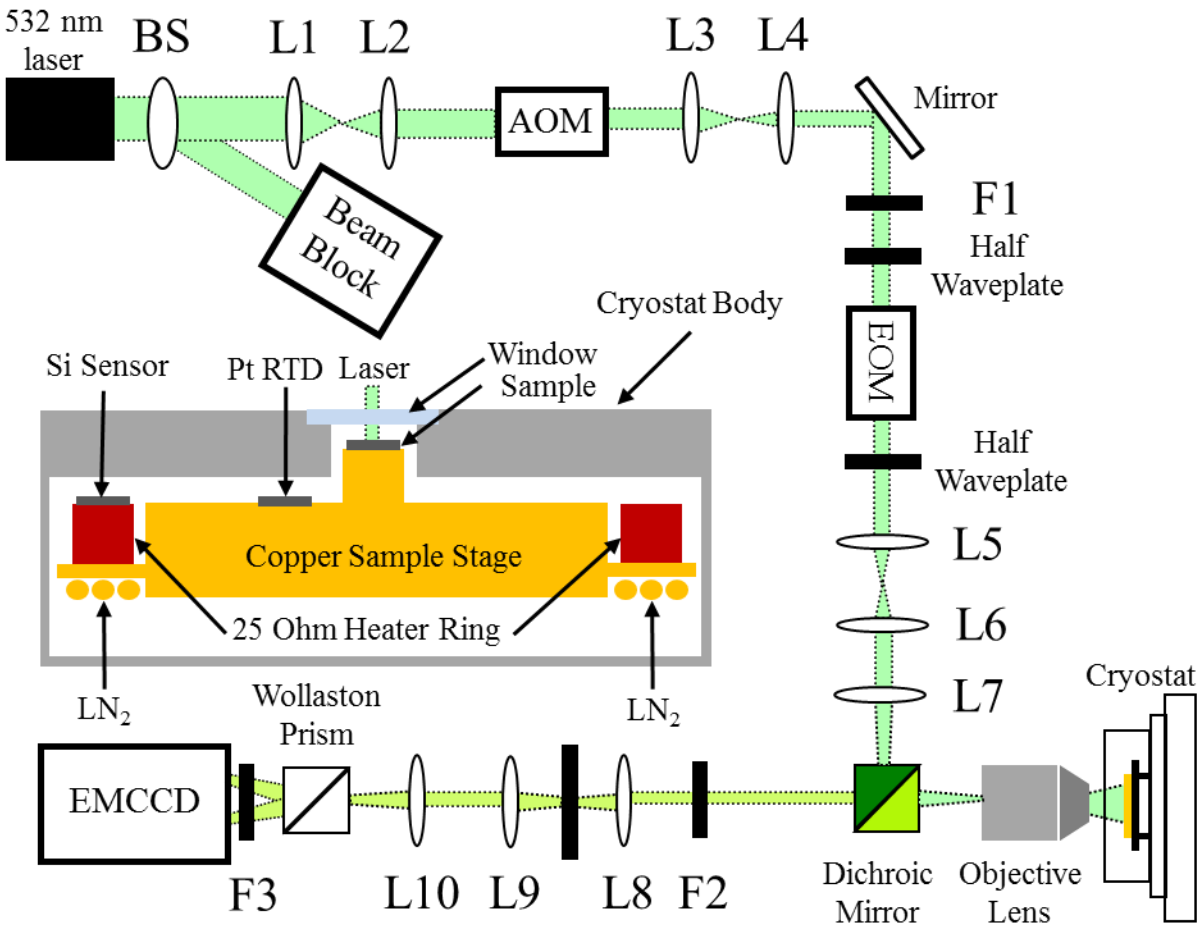

Figure 2.3 Schematic diagram of home built epifluorescence SM microscope. BS= beam splitter, L=lens, F= filter, AOM=acousto-optic modulator, EOM=electro-optic modulator. Inset shows detail of the cryostat. The cryostat has two temperature sensors, but only the Pt RTD is used to determine sample temperature, as the built-in Si sensor sits atop the heating ring. The window has a thickness of 0.5 mm, and the distance between window and sample is 0.2 mm. The cryostat is cooled with liquid nitrogen (LN_2). The size of the sample is 0.5x0.5 mm^2.

. The drawing is not to scale.

Data is collected at temperatures between 198 – 212K.The frame rate is adjusted to ≈ 20 frames per expected median rotational relaxation time of the probe, $\langle\tau_c\rangle$, as determined from preliminary experiments. For frame rates of 5 – 20 Hz (as are used for dpPDI at temperatures ≥ 208K, dapPDI at temperatures ≥ 206K, and tbPDI at temperatures ≥ 204K), sample illumination is continuous, and exposure times are the inverse of the frame rate. The laser powers used for

data collected at these frame rates are 6 – 24 mW, as measured before the objective. For frame rates of < 5 Hz, sample illumination and exposure times are 0.2s followed by a period without illumination of 0.3s (2 Hz), 0.8s (1 Hz), 1.3s (0.67 Hz), 1.8s (0.50 Hz), 2.8s (0.33 Hz), 3.8s (0.25 Hz), or 5.8s (0.167 Hz). During the period without illumination, the laser is shuttered with a mechanical shutter. Average powers used at these frame rates are 3 - 8 mW at 2 Hz, 1- 4 mW at 1 Hz, 1 – 2 mW at 0.67 Hz, 1 mW at 0.5 Hz, 0.5 – 1 mW at 0.33 Hz, and 0.5 mW at 0.25 and 0.167 Hz. For a given sample at a given stage set temperature, data is collected at multiple laser powers to test and potentially correct for heating of the system, as described in Appendix A. The excitation powers and frame rates chosen yield data with similar signal to noise ratios across temperatures and allow collection of $\approx$ 5000 frames per movie (at least 150 $<\tau_c>$) with few molecules photobleaching early in the experiment. A total of 23, 29, and 51 movies are collected for dpPDI, dapPDI, and tbPDI, respectively. For dpPDI, all movies are collected on one sample over two days. For dapPDI and tbPDI, data is collected on two samples over three days each. Number of molecules analyzed at all temperatures for all probes is shown in Table 2.1.

2.4 Data Analysis

Data analysis is performed using in house IDL based software (ITT Visual Information Solutions). The first 500 frames in a given movie are summed prior to identification of single molecules. The resulting summed movie image is filtered by convolution with a Gaussian intensity distribution. Individual features of a reasonable intensity above the background are then matched up into pairs -- one from the left channel and one from the right channel -- by using the known separation of the channels on the CCD chip. Only features that are identified in both

channels and have characteristics consistent with single molecule fluorophores (reasonable intensity and single step bleach) are analyzed.

Once the locations of the fluorophores are established, all further analysis is performed on the raw, unfiltered images. The intensity of the fluorophore is calculated in both channels by integrating the intensities of pixels within 2-2.5 pixels of the identified feature center. In order to extract true fluorophore intensities, a spatially varying background that mimics the excitation beam profile is subtracted. The background is calculated for each molecule individually by averaging the intensities of the pixels surrounding the molecule from the limit of the intensity integration out to a radius of 4.5 pixels. In order to reduce the effect of other fluorophores that may border this background region, the top and bottom 10% of this distribution are excluded from the average. Background subtracted intensities are then recorded for each molecule in each frame of the movie. These intensities are denoted $I_{\parallel}$ and $I_{\perp}$. Linear dichroism (LD) is then constructed from each frame of the movies as

$$\mathrm{LD} = \frac{I_{\parallel} - I_{\perp}}{I_{\parallel} + I_{\perp}}. \tag{2.1}$$

LD values should span the range -1 ≤ LD ≤ 1; however, due to inaccuracies in background estimation and subtraction, LD values outside the expected range are sometimes present. In order to exclude these unphysical values, when a negative intensity is present in one channel of the background subtracted signal, that value is set to zero. This procedure does not affect information subsequently obtained from the LD trajectory.[15]

The deviation of the LD signal from a mean, $a(t) = \mathrm{LD}(t) - \langle \mathrm{LD}(t) \rangle$, is used to construct an autocorrelation function (ACF):

$$C(t) = \frac{\sum_{t'} a(t')a(t'+t)}{\sum_{t'} a(t')a(t')} \quad . \tag{2.2}$$

As detailed in Ref. 15, while the ACF constructed from the SM LD signal is not an orientational correlation function of a single rank, given the experimental setup employed here, it is strongly dominated by $C_2(t)$, where $C_l(t) = e^{-Dl(l+1)t}$ with D the rotational diffusion constant, and thus this experiment is a single molecule analogue to fluorescence anisotropy.[15,22,88,89] When the ACF is well fit by an exponential decay with time constant τ_{exp}, that value can be taken as the rotational correlation time, τ_c, of the probe. When the ACF is best fit by a stretched exponential decay given by

$$C(t) = Ae^{-(\frac{t}{\tau_{fit}})^{\beta}} \tag{2.3}$$

with β the stretching exponent, the extracted relaxation time is given by

$$\tau_{\text{str exp}} = \frac{\tau_{fit}}{\beta}\Gamma\left(\frac{1}{\beta}\right). \tag{2.4}$$

Due in part to the limited length of the LD trajectories, better fits are generally obtained from the stretched exponential fits;[15,19,22,90] thus, all ACFs are first fit with the stretched exponential form. Because the goodness of fit for the stretched exponential varies with trajectory properties, trajectory dependent fitting is performed.[15] For molecules with low sampling rates (< 20 points per $\tau_{str\ exp}$), $\tau_{str\ exp}$ is considered the relaxation time, and $\tau_{str\ exp} = \tau_c$. For trajectories with high sampling rate and trajectories longer than $50\tau_{str\ exp}$, $\tau_{str\ exp}$ is also set as the relaxation time, τ_c. For high sampling rate trajectories shorter than $50\tau_{str\ exp}$, a linear fit to the ACF is found to be more

accurate than the stretched exponential fit.[15,91] Thus, these trajectories are re-fit to a line, ACF = mt + b for the longer of either 20% of $\tau_{str\ exp}$ or five points. τ_c is then given by b/m.

2.5 Simulation Studies of Homogeneous Rotational Diffusion

Criteria with which to assess the reliability and sensitivity of the two methods we use to detect molecules undergoing dynamic exchange are obtained using simulations of three dimensional *homogeneous* rotational diffusion of a fluorophore along the surface of a sphere. The transition dipole of a fluorophore is represented by a unit vector that is rotated, with the rotation axis chosen randomly for each step. The vector is rotated about this axis by an angle whose magnitude is chosen from a Rayleigh distribution, with the diffusion constant chosen to give the desired time constant, τ_c. Simulations are performed at 20 points per τ_c for a trajectory length of 200 τ_c, which approximates experimental conditions in this study.

From the simulated trajectories, x-, y, and z-components of the dipole orientation are used to calculate intensity and linear dichroism as they would be detected experimentally. Specifically, $I_{\parallel}$ and $I_{\perp}$ are calculated assuming collimated excitation and epi-collection with an objective of NA = 0.75, as described in Ref. 15. These intensities are scaled such that the average intensity correlates with that of a typical background subtracted experimental signal. Noise contributions are added to the simulated data. First, detector noise due to EM amplification of the CCD camera is considered. Detector noise has a variance (σ^2) two times the intensity of the signal[92], and to add noise of this type to the simulations each scaled intensity in the simulated trajectory is multiplied by a random number from a Gaussian distribution with mean equal to that intensity and variance equal to two times that intensity. Noise that may emerge from subtracting

the spatially varying background is also included. Experimentally, after the probe fluorophore bleaches, the standard deviation of the (background subtracted) intensity fluctuations is at maximum 30% of the mean intensity of the signal before bleaching. Given that these fluctuations arise from several sources, 30% is considered an upper bound on the noise introduced by background subtraction. This additional "background noise" is added to the simulated signal. At every point in the simulated trajectory, a randomly chosen value from a Gaussian distribution centered at zero with standard deviation set to 30% of mean signal intensity (or $\sigma^2 = (0.3\mu_{signal})^2$) is added to the signal. After noise is added to the $I_{\parallel}$ and $I_{\perp}$ trajectories, as in the experimental traces, any negative intensities are set to zero. LD trajectories and ACFs are then calculated.

2.6 Median Probe Rotational Relaxation Times

In typical liquids, the temperature dependence of the host viscosity allows prediction of the rotational relaxation time of a probe of known size in the liquid via the Debye – Stokes - Einstein (DSE) equation,

$$\tau_c = \frac{V_h \eta(T)}{k_B T}. \qquad (2.5)$$

The rotational relaxation time of the probe is given by τ_c, V_h is the hydrodynamic volume of the probe, T is the temperature in Kelvin, k_B is the Boltzmann constant, and $\eta(T)$ the temperature dependent host viscosity. The DSE equation assumes a non-perturbative and spherical probe. Using the DSE equation to predict probe rotational relaxation time in a supercooled liquid also

requires the assumption that DSE behavior holds in such systems. Experiments show that DSE behavior does describe probe rotations in small molecule supercooled liquids.[13,14,80–85,93–95] For the SM experiments described in this work, the rotational DSE equation is used primarily to confirm that measured SM probe dynamics are reflecting behavior of the host. We use the DSE equation both to compare the temperature dependence of the rotational relaxation of the probe to the known temperature dependent viscosity of glycerol and to extract a hydrodynamic volume, V_h, for the probe. Using the DSE equation allows us to confirm (1) collection of a statistically significant sample set, (2) that the temperature dependence of the probe's relaxation time tracks the viscosity of glycerol and thus reflects the host system's behavior on some level, and (3) a reasonable size for the probe.

Fig. 2.2 shows the structure and abbreviations for the three PDI probes used in this study: dpPDI, dapPDI, and tbPDI, the last of which was also used by Zondervan et al. for SM studies of supercooled glycerol.[14] The three molecules have similar photophysical properties, quantum yields near unity, and fluorescence anisotropy near the theoretical maximum of 0.4, making them well suited for SM measurement of rotational dynamics.[96–98] Median rotational relaxation times measured for each of the three probes as a function of temperature are plotted in Figure 2.4. Each point represents the median τ_c from an individual movie (typically containing 100 – 200 analyzed probe molecules), which has been corrected for heating as described in Appendix A. The data is fit to the DSE equation using the known temperature dependence of the glycerol viscosity.[99] The determined hydrodynamic volumes of dpPDI, dapPDI, and tbPDI and are V_h = 2.02 nm^3 (r_h = 0.79 nm), V_h = 1.27 nm^3 (r_h = 0.67 nm), and V_h = 0.36 nm^3 (r_h = 0.44 nm), respectively.

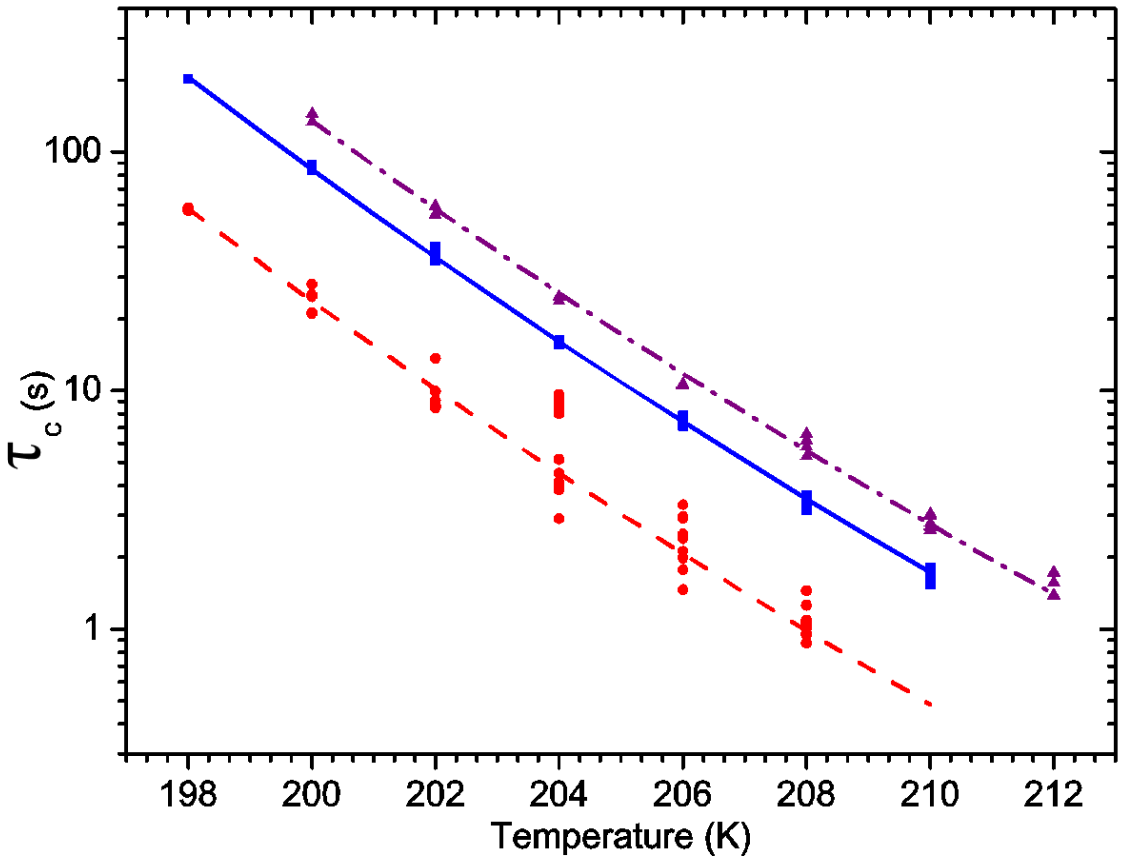

Figure 2.4 Rotational relaxation times versus temperature for tbPDI (red circles), dapPDI (blue squares), and dpPDI (purple triangles). Each point represents the heating corrected median τ_c for all molecules in a given movie. The lines are the fit of the DSE equation with best-fit hydrodynamic volumes for each of the probes. Red dashed line (tbPDI): V_h = 0.36 nm^3, blue solid line (dapPDI): V_h = 1.27 nm^3, and purple dash - dot line (dpPDI): V_h = 2.02 nm^3.

The relative hydrodynamic volumes of the probes run counter to initial expectation, as it is generally accepted that a molecule with a larger space filling volume (which often trends with molecular weight) will rotate more slowly than a smaller and less massive molecule. Thus, tbPDI's rotations were expected to be slower and yield a larger hydrodynamic volume than dpPDI's due to the two t-butyl groups in tbPDI compared to the two methyl groups in dpPDI. Instead, the measured hydrodynamic volume of dpPDI is ≈ 5 times that of tbPDI, where our measurement is in close accord with the determined V_h = 0.38 nm^3 obtained by Zondervan et al.[14]

Similarly, the hydrodynamic volume of dpPDI is ≈ 1.6 times greater than that of dapPDI despite the fact that these molecules' molecular weights differ by < 10%. Indeed, the extracted probe hydrodynamic volumes are inconsistent with an explanation based on probe mass or size such as that found by Wang and Richert for a variety of probe/host systems near T_g.[86] In that study, time resolved optical depolarization was used to monitor rotational relaxation of probe molecules while solvation experiments monitored solvent dynamics in the vicinity of the probes. It was found that the ratio of molecular weight of the probe relative to that of the host molecule, R_m, correlated with ratio of the rotational relaxation time of the probe to that of the host. Because our data is inconsistent with that finding, instead we consider the possibility that the measured hydrodynamic volumes reflect a complex mix of probe mass, space filling volume, structural anisotropy, and interactions with the surroundings.

Of the probes employed, dapPDI is expected to be the most polar and tbPDI the least polar.[96] Additionally, while all of these molecules may hydrogen bond with glycerol, in the case of tbPDI there may be steric hindrance that inhibits this interaction. Given the high polarity of glycerol and its hydrogen bonding network, differences in PDI probe polarity and ability to hydrogen bond are expected to affect probe interaction with the host, potentially slowing the rotation of hydrogen bonding probes relative to those that do not participate in the hydrogen bonding network. The suggestion that less polar molecules that can not hydrogen bond with glycerol rotate more quickly than polar molecules of similar size that can participate in glycerol's hydrogen bonding network is also consistent with our previous result for rubrene in glycerol[3]. Rubrene has a similar mass to dapPDI and dpPDI but a significantly faster rotational relaxation time and thus a smaller extracted hydrodynamic volume (V_h = 0.18 nm^3, data not shown) than any of the PDIs measured.[15] A similar slowdown for hydrogen bonding probes relative to non-

hydrogen bonding probes has been noted previously in poly(isobutyl) methacrylate near T_g.[100] Given the slow rotation and large extracted V_h for dapPDI and dpPDI, it is possible that these molecules' rotations are significantly hindered due to participation in the hydrogen bonding network or even that these probes are rotating with a shell or partial shell of glycerol molecules, increasing the effective radius of the probe.

2.7 Breadth of Relaxation Times

One of the chief reasons for evaluating the DSE behavior of the PDI dyes as a function of temperature is to establish the presence of a statistically significant sample size. Having found that all three probes exhibit changes in rotational relaxation time with decreasing temperature in accord with the DSE equation and known temperature dependence of the viscosity of glycerol, we now evaluate results that can only be attained from SM experiments. Fig. 2.5 shows the histograms of the heating corrected τ_c values for dpPDI, dapPDI, and tbPDI in the temperature range of 198K - 212K. Qualitatively, the histograms for each of the PDI molecules look similar, and the histograms (on the log scale) are quite well fit by both Gaussian and Lorentzian functions. The Gaussian distribution is given by

$$y = \frac{1}{\sqrt{2\pi\sigma^2}} \exp^{-\frac{(x-x_c)^2}{2\sigma^2}}, \tag{2.6}$$

where x_c indicates the center of the peak and σ^2 is the variance. The full width at half maximum (FWHM) is given by $2\sqrt{2\ln 2}\sigma$. The Lorentzian distribution is

$$y = \frac{1}{\pi} * \frac{\gamma}{(x-x_c)^2 + \gamma^2} \tag{2.7}$$

with the FWHM given by 2γ. Taking the adjusted R^2 value as an indicator of the quality of the fit, both distributions fit the histograms equally well. In Table 2.1, the number of assessed molecules and the FWHM from the Gaussian and Lorentzian fits are shown for each probe at each temperature investigated, and Fig. 2.5 shows Gaussian fits to the distributions of τ_c values for dpPDI, dapPDI, and tbPDI for all single molecule probes evaluated in this study. While these distributions are well fit by symmetric functions on a log scale, on a linear scale the data is well described by log-normal distributions, which have previously been associated with non-trivial, cooperative dynamics. [101,102]

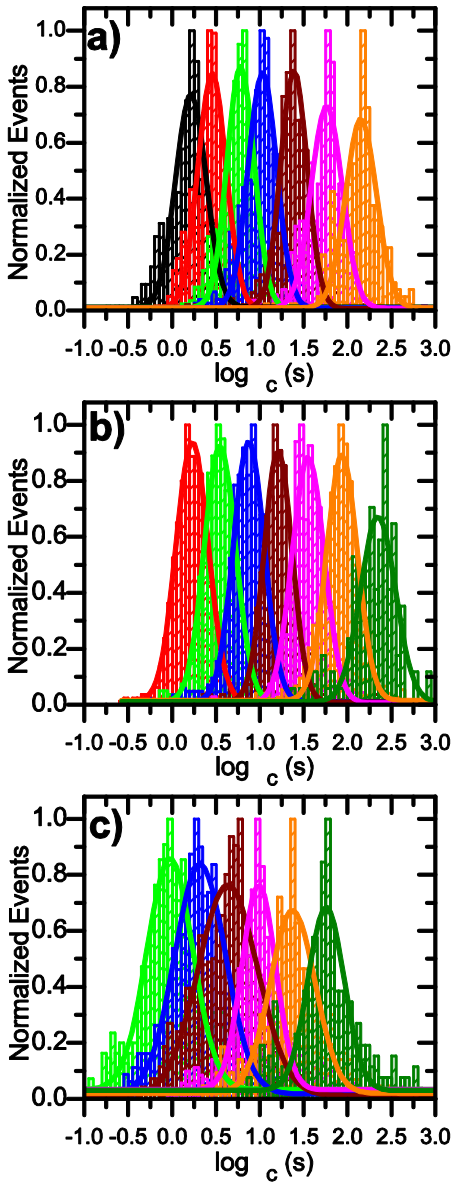

Figure 2.5 Histograms of log(τ_c) values for all PDI probes with Gaussian fits: (a) dpPDI, (b) dapPDI, and (c) tbPDI. Colors indicate temperature: black: 212K, red: 210K, green: 208K, blue: 206K, wine: 204K, magenta: 202K, orange: 200K, forest green: 198K. All histograms are normalized to the maximum number of occurrences at each temperature. Because dapPDI and tbPDI are taken from two data sets, to make this data comparable to that of dpPDI, collected on one sample, a normalization is performed. Two histograms are made (one for each of the data sets collected) for dapPDI and tbPDI and each histogram is normalized such that median τ_c at a given temperature matches that from the best-fit DSE fit. This prevents histogram width from being affected by potential differences between data sets.

	dpPDI			dapPDI			tbPDI		
T/K	Molecules	$FWHM_1$	$FWHM_2$	Molecules	$FWHM_1$	$FWHM_2$	Molecules	$FWHM_1$	$FWHM_2$
198	. . .	. . .	. . .	126	0.47	0.34	244	0.49	0.39
200	270	0.41	0.28	651	0.41	0.43	434	0.60	0.51
202	372	0.41	0.28	578	0.43	0.38	696	0.45	0.37
204	330	0.36	0.29	431	0.38	0.32	1319	0.79	0.67
206	438	0.38	0.29	748	0.41	0.37	1071	0.68	0.60
208	622	0.36	0.29	716	0.42	0.35	749	0.61	0.54
210	877	0.38	0.29	737	0.43	0.38	. . .	. . .	. . .
212	484	0.40	0.30	. . .	. . .	. . .	. . .	. . .	. . .
Average		0.39	0.29		0.42	0.37		0.60	0.51

Table 2.1 Temperature, number of molecules, and FWHM for Gaussian ($FWHM_1$) and Lorentzian ($FWHM_2$) fits to the $\log(\tau_c)$ distributions shown in Fig. 2.5. FWHM are best-fits to within ± 0.02.

The distributions shown in Fig. 2.5 indicate there is a spread of rotational relaxation times reported by all of the probes in supercooled glycerol at all of the temperatures investigated, with molecules exhibiting rotational relaxation times that span at least an order of magnitude at all temperatures and for all probes studied. This implies that dpPDI, dapPDI, and tbPDI all report spatial heterogeneity in supercooled glycerol. While the log-normal distributions evident here represent a large spread of time constants, the histograms are significantly different in shape from that of rubrene in glycerol at 204K, which had a more prominent long time tail and a spread of time constants that spanned nearly three orders of magnitude.[15] This suggests that rubrene accesses and reports a larger breadth of the environments in supercooled glycerol than do the larger, more slowly rotating PDI probes. It is also evident that the distributions of time scales reported by the SM probes are narrower and somewhat different in shape than would be expected from results of a variety of bulk measurements in supercooled glycerol.[99,103,104]

When one considers spatially heterogeneous dynamics, it is not obvious that the extent of heterogeneity should be the same over the full supercooled temperature regime. It may then be

expected that observables that probe these heterogeneities directly may vary with temperature even if TTS holds when probing bulk observables. Despite this, for PDI probes, the shape and width of histograms detailing spatial heterogeneity via SM microscopy are found to be constant as a function of temperature in supercooled glycerol in the range of 1.04 - 1.12 T_g.

The fact that the distributions of rotational relaxation times measured are not changing shape with temperature suggests that degree of spatially heterogeneous dynamics in glycerol is constant over the temperature range probed. However, comparing the widths of the distributions at each temperature across PDI probes reveals the dapPDI τ_c distributions to be slightly wider than those of dpPDI at all temperatures. A more notable difference is apparent between the τ_c distributions for tbPDI and those for dpPDI and dapPDI. Data collected using tbPDI is more variable than for either of the other two probes, with the histograms for relaxation times at some temperatures slightly broader than those for dapPDI and at some temperatures significantly broader, though with no clear trend as a function of temperature. The breadth of the tbPDI histograms is confirmed not just for the pooled data over the two samples and 53 movies represented in Fig. 2.5 but also for the 100 - 200 molecules in individual movies, showing that the increased breadth of rotational relaxation times in the tbPDI data is not due to movie to movie or sample to sample variation in median relaxation time that can be seen in the spread of points for tbPDI at a given temperature in Fig. 2.4.

Given the similar size of the three PDI probes used in this work and the fact that tbPDI is the largest of these probes, we suggest that the narrower τ_c distributions seen for the dpPDI and dapPDI relative to those of tbPDI are unlikely to be due to a differential in spatial averaging by the probes. Instead, the broad distribution found for tbPDI suggests that more quickly rotating probes can report the presence of a more significant breadth of spatially heterogeneous dynamics

in the glycerol host and that the narrowing of dpPDI and dapPDI histograms relative to those seen for tbPDI is driven by the increased temporal averaging of the more slowly rotating dpPDI and dapPDI probes. This is also supported by comparing τ_c distributions for two probes in glycerol at different temperatures chosen such that the median probe τ_c overlaps. In Fig. 2.6, the τ_c distributions for tbPDI at 200K and dpPDI at 204K are shown: both distributions peak at ≈ 20s, but the tbPDI distribution is broader. In this comparison, the time averaging in absolute time performed by the probes over the spatially heterogeneous dynamics is the same for most probe molecules in the glycerol. Given the similarity in probe molecular structure, the spatial averaging is also expected to be very similar, with tbPDI averaging slightly more than dpPDI in space owing to its t-butyl groups. Comparing these two distributions from probes that have performed very similar temporal and spatial averaging over their surroundings may suggest that glycerol at 200K is more heterogeneous than glycerol at 204K, as judged from the breadth of the distributions at the two temperatures. However, taken in the context of Fig. 2.5, in which we find no broadening with decreased temperature for a given probe, we suggest this behavior is further evidence for temporal averaging by the probes being the primary determinant of the breadth of τ_c distribution: even while the absolute time averaging between the two probes is the same in the two distributions shown in Fig. 2.6, the relative τ_c/τ_α values are ≈ 16 for tbPDI at 200K and 90 for dpPDI at 204K. As such, the effective time averaging relative to the structural relaxation time of the surroundings is greater for the slower probe at the higher temperature, consistent with the narrower distribution found. Such temporal averaging has been implicated previously in probe molecules' inability to report the full breadth of heterogeneity in a supercooled liquid in ensemble and sub-ensemble measurements[10]. This conclusion is also consistent with results for

rubrene probes in glycerol at 204K, which show a distribution of probe rotational relaxation times that has a long time tail and a distribution spanning nearly three orders of magnitude.[15]

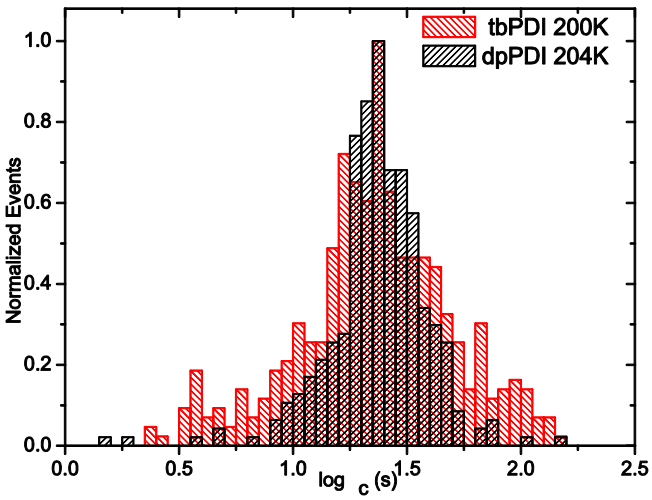

Figure 2.6 Histograms of log(τ_c) values for dpPDI at 204K and tbPDI at 200K. The two distributions are centered at approximately the same value, and absolute temporal and spatial averaging performed by the probe are expected to be very similar.

The conclusion that time averaging is responsible for the differential in rotational relaxation time distribution breadth between the probes suggests that dynamic exchange occurs on time scales shorter than or similar to probe rotation. While other measurements have also led to the finding that large probes will average over spatially heterogeneous dynamics in space and/or time, as depicted in Fig. 2.1, we note here that we find strong evidence for spatially heterogeneous dynamics in supercooled glycerol in these SM experiments for probes that are quite large. While other studies report that probes of molecular weight $\geq$ 1.2 times that of the host and/or relaxation times $\geq$ 20 times the solvent relaxation time only report exponential decays in optical depolarization experiments[86], implying full averaging over the spatially heterogeneous dynamics in the sample, in these experiments we find a broad spread of spatially heterogeneous dynamics even for tbPDI, whose molecular weight is 8.3 times that of the host

molecule. This behavior is further investigated by considering the average ACF as would be measured via bulk experiments. Averaging the LD ACFs for 629 tbPDI molecules at 204K and fitting the resulting ACF to a stretched exponential yields a best-fit stretching exponent of 0.88. This is the first time a molecule as large as tbPDI (≈ 8 times the molecular weight of and ≈ 20 times slower than glycerol) has demonstrated deviations of the stretching exponent from unity. These findings confirm that in supercooled glycerol even the relatively large and slow probes used in SM studies to date are sensitive to spatially heterogeneous dynamics in supercooled glycerol.

2.8 Dynamic Exchange

The broader spread of rotational relaxation times seen for probe molecules that, on average, rotate most quickly despite similar molecular weight and structure suggests the presence of dynamic exchange on time scales on or shorter than that associated with probe rotation (≈ 100 τ_α for dpPDI and 20 τ_α for tbPDI). To more directly assess temporal heterogeneity and dynamic exchange, two techniques that directly interrogate dynamic exchange on time scales from 10^3 – 10^6 τ_α are employed.

2.8.1 Window Shifting Technique

A method proposed by Schob et al. is employed to detect changes in dynamics during the collected trajectories.[105] The LD trajectory is split up into segments by a window that is slid across the trajectory, and an ACF is calculated and fit for each segment. This results in a trajectory of rotational time constants, subsequently called τ–trajectory. A sliding window of 20

τ_c, with τ_c the rotational relaxation time obtained from the full trajectory, is selected to balance sensitivity to relatively short changes in dynamics and accuracy and precision of ACF fits. The window is moved by 10 points ($\approx 0.5\ \tau_c$) between each fitted window. Linear fitting is used to derive τ_c in each window due to the short window width and insensitivity of linear fits to window width.[15] After τ–trajectory is obtained, a molecule is classified as either temporally heterogeneous or homogenous using criteria set with simulations described in the Experimental Section.

For simulations of homogeneous rotational diffusion, 95% of the trajectories are found to have 95% of their τ–trajectory values within 2.6 times the median relaxation time in τ–trajectory ($\tau_{traj,med}$). This criterion thus has a false positive rate of 5%. A second criterion is based on the finding that 95% of the homogeneous trajectories have τ–trajectory distributions with standard deviations < 0.68. The second criterion is thus satisfied if the standard deviation of τ–trajectory is > 0.68. These criteria were developed for trajectories of 200 τ_c with a point density of 20 points per τ_c, properties chosen to well match the experimental data. Molecules are assigned as heterogeneous if either the first or second criteria is met. Using these criteria, between 5 and 10% of homogeneous molecules are expected to be incorrectly identified as heterogeneous.

This approach has been applied to data collected on dpPDI at all temperatures as well as for dapPDI and tbPDI at 204K. For dpPDI, all molecules in all movies are investigated for potential temporal heterogeneity via this approach. For dapPDI and tbPDI, at least two movies each collected at 204K are assessed. In all cases, the total number of molecules in the movies are only assessed for temporal heterogeneity with the sliding window technique when the LD trajectory is > $50\tau_c$ and τ-trajectory contains both at least 50 points and at least 33% of the

expected points based on window step, window size and trajectory length. Missing points in τ-trajectory are usually due to a noisy ACF obtained from a particular window. This typically manifests as a poor fit to the ACF, with τ_c from a linear fit and an exponential fit differing by more than a factor of 3 or a pre-exponential factor lower than 0.3, either of which results in the point being excluded from τ-trajectory. With these criteria, ≈ 75% of molecules that are present in each movie are assessed for temporal heterogeneity with the window shifting approach. As can be seen in Table 2.2, 26 – 36% of dpPDI molecules assessed are found to be heterogeneous by this approach, with no clear dependence on temperature. At 204K, dapPDI shows similar results, with ≈ 25% of molecules found to be heterogeneous; however, for tbPDI at 204K only 15% of the assessed molecules satisfy the criteria for heterogeneity. Taken together with previous work showing 15% of rubrene molecules in supercooled glycerol at 204K were classified as heterogeneous with this approach, the tbPDI data suggests that faster probes may be less likely to be classified as heterogeneous in the sliding window approach. This may be related to the fact that dpPDI and dapPDI show a relatively narrow distribution of τ_c values relative to rubrene and tbPDI. Thus, the dynamic exchanges likely to occur for dpPDI and dapPDI (alterations in time constant of a factor of ≈ 2 - 3) may be more readily picked up by the window shifting technique than are those that rubrene and tbPDI undergo. Indeed, unlike in the rubrene data, no evidence of molecules exchanging between dynamically disparate environments is present for dpPDI or dapPDI though a small proportion of tbPDI molecules do exhibit large, abrupt changes in dynamics (data not shown) as were also seen for rubrene.[15]

T/K	Assessed molecules	Heterogeneous molecules	Percent heterogeneous
	dpPDI		
200	166	59	35.5
202	226	80	35.4
204	243	70	28.8
206	319	84	26.3
208	307	80	26.1
210	606	166	27.4
212	321	114	35.5
	dapPDI		
204	220	54	24.5
	tbPDI		
204	194	29	15.0

Table 2.2 Number of molecules assessed for heterogeneity and found to be heterogeneous with the sliding window approach.

For dpPDI at all temperatures as well as for dapPDI and tbPDI at 204K, for each molecule assigned as heterogeneous, τ-trajectory is evaluated for time until the first change in dynamics and, potentially, for time between dynamic exchanges. The time before the first change in dynamics is termed the persistence time (τ_{pers}) and that between changes in dynamics is the exchange time (τ_{ex}), in keeping with definitions employed for kinetically constrained models.[106] The values and temperature dependence of persistence and exchange time need not be the same, and thus we distinguish between them. Lower bounds on exchange times (time from last exchange of a heterogeneous molecule to the end of the evaluated portion of the LD trajectory) as well as lower bound on persistence time (time to the end of the evaluated portion of the LD trajectory for homogeneous molecules) are also tabulated. Histograms of the ratios of exchange,

lower bound on exchange, persistence, and lower bound on persistence time to the molecules' rotational relaxation times for the 70 heterogeneous molecules identified in dpPDI at 204K are shown in Fig. 2.7. The median ratio of the molecules' lower bound on persistence times relative to their rotational correlation times ($\tau_{pers,lower\ bound}/\tau_c = 145$) is significantly longer than the that of persistence times relative to rotational correlation times measured on molecules that experience exchange ($\tau_{pers}/\tau_c = 26$). This is similar to the findings in rubrene at 204K and consistent with the idea that a molecule undergoing exchange is likely to continue to do so. Exchange and lower bound on exchange times relative to rotational relaxation time from molecules deemed heterogeneous are found to be $\tau_{ex}/\tau_c = 36$ and $\tau_{ex,\ lower\ bound}/\tau_c = 43$. Examining these quantities as a function of temperature reveals they are relatively insensitive to temperature (Fig. 2.8). Only the lower bound on persistence time exhibits a clear trend with respect to temperature, increasing monotonically with temperature from $\tau_{pers,lower\ bound}/\tau_c \approx 110$ at 200K to ≈ 170 at 210 and 212K. However, this trend appears correlated with the total median trajectory lengths of the assessed molecules. Indeed, the trajectory lengths of not only the molecules classified as homogeneous but also those classified as heterogeneous follow this trend. This is displayed in a quantity termed $\tau_{pers,\ lower\ bound\ (het)}/\tau_c$ in Fig. 2.8. For dapPDI (tbPDI) at 204K, the median values are $\tau_{pers,lower\ bound}/\tau_c = 96$ (79), $\tau_{pers}/\tau_c = 28$ (30), $\tau_{ex}/\tau_c = 27$ (31) and $\tau_{ex,\ lower\ bound}/\tau_c = 32$ (31), with similar distributions for each of these quantities as those shown for dpPDI in Fig. 2.7 (data not shown).

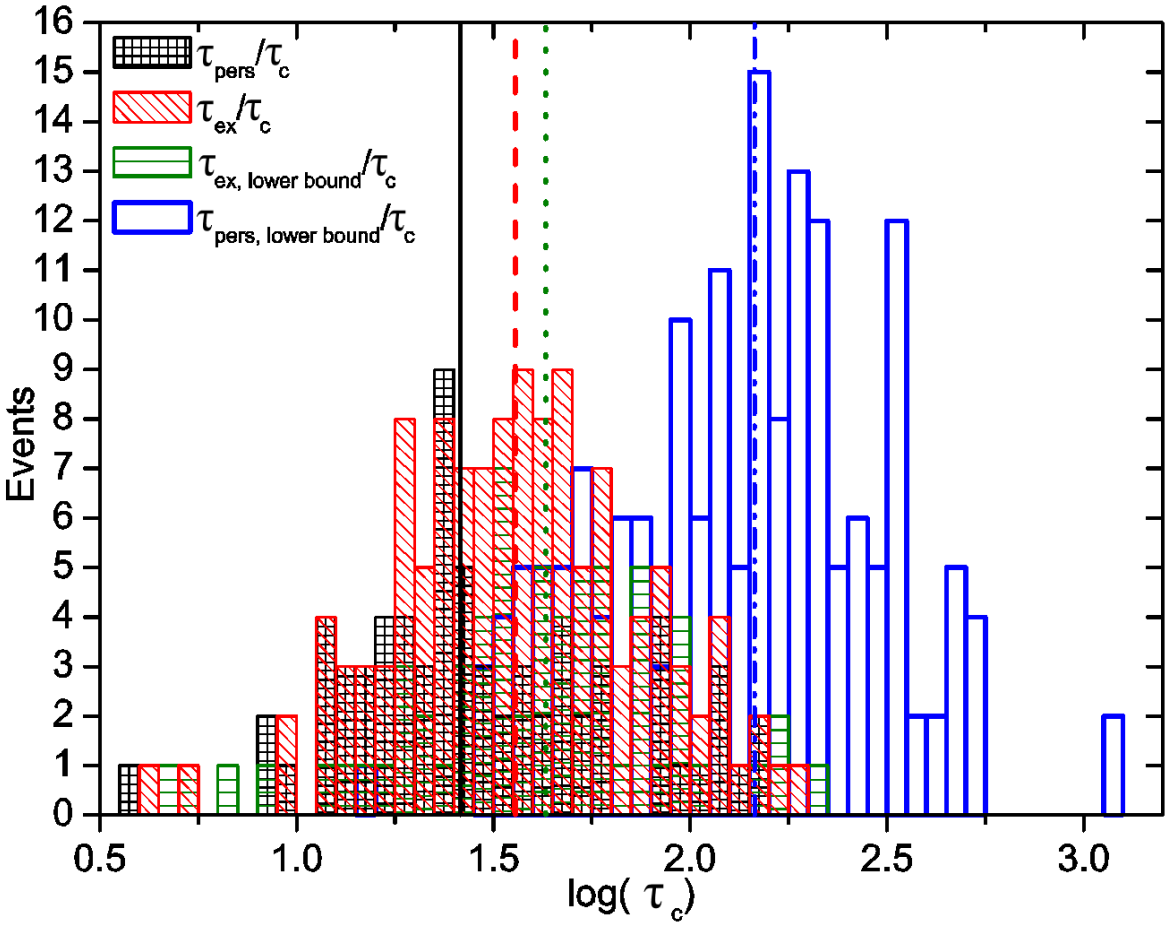

Figure 2.7 Histograms and median values (lines) of τ_{pers}/τ_c (black bars with checks; black solid line), τ_{ex}/τ_c (red bars with diagonal lines; red dashed line), $\tau_{ex,lower\ bound}/\tau_c$ (olive bars with horizontal lines; olive dotted line), and $\tau_{pers,lower\ bound}/\tau_c$ (blue bars; blue dash-dot line) as compiled from the 243 dpPDI molecules assessed for temporal heterogeneity at 204K.

The various time scales shown in Fig. 2.8 can be translated into values relative to τ_α using the ratio τ_c/τ_α for each of the probes. This ratio varies between ≈ 100 for dpPDI to ≈ 20 for tbPDI. As such, $\tau_{ex}/\tau_\alpha \approx 3600$ for dpPDI and $\tau_{ex}/\tau_\alpha \approx 600$ for tbPDI (and was ≈ 200 for rubrene) in glycerol at 204K. Given the similarity in τ_{ex}/τ_c values for the various probes, the large spread in τ_{ex}/τ_α values highlights how probe speed sensitively influences time scale on which dynamic

exchange can be assessed. Despite the fact that for all probes at all temperatures the window shifting technique is sensitive to exchange on the order of ≈ 10 – 200 τ_c, this translates into different sensitivities in the "dynamic exchange phase space" relative to τ_α. As will be described further below, the insensitivity of τ_{ex}/τ_c and related values to temperature and probe also suggests that the window shifting technique is reporting a bound on average exchange time rather than an absolute value of this quantity.

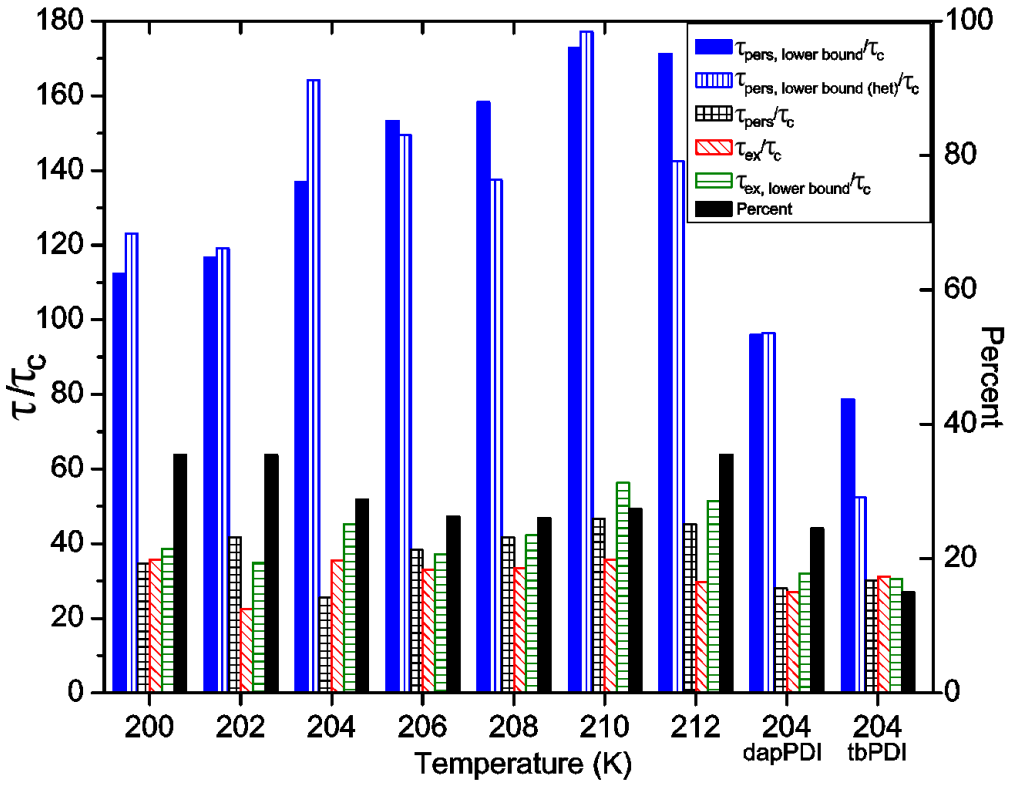

Figure 2.8 Median τ_{pers}/τ_c (black bars with checks), τ_{ex}/τ_c (red bars with diagonal lines), $\tau_{ex,lower\ bound}/\tau_c$ (olive bars with horizontal lines), $\tau_{pers,lower\ bound}/\tau_c$ (blue bars), and $\tau_{pers,lower\ bound\ (het)}/\tau_c$ (blue bars with vertical lines) as a function of temperature for dpPDI as well as for dapPDI and tbPDI at 204K.

2.8.2 Long Time Heterogeneity Assessment

To supplement analysis of temporal heterogeneity and dynamic exchange provided by the window shifting technique, a variation on the long time heterogeneity assessment carried out by Zondervan et al. is performed.[14] This technique can directly probe dynamic exchange on time scales longer than those assessed by the window shifting technique. It can thus address whether molecules that do not appear heterogeneous by that method (≈ 65-85% of the assessed molecules) do so because exchange occurs on time scales longer than those associated with typical trajectory length. To perform this experiment, several movies of the same dpPDI probe molecules embedded in glycerol at 210K are collected consecutively. Specifically, we collect a movie of trajectory length ≈ 50 $<\tau_c>$, wait ≈ 10^5 τ_α, collect a second ≈ 50 $<\tau_c>$ movie of the same molecules, wait ≈ 10^6 τ_α, and collect a third ≈ 50 $<\tau_c>$ movie of the same molecules. In one case, the trajectories collected are ≈ 75 $<\tau_c>$ and only two movies are collected, with a waiting time of ≈ 10^6 τ_α. The relatively short trajectories are required to prevent photobleaching of the molecules before the experiment is complete. However, we focus on maximizing trajectory length within this constraint, given that the accuracy of extracted rotational correlation times from the ACFs depends strongly on trajectory length for short trajectories.[15,19,90] This experiment allows comparison of SM relaxation times after fixed waiting times very long compared to τ_α and, as such, provides sensitivity to temporal heterogeneity that may occur on time scales much longer than that provided by the window shifting technique, whose long time sensitivity limit is similar to typical trajectory length (≈ 200 τ_c ≈ 10^3 – 10^5 τ_α, depending on probe). In the long time heterogeneity experiment, a molecule experiencing dynamic exchange

on any time scale faster than the waiting times is expected to have different relaxation times in each of the movies.

As with the window shifting approach, simulations are performed on molecules undergoing homogeneous rotational diffusion to set criteria for heterogeneity and to assess the accuracy and sensitivity of the method. This is especially important given that ACFs constructed from trajectories between 10 - 250 τ_c have intrinsic uncertainty, and even molecules undergoing homogeneous rotational diffusion with unchanging relaxation dynamics may appear to have different time constants over time as a result of this uncertainty.[19,90] Homogeneous rotational diffusion of 1000 molecules is simulated. The population is set to have a τ_c distribution with a full width half max (FWHM) of 0.4 on a log-scale, $<\tau_c>$ of 20 steps, and a trajectory length of 1000 steps ($50 <\tau_c>$), similar to data collected on dpPDI. As described in the Data Analysis section, trajectory dependent fitting of the LD ACFs is performed. The τ_c value for each molecule is normalized to its minimum value over the 2-3 movies (or simulated data sets), and the 2 - 3 τ_c values are plotted for each molecule relative to this minimum. Normalizing τ_c to the minimum value facilitates assessment of temporal heterogeneity by removing the effect of the relatively broad spread of time constants in the simulated or experimental data.

For 3 (2) simulated trajectories of $50 <\tau_c >$, 95% of the molecules are found to have a maximum τ_c value within 3.0 (2.7) times the minimum τ_c value of that molecule, and 90% have a maximum value within 2.7 (2.2) times the minimum τ_c value of that molecule. Because one of our experiments of this type was performed with 2 trajectories of $75 <\tau_c>$, simulations for 2 trajectories of that length are also performed. Here, the 95% confidence interval (CI) is 2.1 and the 90% CI is 1.9. Concentrating on the result for 3 consecutive $50 <\tau_c>$ trajectories, we conclude that due to statistical variation, a molecule with homogeneous dynamics can have a

change of τ_c by a factor of 3 as assessed by experiments of this type. This is a greater variation in τ_c than is expected for homogeneous rotational diffusion as examined with the window shifting approach. This is due to the fact that there the assessed trajectories are known to be 20 τ_c in all cases, while in this experiment and simulation the trajectories are 50 $<\tau_c>$, or on average 50 τ_c. Slower than average molecules have trajectories shorter than 50 τ_c, leading to substantial uncertainty in the time constants extracted for these molecules. Moreover, in the window shifting approach, the change in τ_c is relative to $\tau_{traj,med}$, where here it is relative to a value that is likely to be smaller, the minimum τ_c in the 3 windows. For three trajectories of 50 $<\tau_c>$, given that simulations reveal that 95% of molecules will have a maximum τ_c value within 3.0 times the minimum τ_c value, we conclude that if more than 5% of the molecules have a change in τ_c greater than a factor of 3.0, temporal heterogeneity is observed. Figure 2.9a shows the simulation results for 3 trajectories of 50 $<\tau_c>$ length for 100 randomly chosen simulated molecules. It is evident that there is substantial crossing of the lines tracking the rotational relaxation times of particular particles. This may initially look to suggest temporal heterogeneity, but we stress that this simulation is for homogeneous rotational diffusion, and all changes in dynamics are due solely to statistical uncertainties.

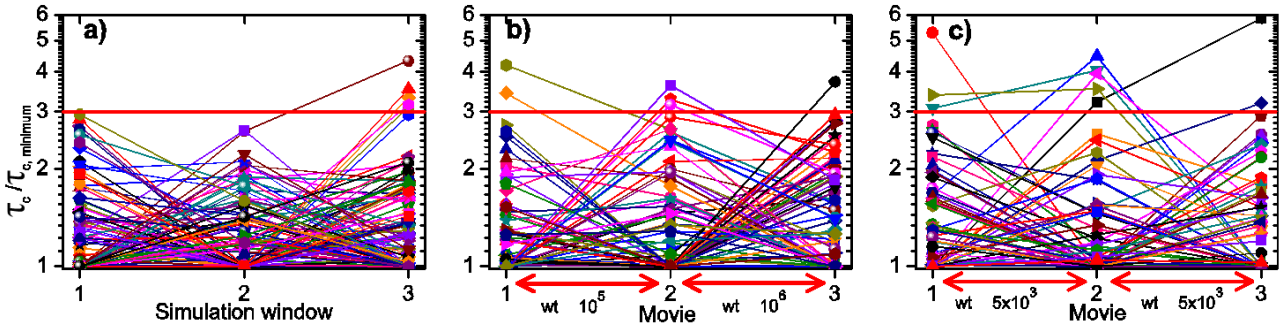

Figure 2.9 Long time heterogeneity assessment for (a) simulations and (b,c) experiments. Each point connected by lines across the three simulated or experimental windows represents a single simulated or experimental molecule. In all cases, the τ_c values are normalized by the minimum τ_c value for each molecule. The red lines indicate the 95% confidence interval (CI) from simulations as described in the text. In panels (b) and (c), "wt" is waiting time. (a) τ_c values for 3 simulated 50 $<\tau_c>$ trajectories. Of the 1000 simulated trajectories, 100 are chosen at random for display. (b) Molecules from one of two experiments in which 3 movies of trajectory length 50 $<\tau_c>$ separated by 10^5 τ_α and 10^6 τ_α, respectively, were collected. Only molecules that have well fit ACFs for all 3 movies are included. In this movie, 6 of 64 (9.4%) molecules are above the 95% CI. (c) Molecules from one movie of dpPDI at 210K collected for ≈ 200 $<\tau_c>$, yielding 4 windows of 50 $<\tau_c>$. All molecules with three consecutive windows of 50 $<\tau_c>$ with LD ACFs that are well fit are included. In this movie, 7 of 58 (12.0%) molecules are above the 95% CI. For the five movies analyzed, 57 of 431 molecules are above the 95% CI (13.2%).

Given that for the 50 $<\tau_c>$ window experiments the lower limit of sensitivity is a change of τ_c of a factor of 3, we consider how likely it is that this experiment will show clear evidence for temporal heterogeneity in the data evaluated. The distribution of $\log(\tau_c)$ values was modeled to be Gaussian with a FWHM of 0.4, consistent with data collected using dpPDI and dapPDI. For such a distribution, the standard deviation, σ, is 0.17. Thus, if this distribution is centered at 20 steps (log(20) = 1.3), ≈ 67% of the molecules are expected to have τ_c values between 13.5 steps (log(13.5) = 1.13) and 29.5 steps (log(29.5)=1.47). 90% (1.64 σ) of the molecules will

have a relaxation time τ_c between 10.5 steps and 38.0 steps. Assuming that molecules undergoing dynamic exchange experience no bias in that exchange (i.e., a molecule in the fastest decile of molecules is as likely to become a molecule in the slowest decile as any other possible exchange), it is expected that even if all molecules exhibit exchange during the full time course of the experiment, only ≈ 10% of the molecules will experience changes of τ_c of a factor of 3 or more[27]. Considering the 95% confidence interval described above, these findings require discrimination of this 10% from the 5% of molecules that may experience this substantial a change even without any change in dynamics. Thus, our initial expectation is that this method will give a null result, neither proving nor excluding the possibility that temporal heterogeneity and dynamic exchange are present. To assess a data set for presence of temporal heterogeneity via the method described here would require a very large number of molecules such that the rare relatively large changes in dynamics possible would be seen in sufficient numbers to discriminate them from those that may occur from statistical variation alone. However, because this approach is similar to the approach used by Zondervan et al., and because it does allow probing exchanges on time scales significantly longer than does the window shifting technique, we describe results from this approach on dpPDI at 210K. The relatively high temperature ($1.11T_g$) is employed so that multiple movies separated by 10^5 – 10^6 τ_α can be collected within several hours, thus avoiding potential issues with mechanical stability.

Fig. 2.9b displays results from such experiments on dpPDI in glycerol at 210K. In the experiment represented by Fig. 2.9b, the first two movies are separated by ≈ 10^5 τ_α and the second and third movies are separated by ≈ 10^6 τ_α. While changes in extracted τ_c are clearly occurring, as evidenced by the many lines that cross each other in Fig. 2.9b, most of the measured τ_c values fall below the 95% CI denoted by the red line at 3.0. Indeed, comparing Figs.

2.9a and b reveals no qualitative differences despite the fact that Fig. 2.9a is based only on homogeneous dynamics. However, subtle differences are noted when evaluating the data shown in Fig. 2.9b as well as related experiments. Specifically, 6 of 64 molecules (9.4%) followed for 3 movies of 50 $<\tau_c>$ (Fig. 2.9b) and 6 of 62 molecules (9.7%) followed for 2 movies of $75<\tau_c>$ (not shown) fall outside the 95% CI as set by simulations of molecules undergoing homogeneous rotational diffusion. In both cases, ≈ 10% of the molecules appear to change their dynamics, double the proportion that would be expected given homogeneous rotational diffusion. As described above, for the breadth of spatial heterogeneity observed for dpPDI, this result is consistent with the presence of temporal heterogeneity and unbiased dynamic exchange. However, the total number of molecules investigated is relatively small (126 molecules). Thus, while this experiment may be evidence of probe molecules exhibiting dynamic exchange, observing a larger number of molecules would be necessary to confirm this finding.

Performing analysis on the molecules represented in Fig. 2.9b not on molecules that have LD trajectories well fit by ACFs in all three of the movies, but on molecules that have LD trajectories well fit by ACFs in either the first two movies (with a waiting time of $\approx 10^5\,\tau_\alpha$) or the second two movies (with a waiting time of $\approx 10^6\,\tau_\alpha$) allows assessment of whether there is more exchange occurring on the longest time scales probed (between 10^5 and $10^6\,\tau_\alpha$) than at all times shorter than $10^5\,\tau_\alpha$. If substantial exchange is occurring on these longest time scales, a higher proportion of molecules should fall outside the 95% CI as waiting time increases. It is found that 9 of 121 molecules and 11 of 123 molecules fall outside the 95% CI (2.7 for 2 movies of 50 $<\tau_c>$) for waiting times of $\approx 10^5\,\tau_\alpha$ and $10^6\,\tau_\alpha$, respectively. The very similar percentage of molecules outside the 95% CI for this comparison suggests no more exchange occurs between 10^5 and$10^6\,\tau_\alpha$ than for times shorter than $10^5\,\tau_\alpha$.

To supplement the analysis described above in a manner that both further investigates the sensitivity of this technique compared to that of the window shifting technique and assesses whether this method can reveal dynamic exchange over periods shorter than 10^5 - 10^6 τ_α, data trajectories from single movies collected at 210K for dpPDI in glycerol are also analyzed. Here, a subset of dpPDI data at 20K that contributes to the histogram in Fig. 2.5 is split into 4 trajectories of 50 $<\tau_c>$ each. Each molecule with at least 3 consecutive 50 $<\tau_c>$ trajectories leading to well fit LD ACFs is analyzed in the manner described above. This analysis thus investigates whether the long time heterogeneity assessment method detects temporal heterogeneity for waiting times of 50 $<\tau_c>$, or $\approx 5 \times 10^3$ τ_α. 431 molecules are analyzed, and it is found that 57 (13.0 %) of these molecules have their slowest rotational relaxation times outside the 95% CI obtained for molecules undergoing homogeneous rotational diffusion. A subset of these molecules, from a single movie collected at 210K, is shown in Fig. 2.9c. The fact that a very similar proportion of molecules is found above the 95% CI in this experiment and in the analysis of molecules experiencing longer waiting times between data collections (Fig. 2.9b) supports the conclusion that no more exchanges occur between 10^3 τ_α and 10^6 τ_α then occur at times shorter than 10^3 τ_α.

Comparing the result of the long time heterogeneity assessment on single trajectories at 210K to the ≈ 27% of dpPDI molecules found to be heterogeneous at this temperature using the window shifting technique demonstrates that the sensitivity to temporal heterogeneity of the window shifting technique is greater than that of the long time heterogeneity assessment. There are several reasons for this: first, the window shifting technique is a molecule specific approach rather than a population based approach; second, the lower bound set by window size (20 τ_c for the window shifting technique vs. 50 $<\tau_c>$ for the long time heterogeneity technique) means the

window shifting technique is sensitive to exchanges on shorter time scales. Even given the limited sensitivity of the long time heterogeneity assessment, the result obtained here is interesting, as it suggests that molecules that do not undergo detectable dynamic exchange during typical data collection and window shifting analysis are not being missed because the trajectories are not long enough. If this were the case, the long time heterogeneity assessment technique would be expected to reveal more heterogeneous molecules for long waiting times than for short waiting times, but this is not the case. Similarly, the results suggest that of the molecules experiencing exchange in the bounds investigated by the window shifting technique, the exchange time measured is not bounded by the upper limit of sensitivity of the time investigated (set by the trajectory length) but instead by the lower limit of sensitivity. As such, we conclude that the exchange times obtained with the window shifting analyses are upper bounds on actual exchange and persistence times.

While our conclusions on average relaxation time and breadth of relaxation times of tbPDI in glycerol near T_g are in close agreement with those of Zondervan et al., our conclusions on temporal heterogeneity differ even though the probes used and the experiments performed are very similar.[14] We can not exclude the possibility that the different conclusions are related to remaining differences between probes employed (tbPDI vs. dpPDI for the long time heterogeneity assessment) or experiments and analysis performed. Given the similarity between probes and experiments, however, we suggest that the different conclusions are due chiefly to the different sample preparation techniques employed, with the slow cooling performed by Zondervan et al. likely to allow for formation of a nearly static network within the sample for which we do not find evidence.[14,74,107] Instead, our results are consistent with the picture of supercooled glycerol as a mosaic of local and interchanging environments.

2.9 Summary

We presented single molecule data of three perylene dyes in glycerol, all three of which report the presence of spatially heterogeneous dynamics in supercooled glycerol despite the fact that these probes are large and slow compared to glycerol molecules. For all three probes, the temperature dependence of the median rotational relaxation times mirrors the temperature dependence of the glycerol viscosity according to the DSE equation. As expected, the obtained hydrodynamic volumes depend on the probe. Unexpectedly, hydrodynamic volume is found not to scale with the size or mass of the fluorophore but instead depends strongly on the polarity and hydrogen bonding ability of the fluorophore, with tbPDI being the largest, least polar, and most quickly rotating of the three dyes studied. The distribution of single molecule τ_c values for all three dyes is qualitatively similar, with none of the distributions displaying the long time tail observed previously for rubrene in glycerol.[15] However, the distribution of rotational relaxation times becomes wider as an inverse function of the extracted probe hydrodynamic volume. For dpPDI and dapPDI, which have similar hydrodynamic volumes, there is only a small difference in distribution width, while for tbPDI, with a significantly smaller hydrodynamic volume, the distribution is much wider. Taken together with results for rubrene in glycerol, this suggests that probe molecules that rotate more quickly report a greater breadth of spatially heterogeneous dynamics in supercooled glycerol than do those that rotate slowly. Given that probe rotational relaxation time distribution breadth appears closely linked to probe rotational correlation time but not to probe molecular size for the probes used in this study implies that temporal averaging by the probe is more important in setting the breadth of reported spatially heterogeneous dynamics than is spatial averaging. For this to be the case requires that at least some dynamic exchange occurs on time scales similar to those required for probe rotation. While distribution

width is found to vary with particular perylene probe, no evidence is found for significant changes in distribution shape or width for the PDI probes as a function of temperature. Similarly, the window shifting technique shows only small changes in the proportion of heterogeneous molecules as a function of temperature for a given probe compared to the difference in proportion of heterogeneous molecules found between tbPDI and the other two probes studied. Additionally, no significant changes in average exchange and persistence times relative to probe correlation time for a given probe as a function of temperature are noted. Long time heterogeneity assessment suggests, consistent with the window shifting analysis, that temporal heterogeneity exists in supercooled glycerol. The similarity in results obtained for such experiments that access exchanges on time scales of $\approx 10^3 - 10^4\ \tau_\alpha$ and $\approx 10^5 - 10^6\ \tau_\alpha$ is consistent with exchange primarily occurring on time scales $\leq 10^3 - 10^4\ \tau_\alpha$. We conclude that the window shifting analysis captures a subset of dynamic exchanges, and those that are not reflected in such analysis occur on faster time scales; thus, we conclude that reported values of exchange and persistence times are upper bounds on those quantities.

Chapter 3. Probe Dependent Studies in Supercooled Ortho-Terphenyl

This chapter is adapted from Reference 108.

3.1 Motivation for Probe Dependent Studies in Ortho-Terphenyl

This chapter continues description of SM probe dependent studies in supercooled glass formers. In Chapter 2, SM studies of the rotational dynamics of three perylene diimide probes in supercooled glycerol yielded intriguing results: The largest probe (tbPDI) unexpectedly displayed the shortest rotational correlation time. Due to the steric hindrance of the bulky side groups, we hypothesized this probe was unable to hydrogen bond with glycerol as strongly as the other probes. Additionally, the breadth of relaxation times was broadest for the fastest rotating

probe. We suspected this was the result of the probes doing less averaging on the dynamics of the host and more accurately reporting the dynamics heterogeneity of the system as a result. To evaluate whether these two hypotheses were true, we chose to perform probe dependent studies in a *non-polar* small molecule glass forming host, *ortho*-terphenyl (OTP). In OTP, we hypothesized probe-host interactions would be much more similar to one another and their rotational relaxation times would be governed by probe size. Furthermore, we expected that probes in OTP would show an increase in the breadth of rotational relaxation times reported with decreasing average probe rotational correlation time, consistent with fast probes doing less averaging and better reporting of dynamic heterogeneity.

In particular, in this study OTP is doped with 3 perylene diimide (PDI) probes, 2 of which were used in the previously mentioned glycerol study.[16] Individual probes' rotational correlation times are measured at temperatures in the range of 1.03-1.06 T_g. The distribution of rotational correlation times as a function of temperature and probe are reported. Individual correlation functions are also combined into a quasi-ensemble for comparison to results of ensemble measurements of supercooled OTP. Results in OTP are compared to previously collected data in glycerol to assess relative heterogeneity of these two glass formers.

3.2 Experimental

3.2.1 Detailed Sample Preparation

Ortho-terphenyl (OTP) (Fluka, spectrophotometric grade) is vacuum-distilled three times and then dissolved in toluene (Sigma Aldrich, spectrophotometric grade) to obtain a 5.0 mg/ml

solution. This solution is photobleached in a home-built bleaching apparatus for 48 hours.[109] Solid *N*,*N'*-bis(2,6-dimethylphenyl)-3,4,9,10-perylenedicarboximide (dpPDI) and *N*,*N'*-bis(2,5-tert-butylphenyl)-3,4,9,10-perylenedicarboximide (tbPDI) are obtained from Sigma Aldrich. Solid *N*,*N'*-bis(triethylglycol)-3,4,9,10-perylenedicarboximide (egPDI) is synthesized and generously provided by L. Campos and co-workers in the Department of Chemistry at Columbia University. dpPDI, tbPDI, and egPDI are provided as solids and are dissolved in toluene to form stock solutions that are ultimately diluted to 1.0 – 5.0 x 10^{-8}M for use in SM imaging. At these concentrations, fluorophores are dilute enough to avoid multiple SMs within a diffraction limited spot but concentrated enough to yield 50-200 analyzable SMs per movie.

Phenylsilane treated silicon wafers are sonicated in acetone for 10 minutes at least twice, rinsed in toluene, and briefly dried on a hot plate at 100°C. This process enhances wetting and film stability of OTP on the wafer. The PDI/OTP solutions are spin coated onto these silicon wafers at 200 rpm, until the toluene has evaporated and a lustrous film forms. After the film has formed, spinning continues for ~10 additional seconds. The spin-coating is performed at room temperature, ~50K above OTP's glass transition temperature (T_g = 243K). The OTP films produced are ~500 nm and rather flat across the sample as judged by interference fringes.

The sample is placed into a liquid nitrogen cooled microscopy cryostat, and vacuum grease is applied to the sample stage to optimize thermal contact between the sample wafer and cryostat stage. The cryostat stage temperature is initially set to 285 K to facilitate rapid cooling of the sample upon contact. Once the sample is placed into the cryostat, the stage temperature is lowered to the desired temperature (250 – 258K, 1.03 – 1.06T_g) at a rate of ~ 5 K min^{-1}. Upon beginning sample cooling, the cryostat is evacuated to ~30 mtorr and flushed with dry nitrogen 5 times. The cryostat is then evacuated to 0.4 mtorr for at least 1 hour to ensure all toluene has

been removed from the sample. The temperature control system is outlined in detail in Ref. 15.

3.2.2 Optical Setup

Data is acquired using a home built microscope in an epi-fluorescence configuration (Fig. 3.1). This configuration is similar to the one described in Chapter 2.[15] One change has been made to the previously described experimental set-up to allow for a more homogeneously illuminated field of view: approximately 150 mW of excitation light (from an Nd:Vanadate 532 nm diode laser) is directed into an objective lens and coupled into a multimode fiber (Newport, F-MCB-T-3FC) that is shaken by a piezoelectric buzzer at 500-4700 Hz (MCM Electronics; PEB in Fig. 3.1) to eliminate the speckle pattern produced by multimode fibers. The unpolarized light is directed out of the fiber via a collimator and is passed through polarization optics and a telescope before being reflected toward the objective lens.

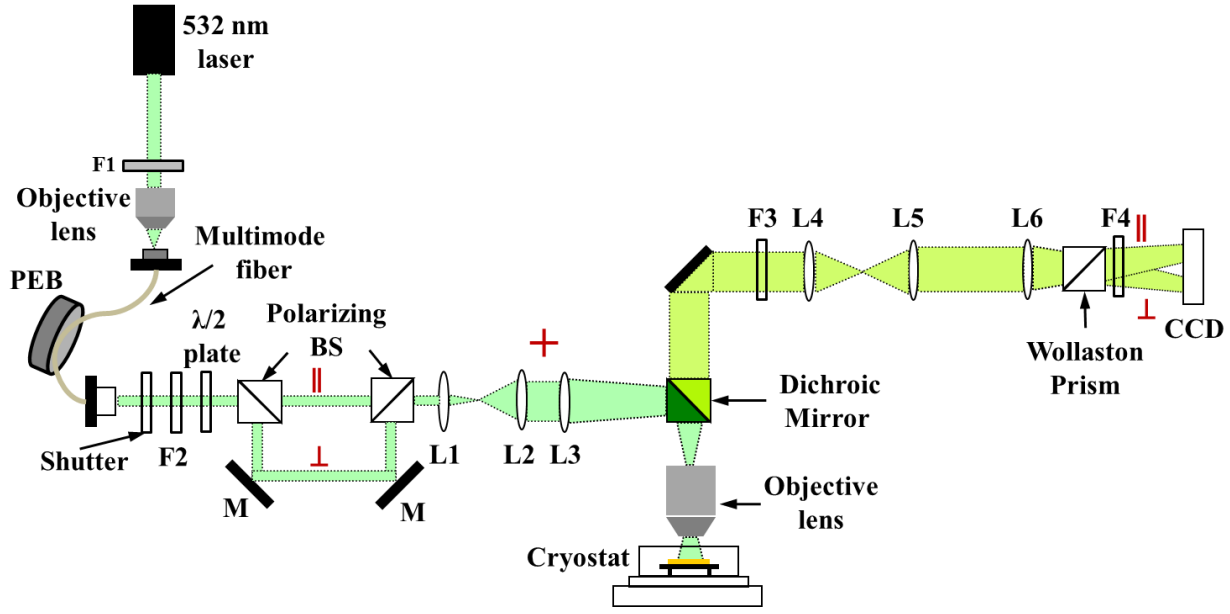

Figure 3.1. Schematic diagram (not to scale) of the epi-fluorescence microscope. BS = beam splitter, F = filter, M = mirror, PEB = piezoelectric buzzer, L = lens.

The fluorescence from SMs in the illuminated area is collected by a long working-distance, high numerical aperture objective (Zeiss, LD Plan-Neofluar, air 63x, NA = 0.75, WD = 1.5 mm), passed through detection optics including a Wollaston prism that splits the signal into two orthogonal polarizations and onto an electron multiplying charge-coupled device camera (Andor iXon DV887; EMCCD in Fig. 3.1). Data are collected at temperatures from 250 – 258K. The optimal frame rate of each movie is determined based on preliminary experiments, and ≈ 20 frames per median rotational relaxation time, $\tau_{c,med}$, are collected at each temperature for each probe. Trial movies are also collected at both faster and slower frame rates to search for molecules whose rotations can not be quantified with the chosen frame rate – in this paper movies collected at additional frame rates are not found necessary, and all molecules described are from movies collected at the typical frame rate. Measurements are taken for several thousand frames, until > 95% of the SMs have photobleached. For measurements taken at 20 Hz, 10 Hz, and 5 Hz, the sample is continuously illuminated, and the exposure time is the inverse of the frame rate. At lower temperatures, measurements are taken at 2 Hz, 1 Hz, 0.5 Hz, and 0.25 Hz with a fixed exposure time of 0.2 s. The laser is shuttered with a mechanical shutter for the remainder of the frame time to limit photobleaching. The laser power used to collect data ranges from 0.75 – 30 mW, as measured before the objective lens. The highest powers are required at the highest frame rates. Signal to noise ratio (SNR) for all movies is at least 2. To allow for correction of heating due to absorption of laser light, movies are collected at several powers at a given temperature for a given sample. Median probe rotational correlation time as a function of set temperature and laser power is used to extrapolate an actual temperature for each sample, as described in Reference 16.

In all, 156 movies were collected and analyzed, 53 for dpPDI, 36 for egPDI, and 60 for

tbPDI. The number of data sets collected at each temperature for each dye can be ascertained from Fig. 3.2 where each data point represents the median rotational relaxation of probe molecules in a single movie. The number of molecules analyzed for each PDI dye at each temperature is given in Table 1. Data was collected over a 4 day period on two different samples for each PDI dye in OTP. During data collection, temperature was varied at random over the full range of measured temperatures.

	tbPDI		dpPDI		egPDI	
T/K	Molecules	FWHM	Molecules	FWHM	Molecules	FWHM
250	. . .	. . .	444	0.71	. . .	. . .
251	402	0.60	524	0.66	327	0.65
252	582	0.61	534	0.57	458	0.70
253	655	0.48	567	0.63	316	0.62
254	613	0.64	1117	0.61	462	0.73
255	509	0.61	619	0.62	468	0.71
256	969	0.51	822	0.59	477	0.70
257	599	0.35	. . .	. . .	493	0.73
258	513	0.60	. . .	. . .	. . .	. . .
Average		0.55		0.63		0.69
Summed	4842	0.54	4627	0.61	3001	0.69

Table 1. Number of molecules and FWHM values of best-fit Gaussian distributions of log(τ_c) values for all SM data shown in Fig. 3.3, left panel. Average FWHM over all temperatures as a function of probe as well as the FWHM value for the combined histograms shown in the right panel of Fig. 3.3 are also given.

In the Discussion, SM data collected in OTP is compared to data collected in glycerol that was reported and described in Ref. 16. Sample preparation and data analysis is described in that publication and is very similar to that outlined here. In that study, tbPDI and dpPDI were employed. The third probe used in that study was *N*,*N'*-bis[3-dimethylamino)propyl]-3,4,9,10-perylenedicarboximide (dapPDI).

3.3.3 Data Analysis

Data analysis is performed using IDL software (ITT Visual Information Solutions), as described in detail in Chapter 2. Due to potential heating from laser absorption, an iterative heating correction outlined Appendix A is applied to determine a true temperature and potentially

adjust all τ_c values to the set temperature. Unless otherwise stated, all τ_c values presented and described are heat-corrected. For evaluation of SM stretching exponents, all SMs (regardless of whether τ_c is determined from a stretched exponential or a linear fit) are fit to a stretched exponential function, and β is recorded.

3.2.4 Simulation Studies of Homogeneous Rotational Diffusion

For comparison to experimental results, simulations of 3D rotational diffusion of a unit vector representing the transition dipole of a fluorophore are performed as described in Chapter 2. Simulations are constructed with median τ_c of 20 steps and are varied in length to match the average length for a given probe molecule in OTP (Table 3.2). For all simulations, as for experiments, LD ACFs are constructed from the LD and are fit as outlined in Section 2.4 to yield a τ_c. Trajectories treated with linear fits are also fit with stretched exponentials to yield a β value, as is also done with experimental trajectories.

Dye	V_h	Lifetime/τ_c	FWHM	$FWHM_{sim}$	β_{med}	$\beta_{med,sim}$	β_{QE}	$\beta_{QE,sim}$
tbPDI	1.87	46	0.55	0.35	1.08	1.08	1.01	1.03
dpPDI	1.17	38	0.63	0.39	1.04	1.11	0.96	1.02
egPDI	0.80	96	0.69	0.34	0.94	1.03	0.78	1.04

Table 2. Various quantities for experiments and simulations for the three employed probes in OTP. Lifetime/τ_c is determined for each movie as the average time each SM is "on" (typically the time until photobleaching) divided by the average τ_c value for that movie. These quantities are then averaged. FWHM, β_{med}, and β_{QE} are experimental quantities as described in the text and shown in Figs. 3.3 and 3.4. $FWHM_{sim}$, $\beta_{med,sim}$, and $\beta_{QE,sim}$ are quantities obtained from simulation as described in the text and shown in Figs. 3.3 and 3.4.

3.3 Results

3.3.1 Median Rotational Relaxation Times

We first investigate the temperature dependence of measured SM probe dynamics, on average, in OTP. In particular, we investigate whether median rotational correlation times of the probe molecules track the temperature dependence of the host viscosity as described *via* the Debye–Stokes–Einstein (DSE) equation,

$$\tau_c = \frac{V_h \eta(T)}{k_B T}, \qquad (3.1)$$

where τ_c is the rotational relaxation time of the probe, V_h is the hydrodynamic volume of the probe, $\eta(T)$ is the temperature dependent viscosity of the host, k_b is the Boltzmann constant, and T is temperature of the host. Previous SM measurements have found that the DSE equation does describe probe rotational dynamics in small molecule supercooled liquids.[13,14,16] We use the DSE equation not only to help establish that probe dynamics reflect host dynamics but also to extract an effective hydrodynamic volume, V_h, for each probe.

Using the heating correction algorithm based on the measurements taken at different powers, a single median τ_c, $\tau_{c,med}$, is obtained from each movie for a given probe. These $\tau_{c,med}$ values are fit to the DSE equation using the known temperature dependence of OTP viscosity (Fig. 3.2).[110] In Figure 3.2, each point represents the $\tau_{c,med}$ value for a single movie containing 50-150 molecules. Each line corresponds to the DSE line of best fit for each probe's $\tau_{c,med}$ values with respect to temperature. The extracted hydrodynamic volumes for tbPDI, dpPDI, and egPDI in OTP are V_h =1.87 nm^3, V_h =1.17 nm^3, V_h =0.80 nm^3, respectively. This reflects the fact that of the three probes at a given temperature in OTP, tbPDI rotates the slowest and egPDI rotates the

fastest.

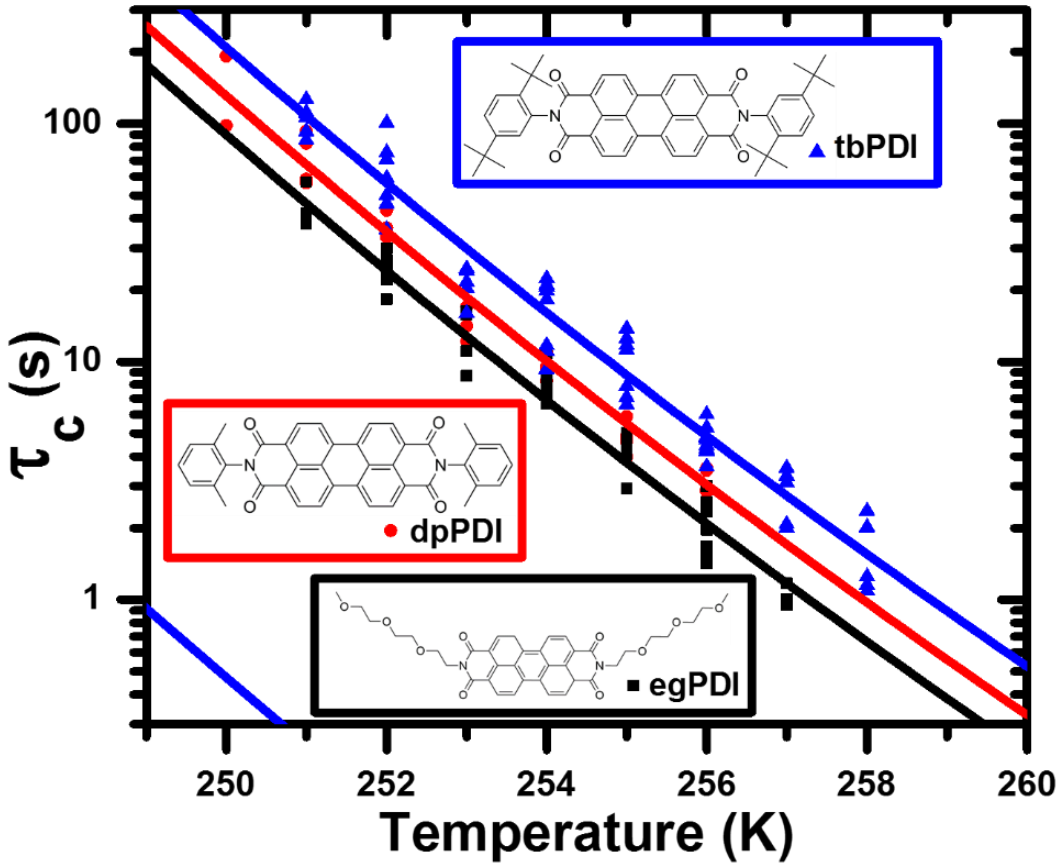

Figure 3.2 Rotational relaxation times vs. temperature for tbPDI (blue triangles), dpPDI (red circles), and egPDI (black squares) together with each dye's molecular structure outlined in the same color. Each point represents the heat corrected $\tau_{c,med}$ value for a single movie. Lines represent the best-fit DSE fit for each PDI dye. Extracted hydrodynamic radii are V_h = 1.87 nm^3 (tbPDI), V_h = 1.17 nm^3 (dpPDI), and V_h = 0.80 nm^3 (egPDI). The structural relaxation of OTP as measured by dielectric spectroscopy[30] is plot as a function of temperature (green line).

3.3.2 Degree of Spatially Heterogeneous Dynamics

Breadth of Relaxation Times

After evaluating the average dynamics of the three PDI dyes in OTP, we assess information attained from individual SM linear dichroism auto-correlation functions for all PDI dyes at each temperature probed. First, heat corrected τ_c values obtained from every individual SM are plot in histograms at each temperature ranging from 250 – 258K for each PDI dye (Fig. 3.3, left panel). There is a substantial spread in relaxation times for all probes at all temperatures investigated, with each histogram spanning over a decade.

Like in Chapter 2, distribution of rotational correlation times is plot on a log scale and fit with a Gaussian and Lorentzian curve. In both cases, fits allowing all variables to float and fits fixing the height to 1 and offset to 0 are performed. As judged by R^2 values, Gaussian fits with floating variables provide the best fits and these are shown in Fig. 3.3. FWHM values are reported in Table 1. For all four types of fits, the FWHM values extracted show the same trend, with the egPDI τ_c distribution having the largest FWHM and tbPDI the smallest.

Regardless of particular fitting procedure, no obvious trend is found for width of the distribution as a function of temperature for any of the probes. As such, in addition to plotting τ_c distributions for each probe at each temperature (Fig. 3.3, left panel), a normalized τ_c distribution for all temperatures is constructed (Fig. 3.3, right panel). These histograms are also fit to Gaussians and Lorentzians with and without constraints as described above. Again, Gaussian fits provide better fits than Lorentzians (for variable amplitude fits, $R^2 \geq 0.98$ for Gaussians vs. $R^2 \geq 0.95$ for Lorentzians). The FWHM values extracted from the combined-temperature distributions are very similar to the average FWHM values for a particular probe's distribution across temperatures (Table 1). Moreover, the trend showing $FWHM_{egPDI} > FWHM_{dpPDI} > FWHM_{tbPDI}$

for τ_c distributions at individual temperatures also holds for this combined data.

For all probes, at all temperatures, the observed τ_c distributions are broader than would be expected for a normal liquid, even given the experimental constraint of short trajectories. Simulations of 1000 trajectories of homogeneous rotational diffusion, all with the same τ_c, were performed with trajectory length set to average trajectory length for each of the probe molecules in OTP: $46\tau_c$, $38\tau_c$, and $98\tau_c$ for tbPDI, dpPDI, and egPDI, respectively (Table 3.2). In all cases, the simulations yield distributions (red lines, Fig. 3.3, right panel and Table 3.2) narrower than those measured experimentally, though broadened relative to the delta functions that would be expected for infinitely long trajectories. Performing simulations such that the trajectory length distribution (rather than simply the average trajectory length) matches that of experimental results yields very similar distributions, with a FWHM a maximum of 3% larger than that obtained using average trajectory length. We note that egPDI is the broadest of the three experimental distributions but would be expected to have the narrowest distribution in the absence of spatially heterogeneous dynamics since it has the longest trajectories. The experimentally recorded spread of τ_c values confirms that spatially heterogeneous dynamics exists in supercooled OTP and that all probes used in this study report on these heterogeneous dynamics.

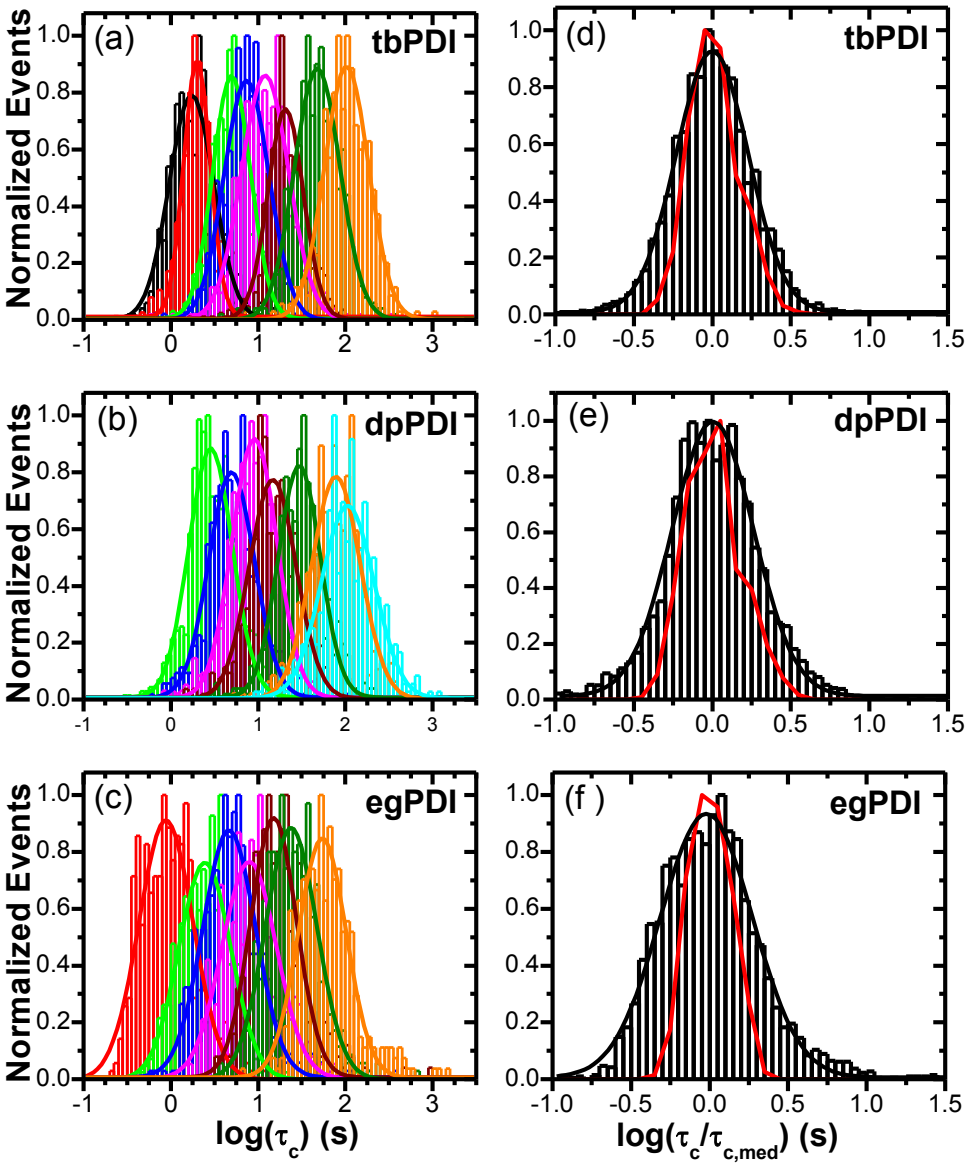

Figure 3.3 (left) Distribution of SM τ_c values for (a) tbPDI, (b) dpPDI, and (c) egPDI in OTP at 258K (black), 257K (red), 256K (green), 255K (blue), 254K (magenta), 253K (wine), 252K (olive), 251K (orange), and 250K (cyan). All histograms are normalized to the maximum number of occurrences. Each histogram is taken from two data sets for each dye, with the histograms across data sets normalized to the median τ_c value at one of the data sets for that particular PDI dye. This alleviates any potential widening of the distribution arising from differing thermal contact of the sample and stage between data sets. (right) SM data from all temperatures normalized to $\tau_{c,med}$ = 10s and combined to form a single histogram for (d) tbPDI, (e) dpPDI, and (f) egPDI. Each histogram is fit with a Gaussian function (black line). Histogram of τ_c distribution of simulations of homogeneous rotational diffusion with trajectory

length for each simulation tuned to match experimental trajectory length as described in the text is shown by the red lines.

Evaluation of Stretching Exponent

In bulk experiments, which can not access distributions of individual relaxation times as described above for SM probes, exponents derived from stretched exponential fits of ensemble ACFs of a variety of observables have been used to assess degree of spatially heterogeneous dynamics in supercooled liquids. In SM experiments, stretching exponents can also be assessed, both from individual SM ACFs as well from quasi-ensemble ACFs constructed from SM ACFs.

Time-limited trajectories may display ACFs with best-fit stretching exponents differing from 1.0 even for systems displaying homogeneous rotational dynamics, with strong effects still seen for trajectories 100 times longer than the characteristic rotational correlation time[19,20], longer than the typical trajectories recorded here. For this reason, attributing the small stretching exponent of a given SM ACF to that SM probe experiencing different dynamic environments over the course of the experiment is not advisable.[12] Distributions of β values across SM ACFs are also affected by short trajectories but may yield some information about degree of heterogeneity in a supercooled liquid. Figure 3.4 shows the distributions of β values for all individual SM traces, each of which was fit to a stretched exponential decay, for each of the three probes. β is allowed to float from 0.3 – 2.0 when each ACF is fit with a stretched exponential. Tails at 0.3 and 2.0 are removed from the figures and not included in the calculation of β_{med}. The difference in β_{med} with and without tails included is less than 1%. Fits were also performed allowing β to float from 0 – 2.0 when fitting ACFs of egPDI in OTP, and this results in < 2% difference in the β_{med} value. As with the τ_c value distributions, the distributions of and median β values do not show any clear trend with temperature (data not shown); therefore, these

distributions are constructed using data for all temperatures. A median stretching exponent, β_{med}, is determined from these distributions: the β_{med} values are 1.08, 1.04, and 0.94 for tbPDI, dpPDI, and egPDI, respectively. We estimate the error on these values as $< \pm 0.01$ as follows: least squares fitting of individual LD ACFs yields scaled uncertainties for β of approximately ± 0.2; propagating error through calculation of the average for a given movie yields β_{med} error of $\pm$ 0.02 – 0.04 and then is reduced further by averaging over all movies. The β_{med} values are shown as solid black lines in Fig. 3.4 and are reported in Table 3.2.

Fig. 3.4a-c also shows distributions of β values for the simulations of homogeneous rotational diffusion described above, with trajectory length set to average trajectory length for each of the probes. In all cases, the simulation data is treated as the experimental data and yields distributions that are somewhat different than the experimental distributions, with the simulated distributions somewhat narrower than the experimental ones. Unlike for the τ_c distributions, where the experimental FWHM values are distinct from those yielded by simulation, the overall experimental and simulated distributions of β values and the β_{med} values are quite similar, particularly for tbPDI and dpPDI. These results suggest that the time-limited nature of typical trajectories affects individual SM ACF β values such that neither a particular β value nor the full distribution of an ensemble of SM β values can necessarily discriminate between a homogeneous and heterogeneous population.

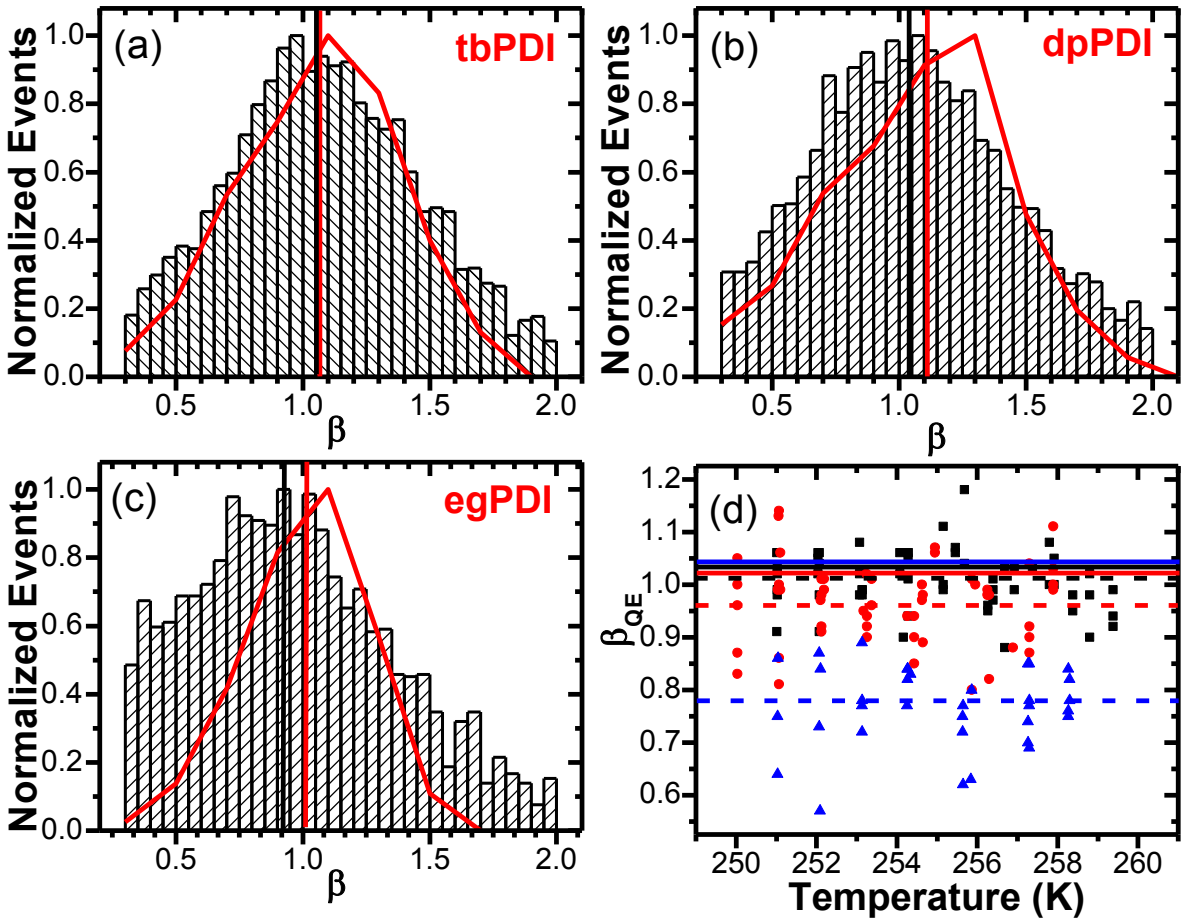

Figure 3.4 Distributions of β values from individual SM ACF fits for (a) tbPDI, (b) dpPDI, and (c) egPDI. The solid black lines indicate the median value, β_{med}, of these distributions. The red curve represents distributions from simulations of homogeneous rotational diffusion with trajectory length set to match average experimental trajectory length. For all experimental and simulated data, β is allowed to float from 0.3 – 2.0 when each ACF is fit with a stretched exponential as described in the text. (d) β_{QE} values for each probe for each movie collected as a function of true temperature for tbPDI (black squares), dpPDI (red circles), and egPDI (blue triangles). The dashed lines of corresponding color represent the mean β_{QE} value for each probe for all temperatures studied. The solid lines of corresponding color represent the β_{QE} values from the corresponding simulations.

Another method that allows evaluation of SM data for indications of host temporal heterogeneity as well as comparison to bulk experiments requires construction of a quasi-ensemble ACF (ACF_{QE}). As described in Reference 16, for each movie all individual SM ACFs are summed to produce a single ACF_{QE}, which is fit with a stretched exponential function. Each ACF_{QE} yields a τ_{QE} and a β_{QE} value. The τ_{QE} values can be used in much the same way the $\tau_{c,med}$ values are used to extract a V_h for each probe. Doing so leads to the following V_h values: 1.82, 1.15, and 0.87 nm^3 for tbPDI, dpPDI, and egPDI, respectively – a maximum of 11% difference from the results obtained with the approach represented by Fig. 3.2. This similarity validates the use of the ACF_{QE}s for data analysis. The quasi-ensemble stretching exponents, β_{QE}, are shown for each probe as a function of true temperature in Fig. 3.4d. While τ_c values can be heat-corrected using the DSE curve as a guide, ACFs can not be straightforwardly heat-corrected. Because multiple movies collected at the same set temperature may have different degrees of heating, data across movies can not be combined in constructing ACF_{QE}s, and therefore these ACF_{QE}s are constructed from SMs in a single movie. The obtained β_{QE} values, again, show no clear trend with temperature, while a trend as a function of probe is apparent. The mean β_{QE} values obtained for tbPDI, dpPDI and egPDI are 1.01, 0.96, and 0.78 respectively (Table 3.2). The scaled uncertainly for the β_{QE} value for each movie is ± 0.02 – 0.04; thus, the error bars are around the size of the data points in Fig. 3.4d. The median β_{QE} error is lower by approximately an order of magnitude; however, as discussed below, scatter between points representing different movies exists in part due to differences in average trajectory length of the movies. Average β_{QE} values for each probe are lower than the β_{med} values in all cases. This result stands in contrast to results for simulations, where β_{QE} values obtained from the same simulations used

to construct the τ_c and distributions of β values shown in Figs. 3.3 and 3.4 are very similar to the β_{med} values and very close to 1.0 (Figure 3.4d and Table 3.2).

3.4 Discussion

3.4.1 Rotational Relaxation Rates

In a previous study, three PDI probes, including dpPDI and tbPDI, were used to assess spatially heterogeneous dynamics in glycerol. The extracted hydrodynamic volumes were found to be counter to what was initially expected: although tbPDI has the largest molecular weight and space filling volume of the three probes used, it demonstrated the fastest rotational relaxation and in turn had the smallest extracted V_h. Indeed, dpPDI's V_h was found to be more than 5 times larger than that of tbPDI even though tbPDI has a van der Waals volume that is nearly 25% larger than does dpPDI (Table 3.3). We speculated that steric hindrance from the *tert*-butyl groups on tbPDI precludes the hydrogen-bonding interactions that could occur between glycerol and other PDI probes. We predicted that in OTP these two probes would show the opposite behavior, with tbPDI being slower than dpPDI and therefore yielding a larger extracted V_h. As shown in Fig. 3.2 and Table 3, this is indeed the finding in OTP, where the extracted hydrodynamic volumes for tbPDI, dpPDI, and egPDI are 1.87, 1.17, and 0.80 nm^3, respectively. These extracted hydrodynamic volumes reflect the fact that $\tau_{c,med,tbPDI} > \tau_{c,med,dpPDI} > \tau_{c,med,egPDI}$ at all measured temperatures.

Probe	MW (g/mol)	V_V (nm^3)	$V_{h\ (OTP)}$:V_V	$V_{h\ (Glycerol)}$ (nm^3)	$V_{h\ (Glycerol)}$:V_V	τ_c:$\tau_{\alpha,OTP}$	τ_c:$\tau_{\alpha,glycerol}$
tbPDI	766.38	0.67	2.77	0.36	0.53	297	14
dpPDI	598.65	0.46	2.56	2.02	4.42	193	66
egPDI	684.73	0.54	1.48	. . .	. . .	168	. . .
dapPDI	560.64	0.45	. . .	1.27	2.82	. . .	42

Table 3. Molecular weight (MW), extracted hydrodynamic volumes (V_h), van der Waals volume (V_v), V_h/V_v ratios, and τ_c/τ_α values as described in the text for the three probes investigated in OTP and in glycerol.[16]

While the findings for the relative rotational relaxation rates and hydrodynamic volumes of tbPDI and dpPDI in OTP are in accord with these probes' molecular weights, we note that egPDI has the shortest rotational relaxation time and smallest extracted hydrodynamic volume of the three probes even though its molecular weight is greater than that of dpPDI. To explain this finding, we consider additional measures of probe size and shape. The van der Waals volumes (V_v) of tbPDI, dpPDI, and egPDI are 0.67, 0.46, and 0.54 nm^3, respectively, as computed with ChemBio3D via a Connolly excluded volume calculation. The extracted hydrodynamic volumes of the three probes are larger than the calculated van der Waals volumes in all cases (Table 3.3). The ratio of V_h to V_v for egPDI is the closest to unity, with $V_{h(egPDI,OTP)}$:$V_{v(egPDI)}$ = 1.48 while $V_{h(tbPDI,OTP)}$:$V_{v(tbPDI)}$ = 2.77 and $V_{h(dpPDI,OTP)}$:$V_{v(dpPDI)}$ = 2.54. The fact that egPDI rotates more quickly than the smaller, less massive dpPDI suggests that its rotations may be governed by its core, with the extended hydrocarbon chains providing little hindrance to molecular rotation whereas the bulky phenyl groups of tbPDI and dpPDI may cause more hydrodynamic drag in OTP, slowing their rotational dynamics. The van der Waals volume of the core of the PDI probes is 0.26 nm^3, which would yield $V_{h(egPDI,OTP)}$:$V_{v(egPDI,core)}$ = 3.08, quite similar to that for the other two probes. Additional differences between V_h and V_v for all probes likely emerge because of the assumption of a spherical probe in the DSE equation.

V_h may additionally differ from V_v due to the degree of intermolecular forces between the probe and host. Although $V_{h(dpPDI,OTP)}$:$V_{v(dpPDI)}$ is not unity, it is much smaller than that ratio for dpPDI in glycerol, $V_{h(dpPDI,glycerol)}$:$V_{v(dpPDI)}$ = 4.39 (Table 3.3). This is consistent with the idea proposed (but not endorsed) by Zondervan et al. that strong intermolecular interactions such as hydrogen bonding between PDIs and glycerol can lead to a temporary glycerol shell around the probe, resulting in an effective probe with a larger size and slower rotations than the bare probe.[14] dpPDI's presumed hydrogen-bonding interactions with glycerol slow its rotations in glycerol by a much greater degree than dpPDI's interactions with OTP. If tbPDI can not hydrogen-bond with glycerol, as proposed, it would lack the glycerol shell and have a smaller V_h:V_v in glycerol, as was found (Table 3.3).[14,16] We note that the discrepancy between the V_h:V_v ratios for tbPDI in glycerol and OTP is not fully understood, as tbPDI in glycerol appears to relax more quickly than would be expected in glycerol even for the bare probe.

3.4.2 Breadth of Relaxation Times

One of the key observations emerging from the previous SM study in glycerol was that as probe median rotational correlation time in glycerol decreased, the breadth of reported rotational relaxation times increased.[16] This suggested that as the rate of rotational relaxation of the probe approaches that of the host, the probe can sample and report a greater proportion of the true heterogeneous dynamics of the host. In other words, faster probes do less temporal averaging over these dynamically heterogeneous systems, which leads to an increase in the breadth of distribution of τ_c values. In the study in glycerol, as described above, the fastest probe happened to be that with the highest molecular weight and space filling volume. This implied that within the set of probes used, the differences in rotational relaxation rate, not space filling volume, were

most important in setting the breadth of heterogeneous dynamics reported. These results further suggest that at least a subset of dynamic exchanges occur on time scales similar to that of probe rotation.

The same trend found in glycerol is found in OTP, with FWHM of τ_c distributions increasing monotonically with decreasing probe $\tau_{c,med}$ even when this relaxation time does not track with probe molecular weight or van der Waals volume. Of the three dyes studied in OTP, egPDI, the fastest rotating probe, has the largest FWHM of τ_c values across all temperatures studied (Table 1 and Fig. 3.3). To highlight this point, Fig. 3.5a shows the histograms also shown in the right panel of Fig. 3.3 overlaid for all three probes in OTP together with best-fit Gaussians to the log(τ_c) histograms. In this case, the Gaussian fits are performed with fixed amplitude and zero offset. FWHM increases as τ_c decreases, with egPDI demonstrating the widest distribution of τ_c values as well as the shortest average rotational correlation time. The fastest rotating probe is also that which exhibits dynamics on a time scale most similar to the structural relaxation of the host: for the three PDI probes in OTP, this ratio ranges from $\tau_c/\tau_\alpha = 168$ for egPDI to $\tau_c/\tau_\alpha = 297$ for tbPDI (Table 3). Determination of τ_c/τ_α values is described in the Appendix A. As in glycerol, the fact that the faster probe reports the greatest breadth of heterogeneity supports the idea that at least a proportion of the dynamic exchange occurs on time scales similar to those associated with probe rotation.

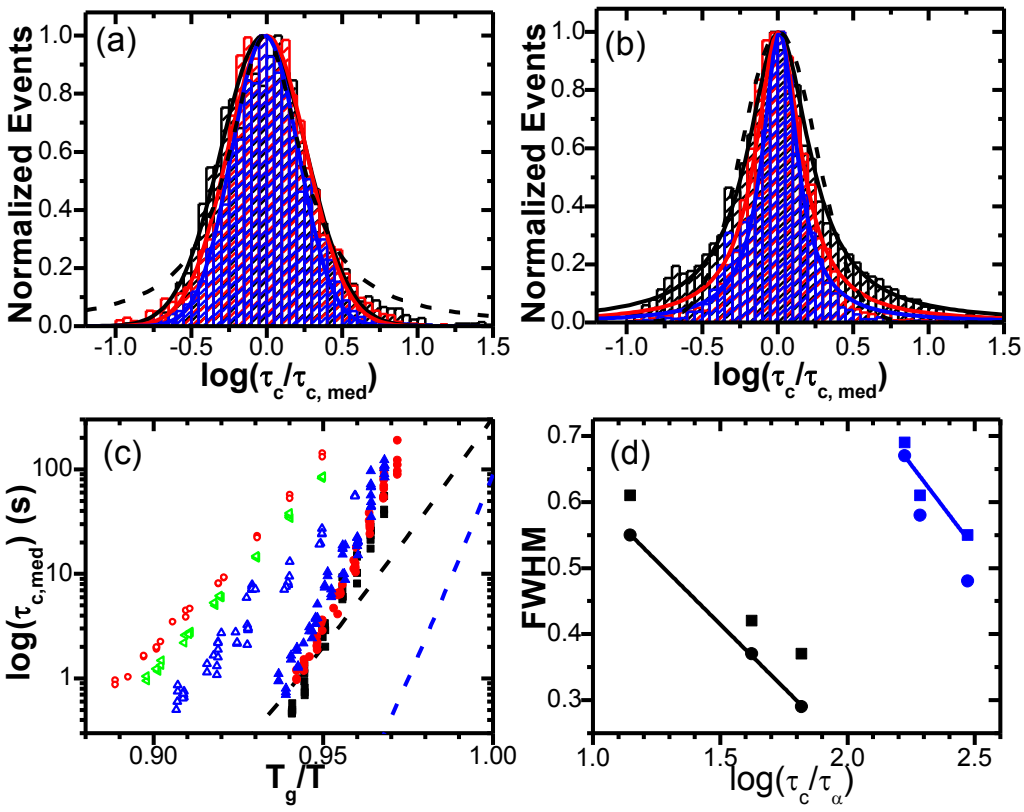

Figure 3.5 SM data from all temperatures normalized and combined to form a single histogram for (a) each PDI in OTP: tbPDI (blue), dpPDI (red), and egPDI (black) and (b) each PDI in glycerol: dpPDI (red), dapPDI (green), and tbPDI (blue). All histograms are normalized to their maximum number of occurrences. Each PDI in OTP histogram is fit with a fixed height Gaussian and each PDI in glycerol histogram is fit with a fixed-height Lorentzian (lines of solid colors corresponding to histogram colors). The histogram for egPDI in OTP is additionally fit with a fixed-height Lorentzian (black dashed line in a) and tbPDI in glycerol is fit with a fixed-height Gaussian (blue dashed line in b). (c) $\tau_{c,med}$ from each movie plot with respect to T_g/T for egPDI (black squares), dpPDI (red circles), and tbPDI (blue triangles) in OTP and tbPDI (open blue triangles), dapPDI (open green sideways triangle), and dpPDI (open red circles) in glycerol. Structural relaxation data for OTP (dashed blue line)[111] and glycerol (dashed black line)[112] are plot with respect to T_g/T. (d) FWHM from Gaussian (squares) and Lorentzian (circles) fits to each of the OTP (blue) and glycerol (black) histograms pictured in (a) and (b) plot as a function $\log(\tau_c/\tau_\alpha)$. FWHM from Gaussian fits of OTP (blue squares) and from Lorentzian fits of glycerol (black circles) τ_c distributions vs. $\log(\tau_c/\tau_\alpha)$ are fit to lines. y-intercepts correspond to FWHM for τ_c/τ_α =1.

We may also consider the breadth of heterogeneity reported by these probes in OTP compared to in glycerol. Taking the same data shown in Fig. 3.2 as well as that for 3 PDI probes in glycerol and plotting it as a function of T/T_g – as in an Angell plot – reinforces that in both cases probes follow the dynamics of the host, here as captured by structural relaxation data measured for OTP and glycerol (Fig. 3.5c).[111,112] From this plot, it is also apparent that OTP dynamics (and probe reports of said dynamics) change more quickly with temperature than do those of glycerol over the same temperature range relative to T_g. This highlights the fact that OTP is more fragile than glycerol, with fragility a measure of the degree of non-Arrhenius change in viscosity with temperature upon approach to T_g.[3,29] It has been proposed that more fragile systems may display a greater degree of heterogeneous dynamics than less fragile ones,[2,29] and we investigate whether our results provide evidence for different degrees of heterogeneous dynamics in OTP and glycerol.

Fig. 3.5a and b show the combined histograms across temperatures for three probes in OTP and glycerol, respectively. In both cases, best-fit amplitude-fixed and zero-offset Gaussian and Lorentzian fits are performed. While all fits are relatively good, the Gaussian fits better describe the summed OTP histograms ($R^2 = 0.98$ for all probes for Gaussian fits vs. 0.92-0.95 for Lorentzian fits) while the Lorentzian fits better describe the summed glycerol τ_c histograms ($R^2 = 0.91$- 0.99 for all probes for Gaussian fits vs. 0.97-0.99 for Lorentzian fits). Considering either Gaussian or Lorentzian fits, the τ_c histograms measured in OTP are broader than those measured in glycerol (Fig. 3.5d). While probes in OTP tend to display shorter trajectories in terms of probe τ_c than in glycerol, egPDI in OTP and dapPDI in glycerol have nearly identical average trajectory lengths of 98 and $102\tau_c$, respectively. Thus, simulation of homogeneous rotational

diffusion in both cases yields FWHM values of $\log(\tau_c)$ distributions of 0.34. The experimental FWHM values, on the other hand are 0.69 for egPDI in OTP and 0.42 for dapPDI in glycerol, with the corresponding τ_c/τ_α values being 168 and 42, respectively (Table 3.3). The fact that a broader τ_c distribution is found in OTP even though this probe is performing a greater degree of temporal averaging than the corresponding probe in glycerol suggests that OTP is more heterogeneous than glycerol. We note that it was initially expected that τ_c/τ_α values for PDIs in OTP would be closer to unity and indeed smaller than those in glycerol. This assumption was based on the fact that OTP molecules are larger than glycerol molecules, and PDI probes are closer in molecular weight and van der Waals volume to OTP than to glycerol molecules. That this is clearly not the case is suggestive of the fact that glycerol, with its hydrogen bonding network, may have a larger effective relaxing unit (perhaps related to cooperatively rearranging sets of molecules) than does OTP.

Figure 3.5d displays the FWHM values of the τ_c distributions of all probes in both glycerol and OTP as a function of $\log(\tau_c/\tau_\alpha)$. In both supercooled liquids the FWHM values of the probe distributions increase with decreasing $\log(\tau_c/\tau_\alpha)$. Extrapolating linear fits of this data to $\tau_c/\tau_\alpha = 1$ (i.e. where probe rotational correlation time is equal to the host structural relaxation time) implies a situation in which no temporal averaging by the probe would be expected. For glycerol, in this limit, the extrapolated FWHM is 0.99 while that of OTP is 1.80. We suggest this is additional evidence that OTP exhibits a greater degree of spatially heterogeneous dynamics than glycerol. We note, however, that other possibilities also exist. First, it has been suggested that OTP has larger regions of distinct dynamics than glycerol.[77,113] The employed probes, with radii along the transition dipole of ≈ 0.2 nm, are more likely to span regions of distinct dynamics in glycerol than in OTP. This could lead to more spatial averaging by the employed PDI probes

in glycerol than in OTP, which could contribute to differences in the widths of the histograms in the two supercooled liquids. Another possibility is that dynamic exchange occurs on quite different time scales in OTP and glycerol. Indeed, while several experiments suggest that dynamic exchange happens on time scales similar to structural relaxation in glycerol and OTP [26,27,80,114] at least one experiment suggests very long-lived heterogeneity in glycerol.[14] If glycerol and OTP have dissimilar characteristic time scales of dynamic exchange (τ_{ex}) relative to the structural relaxation time, the τ_c/τ_{ex} ratio would be decoupled from τ_c/τ_α ratio and extrapolation to $\tau_c/\tau_\alpha = 1$ may not equally correct for temporal averaging in OTP and glycerol.

3.4.3 Evaluation of Stretching Exponent

Just as distributions of probe τ_c values reveal information about host heterogeneous dynamics, so too may distributions of stretching exponents. As described in Section 3.3.2, the β_{med} values in OTP are close to 1.0, as are those attained from simulations of purely homogeneous dynamics (Fig. 3.4a-c and Table 3.2), likely due in part to the time-limited nature of the SM trajectories. Quasi-ensemble interpretation of stretching exponents, however, shows not only that measured $\beta_{med} > \beta_{QE}$ in OTP for all probes but also that β_{QE} obtained from experiments does differ substantially from that attained from these simulations (Fig. 3.4d and Table 3.2). The finding of $\beta_{med} > \beta_{QE}$ is consistent with the fact that greater differences are observed across probes than within probes over time, or that spatial heterogeneity dominates over temporal heterogeneity in these SM measurements. This is because in the limit of long trajectories, the deviation of β_{med} from 1.0 reports on temporal heterogeneity experienced and reported by a probe while β_{QE} reveals both that temporal heterogeneity plus any differences

across probes, i.e. spatial heterogeneity. This conclusion is similar to recent conclusions of Gruebele and coworkers for SM probe-free experiments on a metal glass surface.[115] SM probe report of a greater degree of spatial than temporal heterogeneity is consistent with the spread of τ_c values being larger than expected from simulation of homogeneous dynamics while the distribution of individual β values does not differ substantially from that obtained from those simulations. We note that SM probe reports of a greater degree of spatial than temporal heterogeneity does not necessarily imply this is true of the supercooled OTP itself; indeed, the fact that data collected in both OTP and glycerol show that the fastest probes report the greatest breadth of heterogeneity strongly suggests dynamic exchange on (and likely below) the time scale of probe rotations occurs in these supercooled liquids. The probe-dependent findings further suggest that extrapolating to the limit of no temporal averaging (Fig. 3.5d) can yield important information of instantaneous (spatial) heterogeneity in a supercooled liquid.

As described in Section 3.3.2, to compare β values obtained from SM experiments to those obtained from ensemble studies, a β_{QE} value is extracted from ACF_{QE}s for each type of PDI probe measured in OTP. β_{QE} values remain relatively constant across temperature for all probes studied in OTP, as for FWHM values of τ_c distributions. The fastest rotating probe in OTP, egPDI, exhibits the smallest β_{QE} value with an average $\beta_{QE} = 0.78$ across temperatures. This value is larger than that obtained from probe-free measurements in OTP where $\beta \approx 0.35 – 0.50$.[116,117] However, it is similar to those obtained from most probe-bearing experiments in OTP, which yield β values from 0.60 – 0.90, some of which show temperature dependence in the temperature regime investigated here.[77,118,119] In these measurements, potential probe averaging in space and time can not be distinguished. In our measurements, in which the fastest probes consistently report the greatest degree of host heterogeneity regardless of probe size, the increase

in β_{QE} values relative to β values measured in probe-free experiments points to the importance of temporal averaging rather than spatial averaging by these probes, as has been suggested previously[39-41].

In analogy with the FWHM values obtained from τ_c distributions extrapolated to $\tau_c/\tau_\alpha = 1$, the value of β_{QE} in the limit of no temporal averaging can be estimated. Doing so reinforces that time-limited trajectories affect extracted β values more substantially than FWHM values of τ_c distributions, as described previously.[20] For all probes in OTP, β_{med} is near 1.0 and $\beta_{med} > \beta_{QE}$. This is true, as well, for measurements of dpPDI, dapPDI, and tbPDI in glycerol. In Figure 3.6, β_{QE} values are plot as a function of probe and trajectory length for every movie collected in OTP and glycerol. For the employed probes, probe lifetime in glycerol is significantly longer than in OTP. For dpPDI and dapPDI in glycerol, β_{QE} values exhibit a plateau at a value of $\beta_{QE} \approx 0.9$, regardless of trajectory length. On the other hand, for tbPDI β_{QE} decreases with increasing trajectory length. In OTP, it is not clear whether any of the probes exhibit a plateau, and it appears that the two faster rotating probes, dpPDI and egPDI, show a trend towards lower β_{QE} with increasing trajectory length. For simulations of homogenous rotational dynamics and those with spatial but no temporal heterogeneity, it was previously shown that decreases in β_{QE} occur as a function of trajectory length for trajectories of up to $1000\tau_c$; however, most of the change occurs for systems of up to $100\tau_c$ even though the FWHM of τ_c distributions evolves little in this same trajectory length range.[20] For a system with temporal heterogeneity, additional decrease of β_{QE} with increasing trajectory length may be expected as each individual SM ACF becomes increasingly stretched for probes that do not substantially average over dynamic heterogeneities in these systems. We find evidence for this occurring for tbPDI in glycerol and egPDI in OTP. Because of the short trajectories of the other two probes in OTP, the β_{QE} values may not

accurately represent the degree of heterogeneity in the supercooled liquid. This is illustrated by Fig. 3.6b, where average β_{QE} values averaged over all movies for each probe are plot vs. FWHM of τ_c distributions. In both cases, the relationship between FWHM and β_{QE} is approximately linear. For glycerol, extrapolating to FWHM = 0.98, the value at which probe rotational correlation time is equivalent to host structural relaxation time, β_{QE} is 0.48, very similar to that obtained from ensemble experiments.[99] The same approach for OTP, however, yields an unphysical, negative β_{QE} value, likely because the β_{QE} values are overestimated, particularly for dpPDI and tbPDI due to the short trajectories collected. Despite this, the approximately linear relationship between FWHM and β_{QE} for both glycerol and OTP provides evidence that both quantities are reporting on the same spatially heterogeneous dynamics in the host supercooled liquids.

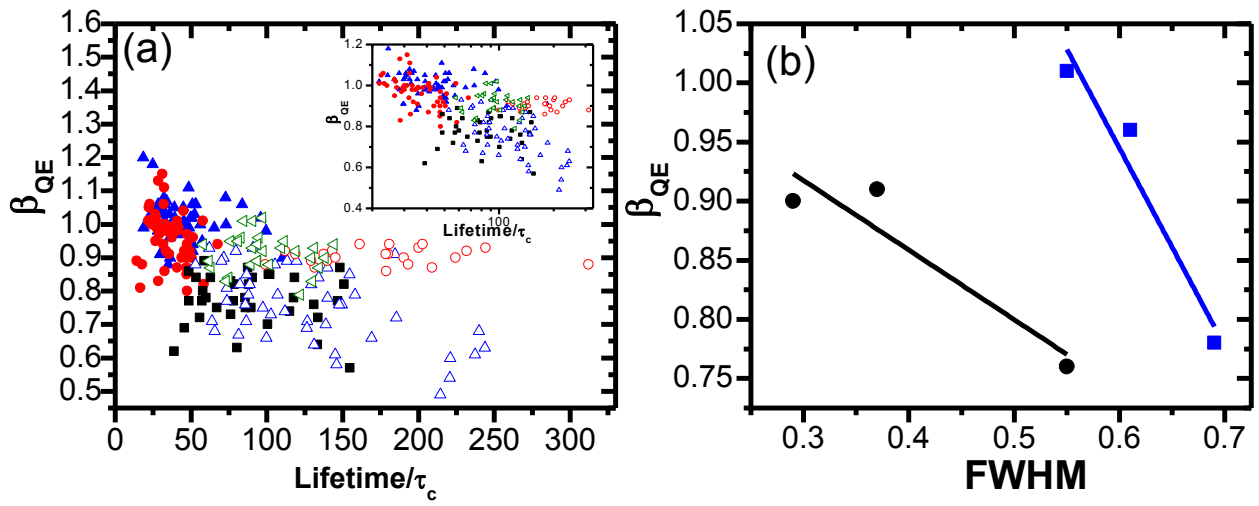

Figure 3.6 (a) β_{QE} with respect to median trajectory length in terms of $\tau_{c,med}$ for each measurement for egPDI (black squares), dpPDI (red circles), and tbPDI (blue triangles) in OTP and tbPDI (open blue triangles), dapPDI (open green sideways triangles), and dpPDI (open red circles) in glycerol. Inset shows the same data with trajectory length plot on a log scale. (b) Average β_{QE} for each PDI studied in OTP (blue) or glycerol (black) with respect to FWHM from Gaussian (OTP) or Lorentzian (glycerol) fits to each histogram pictured in Fig. 5a and b as well as best-fit lines to the data.

3.5 Summary

This study monitored the rotational relaxation dynamics of three PDI probes in OTP near the glass transition temperature. Each of the three probes sampled and reported rotational correlation times that spanned more than a decade, consistent with the presence of spatially heterogeneous dynamics in OTP. As in glycerol, probe rotational correlation time scaled inversely with breadth of SM τ_c distribution, with faster probes having a broader τ_c distribution. This implies that a portion of the full range of dynamic exchange events occurs on probe

rotational correlation time scales. For these probes in OTP, the τ_c/τ_α value is on the order of 100 and thus dynamic exchange reported by these probes is occurring on similar time scales. Extrapolating FWHM of rotational relaxation times to the self-diffusion time scale of the host suggests that the τ_c distribution would span approximately two decades if an instantaneous measurement could be performed. Comparison with SM measurements in glycerol suggests that the more fragile OTP is more spatially heterogeneous than is glycerol, though discrepancies between reports of heterogeneity from τ_c distributions and those from evaluating stretching exponents require additional study. This SM study in OTP not only confirms findings from previous study in glycerol suggesting dynamic exchange occurs on and below the probe rotational time scales, it also demonstrates how probe-dependent studies can be used to extrapolate to a regime in which effects of temporal averaging are eliminated, an important consideration when employing probes to interrogate dynamically heterogeneous systems.

Chapter 4. Single Molecule Studies in Polystyrene Films

In this chapter, results from single molecule studies of polystyrene films doped with perylene diimide (PDI) probes are presented. This study was conducted to investigate the segmental dynamics of high molecular weight polystyrene at high spatial resolution using single molecule (SM) microscopy techniques. Here, as in Chapters 2 and 3,wide field SM microscopy was used to follow the relaxation dynamics of PDI probes in a system near its glass transition temperature, this time polystyrene (PS) rather than a small molecule glass former. These studies were used to reveal the nature of the temperature dependence as well as details of the heterogeneity present in bulk-like films of PS. These experiments were conducted in anticipation of studying confined films via SM experiments, which will help uncover details about the dynamically heterogeneous nature and other physical details of the mobile region present in confined films.

4.1 Motivation

4.1.1 Dynamic Heterogeneity Revealed by Single Molecule Studies

Single molecule microscopy can resolve the shortcomings of experiments attempting to probe the details of dynamic heterogeneity of polymers near their glass transition temperature. Unlike in small molecule glass formers, there have been a relatively large number of single molecule studies probing various aspects of supercooled polymeric systems. These experiments include various techniques including monitoring small molecule probes amongst an unlabeled polymer system [17,24,72,120–127], diffusion of labeled polymers [128], and studying the segmental motion of the polymer chains by tracking the fluorescence lifetime of probes. [126,129–141] All of these studies have helped uncover the physical origins of dynamical heterogeneities within the polymer systems and set up experimental protocols that could be used to investigate confined films.

4.1.2 Previous Single Molecules Studies of Confined Polymer Films

Recently, the first single molecule studies on confined polymer films have been carried out.[71,73,142] These studies reveal many interesting aspects of the mobile region's dynamics and dependence on experimental parameters such as temperature and film thickness. A study carried out by Vacha and coworkers used single PDI probe molecules to investigate poly(methyl acrylate) films supported on a glass coverslip of varying thickness (110 nm, 70 nm, and 20 nm) at T_g + 13 K.[65] Results of these experiments found probes in a 5 nm thick surface layer with increased mobility regardless of the overall thickness of the film (Figure 4.1). This finding

converges with previous ensemble studies done by Paeng, et al., where they additionally concluded that the size of the mobile region is dependent on temperature.[143]

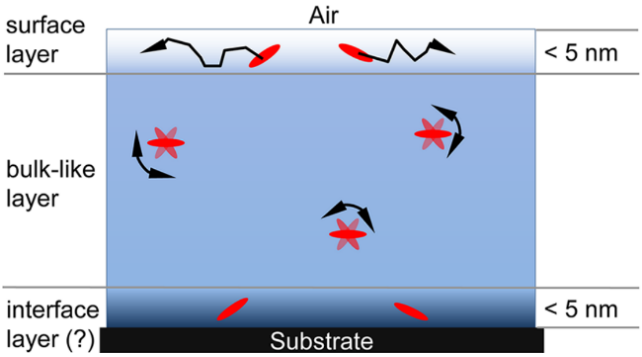

Figure 4.1 A schematic proposal of the structure of the confined supported films of single molecule experimental studies carried out by Vacha et al. Figure 4.1 is reproduced from Reference 66 with permission from the publisher.

To investigate the temperature dependence of the mobile region thickness, Wöll et al. conducted a study of supported films of low molecular weight polystyrene doped with another type of PDI probes. In this study, single probe positions were tracked, yielding translational diffusion constants.[72] They too varied the thickness of the film, from 30 – 250 nm, and also varied temperature from T_g – 1.1T_g. The study showed probe molecules were immobile at temperatures up to T_g, and from T_g to T_g + 40K, mobile and immobile populations were found. The fraction of mobile molecules increased as film thickness decreased, and mobility was observed at lower temperatures for the 30 nm films than for the thicker films. Interestingly, heterogeneous character in the translational diffusion tracks of single molecules were observed in all mobile molecule situations suggesting dynamic heterogeneity within the mobile surface layer of the films. A third study, also investigated thin PS films of two molecular weights (34,000 and 392,000 g/mol) over a wide temperature range and introduced PS chains containing probe molecules chemically attached to each terminal end dilutely.[73,144] Measuring the fluorophores' rotations then revealed terminal chain dynamics of PS thin films. This study complements

findings of another study of this type[144], which found a wide range of rotational fluctuations of individual fluorophores indicating heterogeneous dynamics. Additionally, a characteristic temperature where an abrupt change of terminal chain dynamics from arrested to mobile was found. This temperature was found to be dependent on film thickness and molecular weight of the polymer system. Interestingly, the authors found that this temperature does not coincide with the glass transition temperature, suggesting motion near chain ends differs from that of the internal chain segmental dynamics.

4.1.3 Experimental Shortcomings

The experiments described above have uncovered some details of dynamic heterogeneity within confined polymers, but many questions remain unanswered. The details of spatially heterogeneous dynamics of the mobile layer below (bulk) T_g have yet to be investigated via single molecule techniques in confined polymer films. Recent ensemble measurements suggest the presence of a mobile region of temperature dependent thickness below the glass transition temperature (Figure 4.2). [143,145] A much wider temperature range, above and below the glass transition temperature, should be probed to understand whether heterogeneous dynamics of the mobile layer, thickness of the mobile region, or the gradient of dynamics within the mobile region depend on temperature or film thickness. Vacha's data reveals an undeniable mobile region on the surface of the polymer film with an interior region displaying expected bulk dynamics but only probes a single temperature, above T_g. Wöll and coworkers' single molecule studies probe a wide temperature range, all above T_g. The studies of Zheng et al. investigate temperatures that span T_g, but these studies only provide information about the terminal dynamics of the system, likely distinct from the segmental dynamics in other locations on the

chain. Additionally, the terminal dynamics probed may be altered from the addition of the fluorophore to the chain ends.

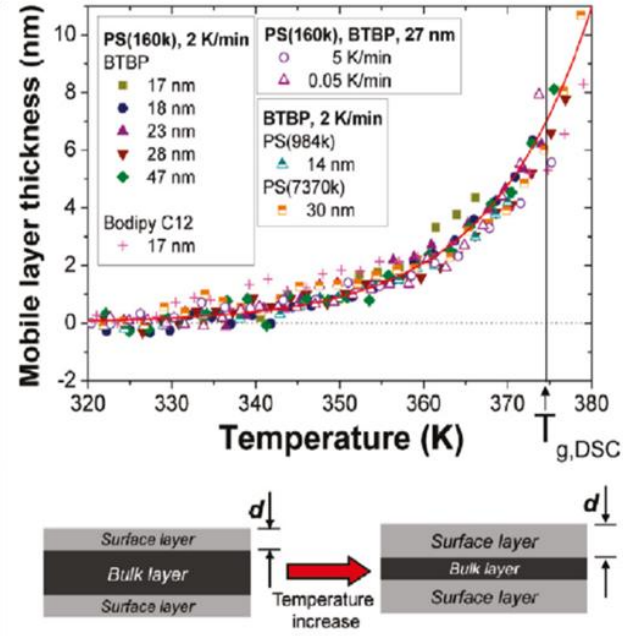

Figure 4.2 The mobile layer thickness with respect to temperature for differing film thickness of PS found via fluorescence anisotropy measurements and complementary schematic. At T_g, the surface mobile layer is 7 nm thick for all film thicknesses investigated. Figure 4.2 is reproduced from Reference 68 with permission from the publisher.

The control or addition of experimental parameters is needed to allow for more extensive conclusions in the single molecule studies probing segmental dynamics: Vacha et al. only reported two film thicknesses, 110 nm and 70 nm, thicker than most thin film studies where evidence of mobile layers have been found. Wöll's studies use low molecular weight polystyrene (3,000 g/mol), which may differ in behavior from high molecular weight polymers, given the importance of chain length relative to entanglement length in setting glassy properties of polymeric thin films. Beyond this, no particular attention was paid to temperature maintenance and avoiding potential temperature gradients in these studies. It is crucial to maintain the

temperature of the sample to ensure seemingly interesting results are not produced from temperature inconsistencies or gradients.

The purpose and main motivation of this final stage of thesis work is to conduct experiments that bridge the gaps and alleviate the shortcomings of the recent efforts to gain a fuller understanding of the spatially heterogeneous dynamics in confined polymer systems through single molecule studies. By probing a wider range of temperatures, especially temperatures below T_g, rotational information can be collected from the bulk portion of the thin film as well the mobile surface region. This will aid in understanding the heterogeneous dynamics and dynamic length scales of the system and as well as reveal the size of mobile and bulk regions as a function of temperature and film thickness.

We plan to perform rotational measurements of PDI type probes in high molecular weight polystyrene doped in a confined thin film environment via single molecule microscopy. First, control single molecule measurements much like the ones in OTP are carried out in a "bulk" 100 nm polystyrene film at $T_g - 1.01T_g$. The purpose of these experiments is to confirm that PDI reports the same temperature dependence as the structural dynamics of PS near its glass transition temperature and to gain insight into the breadth of rotational dynamics present in this system compared to in small molecule glass formers.

4.2 Experimental

4.2.1 Sample Preparation

Polystyrene (PS) of molecular weight M_w = 168,000 g/mol (Polymer Source Inc., p4250-S, M_n = 160,000, polydispersity 1.05) was dissolved in toluene (Sigma Aldrich, spectrophotometric grade) to obtain 2.0 wt% solution. This solution is photobleached in a home-built bleaching apparatus for 48 hours. Solid N,N′-Bis(1-pentyl)perylene-3,4,9,10-bis(dicarboximide) (pPDI) is obtained from Sigma Aldrich and dissolved in toluene to form a 2.6 x 10^{-5} M stock solution. This solution was subsequently diluted to 1.0 x 10^{-8} M solution for use in SM imaging samples. Solutions of pPDI in PS were prepared by mixing 1 uL of 1.0 x 10^{-8} M pPDI in 370 uL of 2.0 wt% PS. These solutions produced films with a pPDI concentration of 1.5 x 10^{-9} M. This concentration produced molecules that were dilute enough that they are separated by a greater distance than the diffraction limit, but concentrated enough such that ~100-150 analyzable molecules were found per measurement.

Films of pPDI/PS were prepared by spin coating onto a silicon wafer. The silicon wafers were cut into 5 x 5 mm pieces in order to fit into the sample holder. The pieces were treated with a 4:1 concentrated sulfuric acid:30% hydrogen peroxide solution for 1 hour. This process produces a native oxide layer of that is smooth and of uniform thickness. Wafers were subsequently flushed with Millipore water followed by 200 proof ethanol (Sigma Aldrich) and stored in ethanol. The native oxide layer ~2 nm thick was measured by ellipsometry. Wafers were sprayed with Millipore water and spun at 8,000 RPM for 1 min to sufficiently dry the surface. The pPDI/PS solutions were spincoated onto the silicon wafer via a glass pipette at 2,000 RPM for 1 minute to produce a 100 nm film. All samples are annealed in a vacuum oven

at 120° C (T_g + 20° C) for 12 hours. Following the annealing process, polymer film thickness was confirmed by ellipsometery measurements.

The sample was placed into the microscopy cryostat (Janis Research Company Inc., Model ST-500-LN) and placed onto the sample stage using Braycote 601EF vacuum grease to ensure thermal contact between the sample and stage. The cryostat was evacuated and the vacuum remained on for the duration of measurements. The cryostat was subsequently heated from room temperature at a rate of ~8 K min^{-1} to desired temperature. The system is held at the measurement temperature until the pressure reached 3.0 mtorr or at least 1 hour time had elapsed to ensure all toluene is removed from the system.

4.2.3 Optical Setup

The optical setup used for these measurements was a variation of that used for rotational measurements collected in Chapter 3. Data was acquired using a home built microscope in an epi-fluorescence configuration similar to Fig. 3.1. Optics on the excitation portion of the setup have been simplified further (Figure 4.3). The excitation light (Nd:Vanadate 532 nm diode laser, Spectra Physics Millenia Vs) was directed into an objective lens and coupled into a multimode fiber (Newport, F-MCB-T-3FC) that was shaken by a piezoelectric buzzer at 500-4700 Hz (MCM Electronics; PEB in Fig. 3.1) and directed out of the fiber via a collimator. At this point the modification from the previously described setup occurs: after the beam was directed through a neutral density filter, a half waveplate used to adjust the ratio of parallel and perpendicular polarized light. The beam was directed through a tube lens and reflected toward the objective lens by a dichroic mirror. The SMs within the sample were illuminated, and their fluorescence was collected by a high numerical aperture objective lens (Zeiss, LD Plan-Neofluar, air 63x, NA = 0.75, WD = 1.5 mm), through detection optics including long and bandpass filters and a

Wollaston prism, splitting the signal into two orthogonal polarizations. The signal was collected by an electron multiplying charge-coupled device camera (Andor iXon DV887; EMCCD in Fig. 4.3).

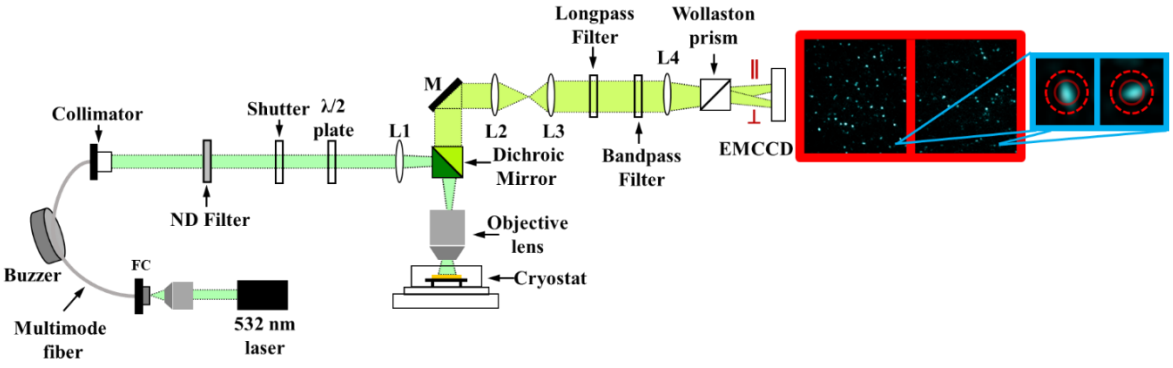

Figure 4.3 Schematic diagram (not to scale) of the epi-fluorescence microscope. F = filter, M = mirror, L = lens. Image on right illustrates a typical field of view and a zoomed in image of a matching pair.

4.2.3 Bulk Film SM Experiments

Data were collected at temperatures from 373.8K – 377.6K. Optimal frame rate for each movie was determined during preliminary experiments to be ≈ 20 frames per median rotational relaxation time, $\tau_{c,med}$. Measurements were taken for 6,000 frames to ensure measurements continued until most molecules photobleached. Measurements were taken at 5 Hz at 377.6 K, 1.67 Hz for 376.3 K, 0.55 Hz for 375.0 K and 0.29 Hz for 373.8 K. The sample was continuously illuminated for data collected at 5 Hz with an exposure time of 0.2s. Data collected at <5 Hz had a fixed exposure of 0.2 s with the laser shuttered the remainder of the frame time to avoid photobleaching.

Most data was collected at a laser power of 10 mW, as measured before the objective lens. This consistently yielded a signal to background ratio of at least 2. To allow for correction

of heating by the laser for continuously illuminated measurements, additional movies were collected at 377.6K at 20 mW and 30 mW. Median probe rotational correlation time as a function laser power were plotted and linearly fit to obtain a correction factor. This correction factor was then used to calculate an adjusted, actual temperature using the VFT equation, $\log(\tau_c) = A + \frac{B}{T-T_0}$, where A = -11.15, B = 404.87, and T_0 = 341.8. These VFT parameters were found by fitting dielectric measurement data of high molecular weight PS.[146] This correction yielded a temperature increase of 0.03 K which is within experimental error of the temperature control of the system (±0.2 K). Therefore, we assume measurements taken at 377.6 K are truly 377.6 K.

4.2.4 Data Analysis

Rotational Data

Data analysis was performed using a variation of the in house IDL based software (ITT Visual Information Solutions) used previously in the Kaufman lab. [15,16,108,147] Frames 1,000 – 1,500 were summed to maximize the chances of choosing a set of molecules with longer lifetimes until photobleaching. This summed image was band-pass filtered by convolution using a Gaussian intensity distribution whose width was on the order of the feature size. Features found whose integrated intensities were above a reasonable threshold were subsequently matched from right and left channels, using a known separation on the CCD chip. Molecules were analyzed only if they have a matching pair, photobleached in a single step, and were free of any closely neighboring fluorophores.

Once the locations of the fluorophores were established, all further analysis was performed on the raw, unfiltered images. The intensity of the fluorophore was determined in both channels by calculating the median intensity of the pixels located within 2-2.5 pixels of the identified feature center. Median intensity values were then recorded for each molecule in each frame of the movie. This differs from previous analysis where intensities were found by integrating intensity and subtracting the background.[16,108,109,147] Because the extracted data was affected by camera noise, median intensity values were used to prevent the addition of further noise due to the propagation of camera noise when integrating several pixels of signal or performing a background subtraction. A linear dichroism (LD) trajectory was then constructed from each frame of the movies as

$$\mathrm{LD} = \frac{I_{\parallel} - I_{\perp}}{I_{\parallel} + I_{\perp}}, \tag{4.1}$$

where -1 ≤ LD ≤ 1 and left and right intensities are denoted as $I_{\parallel}$ and $I_{\perp}$. A smoothed intensity trajectory was formed by calculating a moving average of the raw total intensity ($I_{\parallel}$ and $I_{\perp}$) trajectory with an averaging window of 50 frames. A threshold was set with respect to the smoothed intensity, and all intensity points of the smoothed intensity trajectory that were above threshold were retained. All points of the smoothed intensity trace that fell below the threshold, i.e. where the molecule either blinked or had photobleached, were excluded from the intensity trajectory.

As discussed in chapters 2 and 3, an autocorrelation function

$$C(t) = \frac{\sum_{t'} a(t')a(t'+t)}{\sum_{t'} a(t')a(t')} \tag{4.2}$$

where the deviation of the LD signal from the mean, $a(t) = \mathrm{LD}(t) - \langle \mathrm{LD}(t) \rangle$, was calculated for each SM LD. The SM ACF was then fit by a stretched exponential decay given by

$$C(t) = Ae^{-(\frac{t}{\tau_{fit}})^{\beta}} \tag{4.3}$$

with β the stretching exponent and the extracted relaxation time given by

$$\tau_c = \frac{\tau_{fit}}{\beta}\Gamma\left(\frac{1}{\beta}\right). \tag{4.4}$$

τ_{fit} represents how fast the molecule rotates as represented by the initial decay of the ACF. The resultant τ_c represents the the average rotation time over the full trajectory, incorporating the degree of dynamic heterogeneity the molecule has exhibited.

Initially, individual SM ACFs were fit with a stretched exponential form. Bounding parameters were subsequently enforced to exclude inaccurate fits among these trajectories. It has been shown that extracted relaxation time and associated β are affected by limited trajectory lengths, therefore only trajectories longer than $30\tau_c$ were included. Related to this bound, trajectories with β values falling in $0.3 \geq \beta \geq 2.0$ were retained because β values < 0.3 have been shown to affect the accuracy of the reported τ_{fit} value. Trajectories with sampling rates > 5points/τ_c and >3 points/τ_{fit} were chosen because sampling rates lower than this contain too few rotations to produce reliable fits. Lastly, the prefactor value, A, (from equation 4.3) was used to bound trajectories by $0.3 > A > 1.2$, to avoid fitting trajectories with low signal to noise (lower bound) or including trajectories which have inherently inaccurate fits (upper bound).

Translational Data

A subset of molecules present in the films under investigation appeared to be translating when using the same data collection parameters used to collect rotational data. Analysis of the translating SMs was performed using in-house written IDL based software (ITT Visual

Information Solutions). Frame by frame analysis was performed to locate SM features in every frame. Each individual feature in each frame was subsequently fit with a Gaussian and a tracking algorithm was employed.[148] This tracking algorithm utilizes three parameters when locating and tracking translating features: 1) the maximum displacement is set to indicate the furthest expected movement of a feature between consecutive frames, 2) a memory parameter is set to indicate the maximum number of frames after the disappearance of a molecule that the algorithm will continue to look in that vicinity for the reappearance of the molecule; this is particularly useful for treating photoblinking events or defocusing, 3) a minimum trajectory length is set to exclude trajectories with too few points, to allow meaningful mean squared displacements to be constructed. Once the algorithm is applied, the translating feature intensity data is extracted and the coordinates of each feature are tracked in time.

4.3 Results

4.3.1 Median Probe Rotational Relaxation Times

We first investigated the temperature dependence of the measured rotational dynamics of pPDI on average in PS. The median of the SM rotational correlation times for each temperature investigated were determined. The temperature dependence of these median values over all temperatures probed was investigated to assess whether the probes mimic the structural relaxation of PS, as described by the VFT relationship, determined by dielectric measurements (discussed previously).

A single median τ_c value for all single molecule data collected (all movies) at each temperature probed was obtained (Table 4.1). Figure 4.4 shows median τ_c values with respect to temperature where each scatter point represents a median τ_c value for a given temperature representing 902 – 1971 molecules in total. These data were overlaid with a VFT curve vertically shifted by a constant value. As expected, there was good agreement between the temperature dependence of the probe median rotational correlation time data and that of the dielectric data for PS, suggesting the probes are accurate reporters of the host structural relaxation, which is governed primarily by segmental dynamics. Comparing the shifted VFT line for this data to the original VFT line from dielectric relaxation measurements shows that although the probes' dynamics reflect the temperature dependence of the host dynamics, they do so on a slower time scale than the host dynamics (Figure 4.4).

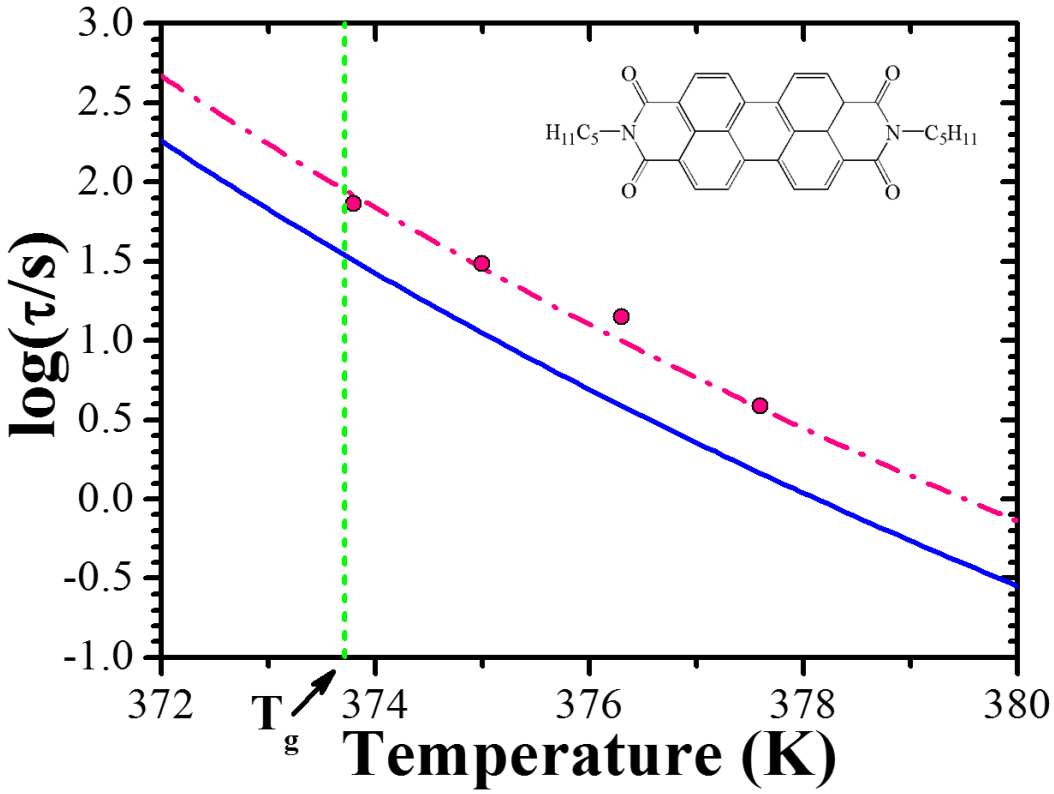

Figure 4.4 Median rotational correlation time values from SM measurements (pink circles) with respect to temperature. Vertically shifted VFT curve (pink dash dot line) shows the temperature dependence of the probe measurements are in agreement with dielectric relaxation measurements. The best fit VFT curve for dielectric data is plotted in blue as a reference. Glass transition temperature of PS is indicated by a vertical green dotted line. The structure of pPDI is pictured (inset).

4.3.2 Breadth of Rotational Relaxation Times

After evaluating the average dynamics of pPDI in PS, we take a deeper look into the information revealed by the single molecule trajectories at each temperature. Specifically, τ_{fit} and subsequent τ_c values (Eqns. 4.4 and 4.5) were obtained from fits of the linear dichroism

autocorrelation functions of each individual single molecule's intensity trajectory. These values were plotted in histograms on a log scale for each temperature probed (Figure 4.5 (a) and (b)). There was a substantial spread for all temperatures probed with each histogram spanning more than 1.5 decades for both τ_{fit} and τ_c.

The full width at half maximum (FWHM) for each τ_{fit} distribution (Figure 4.5 (a)) is determined by simply measuring the width at the half maximum position of the normalized distribution. Each τ_c distribution was fit with a Gaussian function given by

$$y = \frac{1}{\sqrt{2\pi\sigma^2}} \exp^{-\frac{(x-x_c)^2}{2\sigma^2}}, \tag{4.5}$$

where x_c indicates the center of the peak and σ^2 is the variance. The full width at half maximum is given by $2\sqrt{2\ln 2}\sigma$. The fitting procedure allows all variables to float. All τ_c distributions were fit well as indicated by the R^2 value. Corresponding Gaussian fits for each distribution of τ_c were plotted (Figure 4.5 (b)).

The FWHM values as a function of temperature remain constant within error, upholding the time temperature superposition principle (Table 1.1).[112] In addition to plotting τ_{fit} and τ_c distributions for each temperature, normalized distributions for all temperatures were constructed and fit with a Gaussian fit as described above (Figure 4.5 (c) and (d)). The FWHM of the combined temperature distribution was similar to the FWHMs of each individual temperature's τ distribution (τ_{fit} FWHM = 0.63 and τ_c FWHM = 0.63).

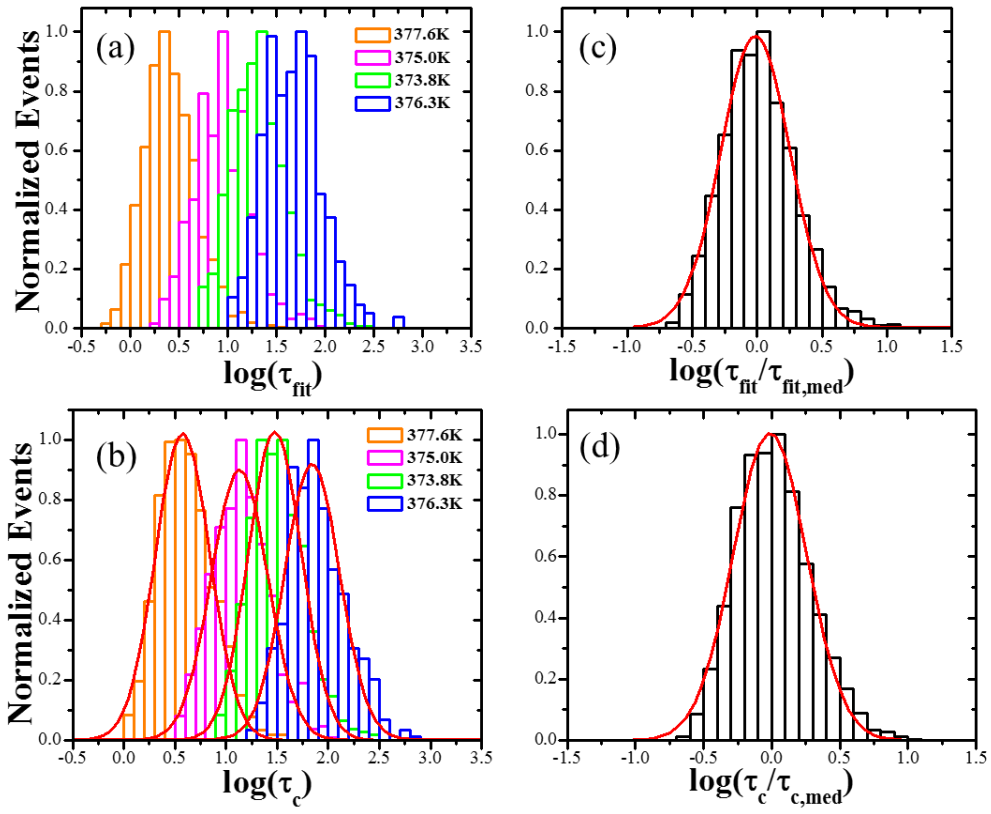

Figure 4.5 Log normal distribution of τ_{fit} (a) and τ_c (b) each individual temperature probed and normalized τ_{fit} (c) and τ_c (d) distributions. Gaussian fit curves of the distributions are shown in red.

The τ_c distributions for each temperature as well as the temperature combined distribution appear to be asymmetric i.e. the fast τ_c tail appears to be undersampled. This may be due to measurements limited by a single frame rate. At least 3 frames per rotation of a single molecule are needed to quantify the dynamics of a probe molecule given our fluorescence microscopy data collection setup and subsequent analysis of LD trajectories. The breadth of dynamics of PS near T_g may be too wide to capture in a single frame rate. Therefore, measurements at faster frame rates may be necessary to assess rotating molecules whose rotations cannot be quantified using a ~20 frames per $\tau_{c,med}$ frames rate, yielding the true full dynamic range of the system at a given temperature. On the other hand, increasing the sampling rate of measurements will decrease the

trajectory lengths of the single molecule measurements, decreasing the accuracy of the extracted τ_c values. Given the FWHM of $\log(\tau_c)$ distributions does not change across all temperatures probed and median τ_c closely follow the temperature dependence of dielectric measurements, the data described in thesis that were collected at a single frame rate for a given temperature are deemed suitable for further analysis.

	377.6 K	**376.3 K**	**375.0 K**	**373.8 K**
No. Molecules	1142	690	724	543
Frame Rate (Hz)	5	1.67	0.56	0.28
$\tau_{fit,\,med}$	2.42	8.72	19.9	46.05
$\tau_{c,\,med}$	3.9	14.1	30.8	73.3
β_{med}	0.62	0.63	0.63	0.63
β_{QE}	0.58	0.56	0.59	0.58
FWHM (τ_c)	0.63	0.65	0.61	0.63
Frame/τ_c	19.5	23.5	17.1	20.94
Trajectory Length/τ_c	180.7	149.3	163.5	138.7

Table 1.1 Number of molecules, frame rate, median $\tau_{fit,}$ τ_c and β of all single molecule trajectories, β_{QE}, FWHM of Gaussian fits of τ_{fit} and τ_c distributions, median frames per τ_c and median trajectory length per τ_c (median on time of molecules until photobleaching divided by their respective τ_c) for each temperature probed.

4.3.3 Evaluation of Stretching Exponent

Spread of SM stretching exponents

As a complement to assessing the spatially heterogeneous nature of the PS system near $T_{g,}$ through the τ_{fit} and τ_c distributions, evaluation of stretching exponents, spatially heterogeneous dynamics are often quantified by the exponent of the stretched exponential fit of the ACF formed from ensemble measurements of observables. In SM experiments, this can be

done by extracting a stretching exponent for each individual SM and also from fitting a quasi-ensemble ACF (ACF_{QE}) constructed from SM ACFs for each movie.

The distribution of β values for each individual temperature across all individual SM ACF fits showed no clear difference, yielding nearly identical β_{med} values ($\beta_{med} \approx 0.63$). Therefore, β values across all individual SM ACF fits for *all* temperatures were combined and are plotted (Figure 4.6). These values are limited to $0.3 < \beta < 2.0$. As you can see, there is a sharp drop off around $\beta = 1$. Additionally, trajectory length has been shown to limit the accuracy of reported β.[20] The median trajectory lengths for each temperature from these experiments are at least $138\tau_c$, well above the lower bound where β values reported suggest a much more heterogeneous environment than is truly present and accessible by single molecule probes given a long enough trajectory length.[20]

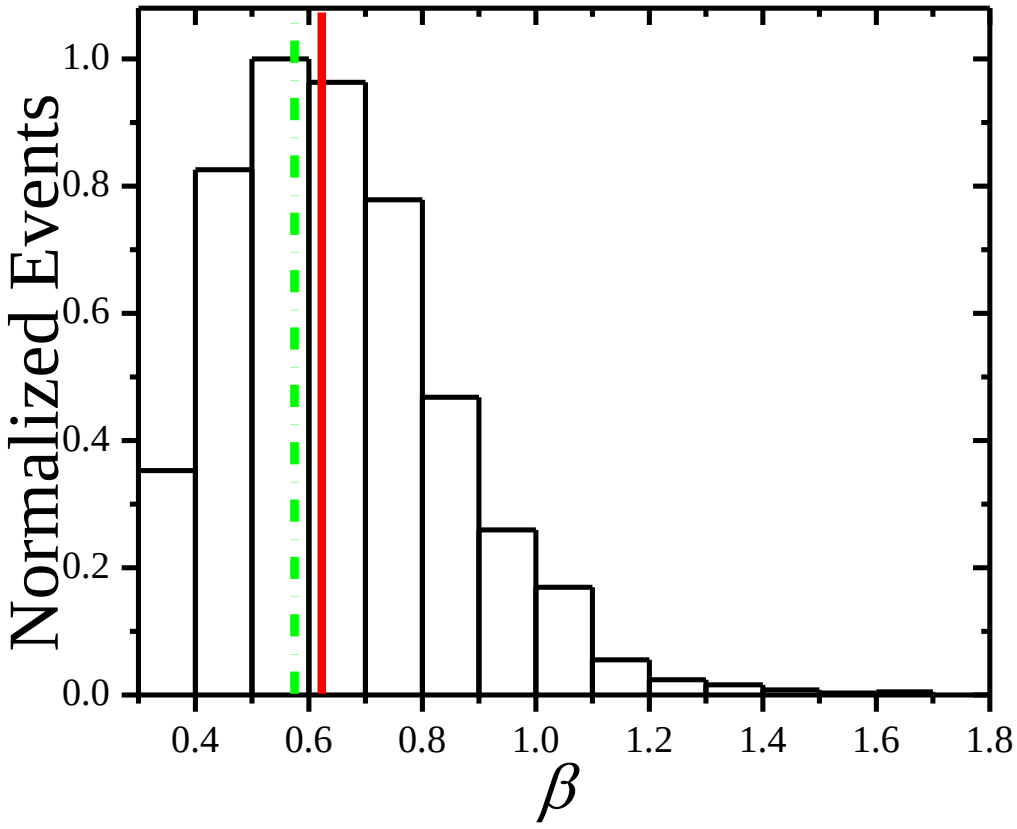

Figure 4.6 Normalized distribution of stretching exponent values for all single molecule trajectories collected at all temperatures probed. Lines denoting β_{med} (solid red) and β_{QE} (dash dot green) values are shown.

Quasi Ensemble Stretching Exponent

Additionally, a method is devised to allow SM data to be directly compared to ensemble studies. Quasi-ensemble ACFs are constructed for each movie for a given temperature by averaging corresponding time points of each individual SM ACF. This ACF_{QE} is fit with a stretched exponential, and β_{QE} values are extracted from this fit. These values serve as guide to assess the validity of median β values from individual SMs, and therefore determine whether probes are a good reporter of the true heterogeneity of the system. β_{QE} values for each movie at a given temperature and also across temperatures were 0.58 with a standard deviation of 0.02

(Table 1.1). This suggests that the degree of heterogeneity across movies as well as temperatures is constant for these experimental measurements of pPDI in PS, at least in this temperature range. Additionally, dielectric measurements of PS report $\beta = 0.5$,[146] which indicates that pPDI could still be averaging some of the heterogeneous dynamics present in the system. This is one of the only representations to date reporting a stretching exponent that is approaching the true degree of heterogeneity via single molecule experiments in a supercooled system.[12,143]

4.3.4 Single Molecule Translation

Unexpectedly, a small subset of molecules appeared to be translating on the same time scale as the rotating SMs in films under investigation. At 100 nm in thickness, an evident mobile layer is unexpected based on past experiments studying this "bulk-like" thickness regime.[65] After translational analysis (described in Section 4.2.4) of a movie measured at 377.6 K (see Table 4.1 for rotational data results at this temperature), single molecule translational trajectories were extracted. These trajectories were mapped onto a summed image of the sum of the first 5 frames of the original movie's images (Figure 4.7 (a)). Some molecules appear to be immobile (Figure 4.7 (b)), while other molecules appear to be translating (Figure 4.7 (c)) creating an interesting mosaic-like picture of rotating and translating spatial areas of the film (Figure 4.7 (a)). Interestingly, the translating molecules appear to be doing so at differing rates spatially and temporally i.e. end to end distances vary across trajectories and for individual trajectories, rate of translation changes over time. Qualitatively, it appears that the molecules in this apparent mobile region are diffusing orders of magnitude faster than the seemingly translationally immobile molecules that are rotating in the bulk-like region of this film.

These preliminary results suggest films under confinement will also exhibit a mobile region near the glass transition that can be probed using our single molecule techniques. These experiments have allowed us to set up an experimental protocol that can be utilized for confined films and help us understand the mobility of SMs in this mobile region. We plan to collect single molecule rotational measurements at temperatures above and below T_g with the intent of probing the rotational dynamics of SMs in the bulk-like, interior region above the bulk T_g and in the mobile, surface region below the bulk T_g. By gathering single molecule rotational data, information about the thickness of the mobile and bulk regions as well as the effects of film thickness and temperature can be discerned. We hope to gain better understanding of the spatially heterogeneous dynamics and dynamic length scales present in confined polymer films. These initial findings of mobile molecules in relatively thick films have also encouraged investigatation of Stokes Einstein behavior and potential rotational-translational decoupling in the mobile layer of thin, confined films above T_g for comparison to data from bulk films.

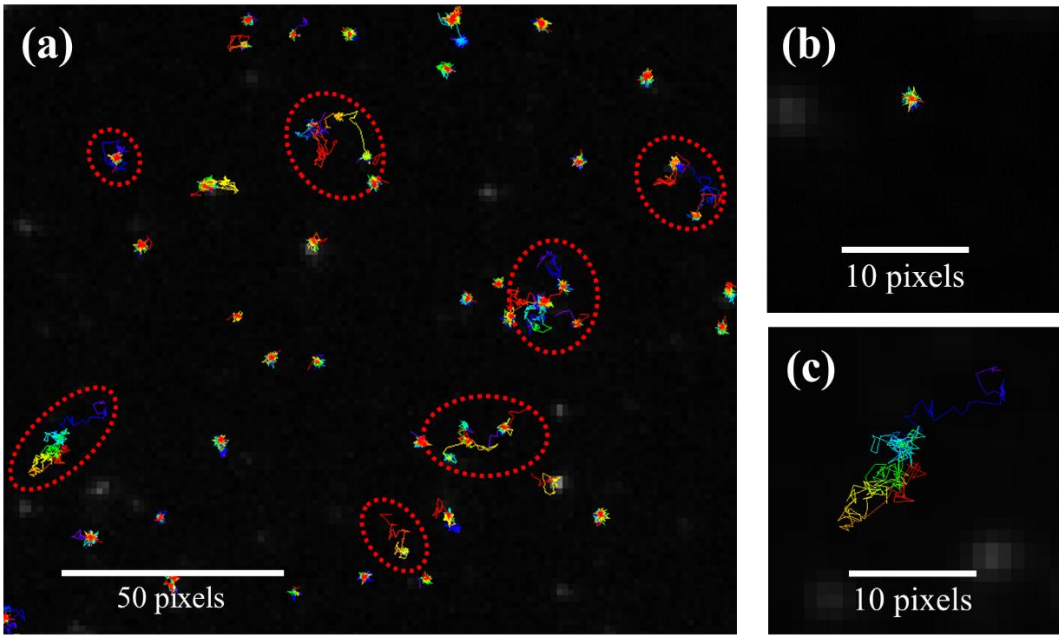

Figure 4.7 (a) Summed image of pPDI in PS at 377.6 K with overlaid trajectories of each single molecule within the sample. Colors indicate the progression of each trajectory in time (time zero is red and colors progress through the visible spectrum to violet) (b) An example of an immobile, rotating molecule. Apparent shift in position of this and similar molecules is due to noise and shift in point spread function that occurs as a result of out-of-plane rotation. (c) Example of a translating molecule that appears fairly immobile during a portion of the trajectory but very mobile during other portions.

4.4 Discussion

4.4.1 How do Relaxation Rates Correspond to Stretching Exponents for SM Studies?

Investigating correlation between β values and their associated τ_{fit} values will allow us to gain a better understanding of whether a lower β_{med} does indeed arise from a faster rotating probe. Faster rotating probes have displayed a lower β_{med} in previous studies, which is believed

to be related to the fact that faster rotating probes are able to report temporal component of heterogeneity of the system more accurately. For this reason, we hypothesize is that the lowest β values of a single molecule distribution are arise from the fastest rotating molecules in the system. To test this hypothesis, τ_{fit} and τ_c of individual SM trajectories for 377.6 K are divided into subsets based on their corresponding β values: $0.3 \leq \beta < 0.5$, $0.5 \leq \beta < 0.7$, $0.7 \leq \beta < 1.0$ and $1.0 \leq \beta < 2.0$. These subsets along with the entire distributions τ_{fit} and τ_c are plotted in histogram form (Figure 4.8).

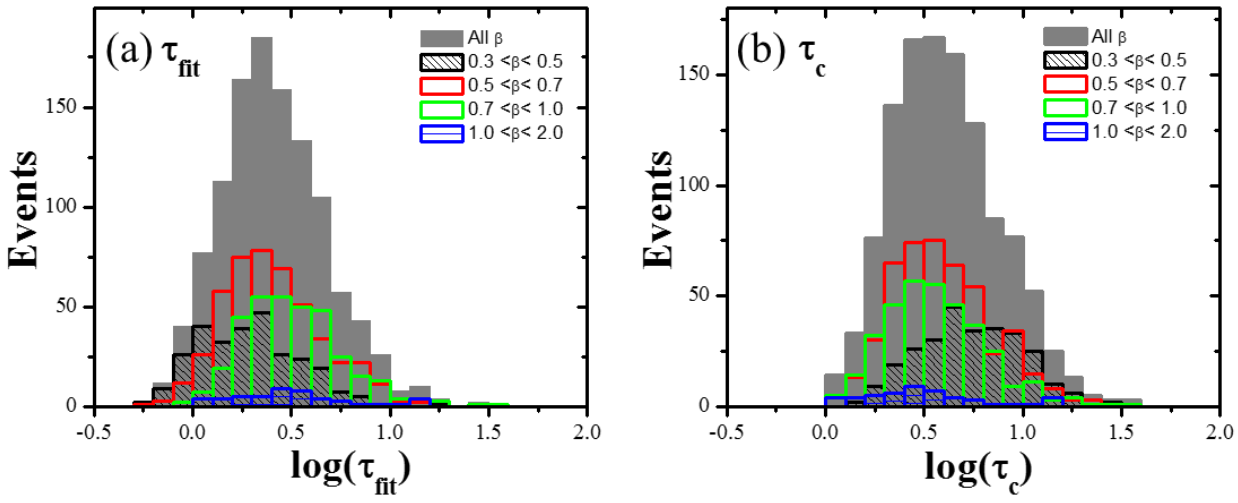

Figure 4.8 Distributions of (a) τ_{fit} and (b) τ_c for measurements taken at 377.6 K. These distributions, which are segregated based on their corresponding β values, clearly illustrate the difference in distribution width as well as τ_{med} values.

The subsets of τ_{fit} values (based on differing β values) are clearly segregated into distinct distributions. These distributions differ from to total τ_{fit} distribution in terms of width and also are centered around different, distinct median τ_{fit} values. The distribution of τ_{fit} values corresponding to $0.3 \leq \beta < 0.5$, are centered around a much lower median value, whereas, the subset corresponding to $0.7 \leq \beta < 1.0$ have a much higher median τ_{fit} value. As mentioned

above, this is most likely due to the fastest molecules having the capacity to explore and report a greater degree of dynamically unique environments by simply rotating at a faster rate. In other words, the faster rotating molecules have the opportunity of accessing dynamic exchange on shorter time scales, and therefore are able to report not only spatial but also a greater breadth of temporal heterogeneity within the system. There is a small population of molecules that report β values greater than 1.0, and as can be seen in Figure 4.8, these molecules report τ_{fit} and τ_c distributions that are centered at more of an intermediate value spanning a wider breadth than the "low" and "high" β value cases discussed above. This suggests trajectories with associated β values greater than one are either reporting a more complex dynamic situation or arise from poorly fit data. Further investigation is needed to more fully understand this subset of data.

Although the fastest rotating molecules undeniably report the lowest β values, β is also correlated with other parameters. As pictured in Figure 4.8, it is evident that the fastest rotating molecules correspond to the lowest stretching exponents, which is also clear when SM τ_{fit} values are normalized and plotted with respect to β in scatter form (Figure 4.9). In addition, the correlation between trajectory length and stretching exponent should also be investigated, given the previous finding that short trajectories may lead to stretching exponents dominated by statistical fluctutations.[20] When trajectory lengths normalized to their respective τ_{fit} are examined with respect to their corresponding β, another strong trend appears (Figure 4.8). As trajectory lengths get longer, β values tend toward lower values. This may result from the molecules being able to experience more rotations in a given trajectory and therefore report more dynamic exchange events. This naturally results in a trajectory reporting a greater amount of temporal heterogeneity and therefore a lower value of β.

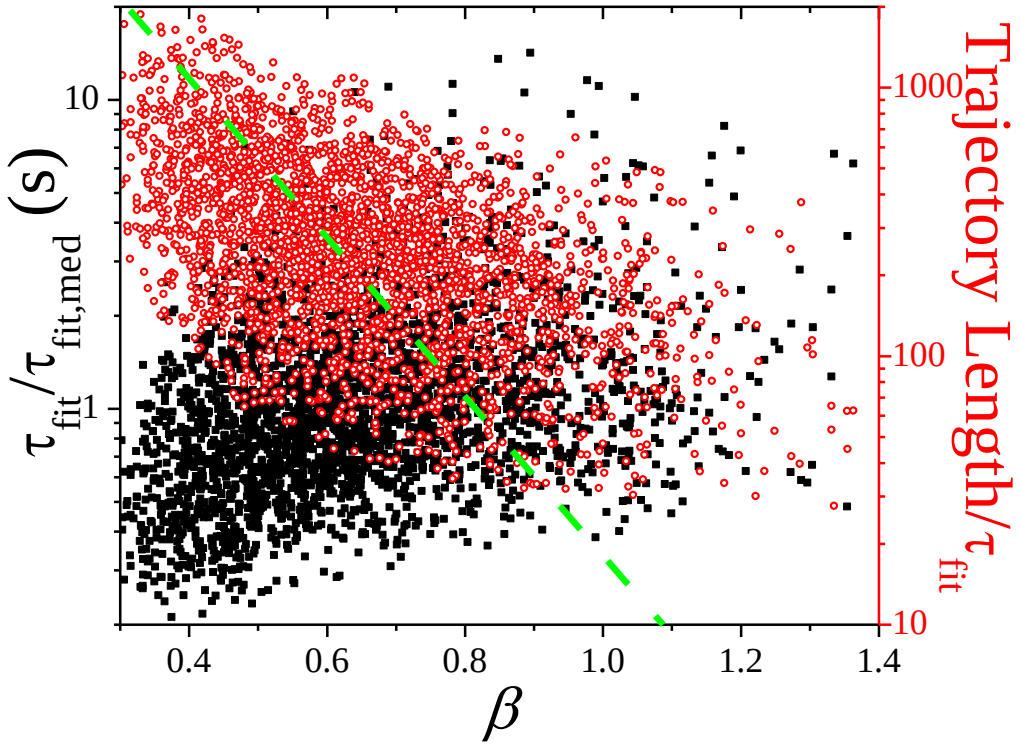

Figure 4.9 SM τ_{fit} normalized to $\tau_{fit,med}$ for each individual temperature measurement (solid black squares) and SM trajectory length (total "on-time" of molecule until photobleaching) normalized to τ_{fit} (open red circles) with respect to their corresponding stretching exponents. Green dashed line is a guide to the eye.

4.4.2 Experimental Comparison of τ_{fit} Distribution to ILT

We devised a method to validate whether the distribution of τ_{fit} values arise from the single molecules' ability to report dynamic heterogeneity of the system as opposed to having spread due to short, noisy trajectories. A stretched exponential function, like the one used to describe the SM ACFs and ACF_{QE} of the data described above, can also be represented as the sum of exponential functions.

$$e^{-\left(\frac{t}{\tau_0}\right)^{\beta}} = \int_{-inf}^{inf} P(\log\tau\,;\tau_0,\beta)e^{-\frac{t}{\tau}}d\log\tau \tag{4.6}$$

This equation mathematically represents the inverse Laplace transform (ILT). Distributions of τ_{fit} can be generated by performing an ILT of a stretched exponential function (as described in equation 4.6) by inputting a dummy value for τ (which is shifted to the appropriate value later) and β value equivalent to β_{QE} (determined above, Table 1.1, Figure 4.10). This provides a visualization of the expected spread of τ_{fit} values if the system is solely spatially heterogeneous case.

We can exploit this process to directly compare the τ_{fit} distribution of the experimental data with that of the ILT curve generated for purely spatial and temporal scenarios. ILT distributions generated from an upper and lower bound β are used to represent the full range of widths experimental τ_{fit} distributions may span, depending how the spatial and temporal components are distributed. The upper bound is set by generating an ILT using β_{QE} from experiments, representing the spatially heterogeneous scenario. A lower bound is simply a delta function, representing the homogeneous case with temporal heterogeneity only. These two distributions are plotted in Figure 4.10, where an ILT of $\beta = 0.99$ is plotted in lieu of $\beta = 1$ such that it has finite height. The area under each curve is normalized by its area, which allows height to act as a measure of the breadth of the distribution.

The upper and lower ILT bounds ($\beta = \beta_{QE}$ and $\beta = 1$ cases) should always be considered when drawing conclusions about the degree of heterogeneity indicated by the width of the τ_{fit} distribution across probes and glass formers. These bounds serve as a guide to how spatial and temporal heterogeneities reported by a given measurement are *distributed* rather than as a measure of the *degree* of heterogeneity. The experimental τ_{fit} for each temperature normalized to

its respective median τ_{fit} in Figure 4.10 appears to lie between the purely spatial and temporal scenarios, implying that the reported heterogeneities have both temporal and spatial character, and cannot be separated using SM experiments or analysis techniques employed thus far. Complicating analysis, it must be noted that there may be averaging of temporal heterogeneity in the systems by the large, slow probes, which limits reporting of the full temporal heterogeneity of the system. On the other hand, since probes are only monitored for a given number of rotations, limited dynamic exchanges may occur, again suppressing reported heterogeneity as assessed through a median stretching exponent. Combining information on measured median stretching exponent, distribution of stretching exponents, and distribution of measured relaxation times may allow untangling of the spatial and temporal components of the underlying native heterogeneity in these systems.[24]

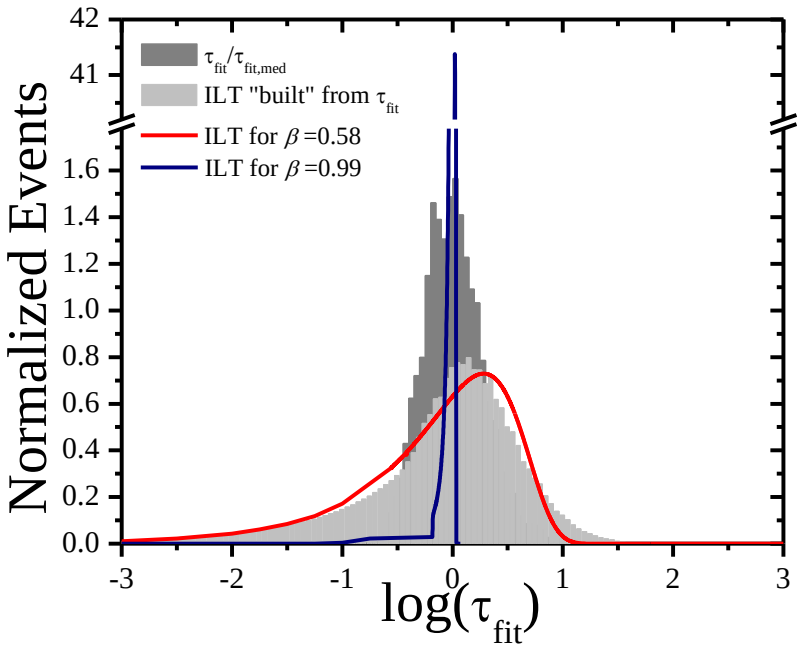

Figure 4.10 Experimental distribution of combined normalized τ_{fit} values for all temperature probed (dark grey histogram). Summation of ILT's built from individual experimental τ_{fit} and corresponding β values (light grey histogram). ILT curve for β = 0.99 (blue line) and β = 0.58 (red line, equal to β_{QE} for experimental distribution).

Additional analysis was performed to confirm that the spread of SM τ_{fit} values emerged from dynamic heterogeneity rather than an uninteresting source such as finite trajectory length data. This was tested by performing an ILT on each individual SM trajectory's stretched exponential fit i.e. the β and τ_{fit} parameters for each SM. SM ILTs were then summed to create an ensemble ILT distribution. This distribution was directly compared to the ILT distribution produced from β_{QE}. The distributions closely resembled one another with just a small mismatch. We hypothesize this mismatch is a result of fitting SM ACFs with a 2 parameter stretched exponential function, which can create an imperfect fit especially for noisy SM ACFs. Despite

the small mismatch, the overall similar shape of the constructed ILT to that obtained from the ensemble stretched exponential function supports the distribution of measured relaxations as truly reflecting system dynamic heterogeneity.

4.5 Summary

This study presents a rotational single molecule data of a perylene diimide probe in PS near the glass transition temperature. The temperature dependence of the single molecule median rotational relaxation times follows that of PS according to the VFT equation, and the relaxation rates are slower by ~0.4 decades, as expected based on the size of the probe. The distributions of relaxation times, τ_{fit} and τ_c, for each temperature span 1.5 decades indicating the probes' ability to sample the spatially heterogeneous dynamics present in PS near the glass transition. A combined distribution of stretching exponents for all temperatures is centered at $\beta = 0.63$ and similarly $\beta_{QE} = 0.58$, another indicator that the heterogeneous nature of the host has been successfully reported by the probes Based on previous studies that suggest that the fastest rotating probes report a larger breadth of relaxation times and subsequently lower median stretching exponents, the probe employed in this study appears to be approaching the limit in which all heterogeneity is reported, given the similarity of stretching exponents measured here to those obtained from dielectric measurements. We also investigated the correlation of τ_{fit} and τ_c values with their associated β values and found that the fastest probes (indicated by τ_{fit}) taken from the full distribution of relaxation times report the lowest stretching exponents, indicating the fastest molecules are able to sample the greatest breadth of dynamics in space and time. Moreover, based on the dynamic range of our sampling rate, our ability to monitor the fastest

rotating molecules is predicated on the fact that they must be exhibiting fluctuations in dynamics into slower regimes during the SM trajectory's lifetime. This is an interesting consequence of single molecule probe data collection in supercooled liquids and a deeper investigation would be appropriate to understand the true origin of the lowest stretching exponents for a given distribution of SM data. Finally, a highly mobile layer containing translating single molecules has been observed in 100 nm films in the temperature regime where rotational molecules are observed. This is the first report of this behavior for a film of this thickness. This finding sets the stage for more SM studies in PS to be conducted in confined systems that employs multiple probes of different size and spans a a wider temperature range,above and below T_g.

Summary

We have presented single molecule (SM) fluorescence study methods and results in supercooled glycerol, ortho-terphenyl (OTP), and polystyrene (PS) using a variety of perylene diimide (PDI) probes. We first introduce the concept of highly viscous glassy systems and the idea that the underlying dynamics of these systems are spatially heterogeneous. By interrogating these dynamics using the SM techniques we have developed, we have uncovered many interesting details about the dynamics near the glass transition temperature of (T_g) supercooled liquids.

First, we presented data collected from three PDI fluorescent probes in supercooled glycerol. For all probes, the average rotational relaxation times (τ_c) obtained from many individual single molecule (SM) trajectories mirrored the temperature dependence of glycerol's viscosity. This upholds the assumption that probe rotations, on average, report the dynamics of the host. Upon investigation of distributions of SM τ_c values for each probe, we show that each

has a wide distribution indicating that all probes report the spatially heterogeneous dynamics of the host. The comparison of the dynamics of three different probes allowed us to investigate the effect of probe size, polarity and structure. We found that the rotational correlation times were correlated with the probe polarity where the least polar probe rotated the fastest. We believe this is due to the fact that the least polar probe has the least amount of dipole intermolecular interactions and was able to rotate the most freely being surrounded by glycerol molecules. Temporal heterogeneity was also investigated on short times scales using a window shifting technique[17] and ~ 30% of molecules was characterized as heterogeneous on these time scales. Heterogeneity on long time scales (10^5 – 10^6 times the structural relaxation) was also investigated and no evidence of temporal heterogeneity was found on these time scales. We conclude that exchange times detected by window shifting techniques are an upper bound on timescales in which exchange occurs.

Given that we believe that the probe polarity plays an important role in dictating the probe rotational rate and therefore its ability to report heterogeneity of the system, we were motivated to investigate a nonpolar glass former, OTP, to test this claim. We presented the data from three PDI probes, two of which were used in glycerol SM studies. As we saw in glycerol, the probes had the same temperature dependence as OTP's viscosity and structural relaxation. Upon examining the SM correlation times, each probe's data showed a wide distribution indicating each reported the heterogeneity of the system. As in glycerol, the widest distribution of relaxation times in OTP arose from the fastest rotating probe. This suggests that only a part of the full range of dynamic exchange that occurs is on probe rotational correlation time scales. In OTP, the fastest probe is also the smallest probe, demonstrating that the lack of strong probe-host intermolecular interactions allows probes to rotate based on the size (and structure) alone. This

study confirms findings from glycerol that suggest dynamic exchange is occurring on or below probe rotational time scales. This study also demonstrated how probe-dependent studies can help uncover the regime in which effects of temporal averaging start to occur, which is important to consider when using probes to investigate dynamic heterogeneity within glassy system.

Finally, we turned to investigating PS using single molecule techniques. When confined to films that are < 100 nm, PS has been shown to contain a mobile surface layer. We set out to investigate the nature of the heterogeneity in "bulk" PS films with the intention of moving to thinner confined films to investigate the details of dynamics within the mobile, surface region. We present the data from a PDI probe in 100 nm thick supercooled PS film. We found that the PDI probes mirror the temperature dependence of the structural relaxation of the host PS, and we on average only 0.4 decades slower than PS. This small difference in probe and host dynamics suggests that the probe is able to report a very close representation of the host dynamic heterogeneity. The distributions of rotational relaxation times spanned 1.5 decades, the widest breadth of relaxation times observed for SM studies to date, indicating the probes' ability to sample the heterogeneous dynamics present in PS near the glass transition. The median of all SM stretching exponents was 0.63, which lies very close to stretching exponents reported by dielectric measurements. Based on the findings of SM studies of glycerol and OTP, this probe appears to be approaching the limit of heterogeneity that is able to be reported by SM probes. Additional investigation was conducted to evaluate the correlation between rotational relaxation times (τ_{fit} and τ_c) and stretching exponent and trajectory length. We found that the fastest probes for a given temperature had the lowest stretching exponent values suggesting the fastest molecules have the ability to report the greatest breadth of dynamics. Moreover, we found that probes with the longest trajectory lengths also have the lowest stretching exponents, indicating

the longest lived molecules have the opportunity to experience the most dynamic exchange events within the sample. Finally, we present observation of a highly mobile layer containing translating molecules in the 100 nm thick PS films under investigation. This is the first report of a mobile surface region in films of this thickness. This discovery is a nice start to the systematic investigation of mobile layers in confined polymer films via SM techniques.

Our work presents evidence for spatially heterogeneous dynamics in a variety of supercooled systems. We have determined the capabilities and limitations of SM microscopy as a technique to study heterogeneity as a function of probe identity, probe rotational rate, probe-host interactions, and SM trajectory lengths. In the future, we will be able to tailor the probe to most accurately interrogate the features of dynamic heterogeneity we want to investigate within a supercooled system. In sum, this work will allow for a deeper understanding of physical picture of polymer systems under confinement. This work will allow the origin of limitations of these systems to be know when utilizing them in applications and commercialization.

References

(1) Debenedetti, P. G.; Stillinger, F. H. Supercooled Liquids and the Glass Transition. *Nature* **2001**, *410*, 259–267.

(2) Ediger, M. D. Spatially Heterogeneous Dynamics in Supercooled Liquids. *Annu. Rev. Phys. Chem.* **2000**, *51*, 99–128.

(3) Angell, C. A. Formation of Glasses from Liquids and Biopolymers. *Science (80-.).* **1995**, *267*, 1924–1935.

(4) Ediger, M. D.; Nagel, S. R. Supercooled Liquids and Glasses. *J. Phys. Chem.* **1996**, *100*, 13200–13212.

(5) Richert, R.; Israeloff, N.; Alba-Simionesco, C.; Ladieu, F.; L'Hote, D. Experimental Approaches to Heterogeneous Dynamics. In *Dynamical Heterogeneity in Glasses , Colloids and Granular Media*; 2011; pp. 152–201.

(6) Richert, R. Heterogeneous Dynamics in Liquids : Fluctuations in Space and Time. *J. Phys. Condens. Matter* **2002**, *14*, R703–R738.

(7) Adam, G.; Gibbs, J. H. On the Temperature Dependence of Cooperative Relaxation Properties in Glass-Forming Liquids. *J. Chem. Phys.* **1965**, *43*, 139–146.

(8) Bouchaud, J.-P.; Biroli, G. On the Adam-Gibbs-Kirkpatrick-Thirumalai-Wolynes Scenario for the Viscosity Increase in Glasses. *J. Chem. Phys.* **2004**, *121*, 7347–7354.

(9) Xia, X.; Wolynes, P. Microscopic Theory of Heterogeneity and Nonexponential Relaxations in Supercooled Liquids. *Phys. Rev. Lett.* **2001**, *86*, 5526–5529.

(10) Sillescu, H.; Böhmer, R.; Diezemann, G.; Hinze, G. Heterogeneity at the Glass Transition: What Do We Know? *J. Non. Cryst. Solids* **2002**, *307-310*, 16–23.

(11) Böhmer, R.; Chamberlin, R. V.; Diezemann, G.; Geil, B.; Heuer, a.; Hinze, G.; Kuebler, S. C.; Richert, R.; Schiener, B.; Sillescu, H.; et al. Nature of the Non-Exponential Primary Relaxation in Structural Glass-Formers Probed by Dynamically Selective Experiments. *J. Non. Cryst. Solids* **1998**, *235-237*, 1–9.

(12) Kaufman, L. J. Heterogeneity in Single-Molecule Observables in the Study of Supercooled Liquids. *Annu. Rev. Phys. Chem.* **2013**, *64*, 177–200.

(13) Deschenes, L. A.; Bout, D. A. Vanden. Heterogeneous Dynamics and Domains in Supercooled O -Terphenyl : A Single Molecule Study. *J. Phys. Chem. B* **2002**, *106*, 11438–11445.

(14) Zondervan, R.; Kulzer, F.; Berkhout, G. C. G.; Orrit, M. Local Viscosity of Supercooled Glycerol near Tg Probed by Rotational Diffusion of Ensembles and Single Dye Molecules. *Proc. Natl. Acad. Sci. U. S. A.* **2007**, *104*, 12628–12633.

(15) Mackowiak, S. A.; Herman, T. K.; Kaufman, L. J. Spatial and Temporal Heterogeneity in Supercooled Glycerol: Evidence from Wide Field Single Molecule Imaging. *J. Chem. Phys.* **2009**, *131*, 244513.

(16) Mackowiak, S. A.; Leone, L. M.; Kaufman, L. J. Probe Dependence of Spatially Heterogeneous Dynamics in Supercooled Glycerol as Revealed by Single Molecule Microscopy. *Phys. Chem. Chem. Phys.* **2011**, *13*, 1786–1799.

(17) Schob, A.; Cichos, F.; Schuster, J.; von Borczyskowski, C. Reorientation and Translation of Individual Dye Molecules in a Polymer Matrix. *Eur. Polym. J.* **2004**, *40*, 1019–1026.

(18) Paeng, K.; Kaufman, L. J. Single Molecule Rotational Probing of Supercooled Liquids. *Chem. Soc. Rev.* **2014**, *43*, 977–989.

(19) Lu, C.-Y.; Vanden Bout, D. A. Effect of Finite Trajectory Length on the Correlation Function Analysis of Single Molecule Data. *J. Chem. Phys.* **2006**, *125*, 124701.

(20) Mackowiak, S. A.; Kaufman, L. J. When the Heterogeneous Appears Homogeneous: Discrepant Measures of Heterogeneity in Single Molecule Observables. *J. Phys. Chem. Lett.* **2011**, *2*, 438–442.

(21) Lu, C.-Y.; Vanden Bout, D. A. Analysis of Orientational Dynamics of Single Fluorophore Trajectories from Three-Angle Polarization Experiments. *J. Chem. Phys.* **2008**, *128*, 244501.

(22) Wei, C.-Y.; Kim, Y.; Darst, R.; Rossky, P.; Vanden Bout, D. A. Origins of Nonexponential Decay in Single Molecule Measurements of Rotational Dynamics. *Phys. Rev. Lett.* **2005**, *95*, 173001.

(23) Bingemann, D.; Allen, R. M.; Olesen, S. W. Single Molecules Reveal the Dynamics of Heterogeneities in a Polymer at the Glass Transition. *J. Chem. Phys.* **2011**, *134*, 024513.

(24) Adhikari, S.; Selmke, M.; Cichos, F. Temperature Dependent Single Molecule Rotational Dynamics in PMA. *Phys. Chem. Chem. Phys.* **2011**, *13*, 1849–1856.

(25) Cicerone, M. T.; Ediger, M. D. Relaxation of Spatially Heterogeneous Dynamic Domains in Supercooled Ortho-Terphenyl. *J. Chem. Phys.* **1995**, *103*, 5684–5692.

(26) Böhmer, R.; Hinze, G.; Diezemann, G.; Geil, B.; Sillescu, H. Dynamic Heterogeneity in Supercooled Ortho-Terphenyl Studied by Multidimensional Deuteron NMR. *Eur. Lett.* **1996**, *36*, 55–60.

(27) Wang, C.; Ediger, M. D. How Long Do Regions of Different Dynamics Persist in Supercooled O -Terphenyl? *J. Phys. Chem. B* **1999**, *103*, 4177–4184.

(28) Ediger, M. D. Spatially Heterogeneous Dynamics in Supercooled Liquids. *Annual* **2000**, *128*, 99–128.

(29) Angell, C. A. Relaxation in Liquids, Polymers and Plastic Crystals - Strong/fragile Patterns and Problems. *J. Non-Cryst. Sol.* **1991**, *133*, 13–31.

(30) Roth, C. B.; Pound, A.; Kamp, S. W.; Murray, C. A.; Dutcher, J. R. Molecular-Weight Dependence of the Glass Transition Temperature of Freely-Standing Poly(methyl Methacrylate) Films. *Eur. Phys. J. E. Soft Matter* **2006**, *20*, 441–448.

(31) Alcoutlabi, M.; McKenna, G. B. Effects of Confinement on Material Behaviour at the Nanometre Size Scale. *J. Phys. Condens. Matter* **2005**, *17*, R461–R524.

(32) Ellison, C. J.; Torkelson, J. M. The Distribution of Glass-Transition Temperatures in Nanoscopically Confined Glass Formers. *Nat. Mater.* **2003**, *2*, 695–700.

(33) Ellison, C. J.; Mundra, M. K.; Torkelson, J. M. Impacts of Polystyrene Molecular Weight and Modification to the Repeat Unit Structure on the Glass Transition - Nanoconfinement Effect and the Cooperativity Length Scale. *Macromolecules* **2005**, *38*, 1767–1778.

(34) Forrest, J. A.; Dalnoki-Veress, K. The Glass Transition in Thin Polymer Films. *Adv. Colloid Interface Sci.* **2001**, *94*, 167–196.

(35) Keddie, J. L.; Jones, R. A. L.; Cory, R. A. Size-Dependent Depression of the Glass Transition Temperature in Polymer Films. *Eur. Polym. J.* **1994**, *27*, 59–64.

(36) Liem, H.; Cabanillas-Gonzalez, J.; Etchegoin, P.; Bradley, D. D. C. Glass Transition Temperatures of Polymer Thin Films Monitored by Raman Scattering. *J. Phys. Condens. Matter* **2004**, *16*, 721–728.

(37) Kim, J. H.; Jang, J.; Zin, W.-C. Thickness Dependence of the Glass Transition Temperature in Thin Polymer Films. *Langmuir* **2001**, *17*, 2703–2710.

(38) Lupaşcu, V.; Picken, S. J.; Wübbenhorst, M. Cooperative and Non-Cooperative Dynamics in Ultra-Thin Films of Polystyrene Studied by Dielectric Spectroscopy and Capacitive Dilatometry. *J. Non. Cryst. Solids* **2006**, *352*, 5594–5600.

(39) Keddie, J. L.; Jones, R. A. L.; Cory, R. A. Temperature in Thin Polymer Films. *Faraday Discuss.* **1994**, *98*, 219–230.

(40) Dalnoki-Veress, K.; Forrest, J.; Murray, C.; Gigault, C.; Dutcher, J. Molecular Weight Dependence of Reductions in the Glass Transition Temperature of Thin, Freely Standing Polymer Films. *Phys. Rev. E* **2001**, *63*, 031801.

(41) DeMaggio, G.; Frieze, W.; Gidley, D.; Zhu, M.; Hristov, H.; Yee, a. Interface and Surface Effects on the Glass Transition in Thin Polystyrene Films. *Phys. Rev. Lett.* **1997**, *78*, 1524–1527.

(42) Forrest, J.; Dalnoki-Veress, K.; Dutcher, J. Brillouin Light Scattering Studies of the Mechanical Properties of Thin Freely Standing Polystyrene Films. *Phys. Rev. E* **1998**, *58*, 6109–6114.

(43) Fukao, K.; Miyamoto, Y. Glass Transitions and Dynamics in Thin Polymer Films: Dielectric Relaxation of Thin Films of Polystyrene. *Phys. Rev. E* **2000**, *61*, 1743–1754.

(44) Kim, S.; Roth, C. B.; Torkelson, J. M. Effect of Nanoscale Confinement on the Glass Transition Temperature of Free-Standing Polymer Films : Novel, Self-Referencing Fluorescence Method. *J. Polym. Sci. Part B Polym. Phys.* **2008**, *46*, 2754–2764.

(45) Roth, C. B.; Dutcher, J. R. Glass Transition Temperature of Freely-Standing Films of Atactic Poly (Methyl Methacrylate). *Eur. Phys. J. E.* **2003**, *12*, S103–S107.

(46) Fryer, D. S.; Peters, R. D.; Kim, E. J.; Tomaszewski, J. E.; Pablo, J. J. De; Nealey, P. F.; White, C. C.; Wu, W. Dependence of the Glass Transition Temperature of Polymer Films on Interfacial Energy and Thickness. *Macromolecules* **2001**, *34*, 5627–5634.

(47) Roth, C. B.; McNerny, K. L.; Jager, W. F.; Torkelson, J. M. Eliminating the Enhanced Mobility at the Free Surface of Polystyrene: Fluorescence Studies of the Glass Transition

Temperature in Thin Bilayer Films of Immiscible Polymers. *Macromolecules* **2007**, *40*, 2568–2574.

(48) Prucker, O.; Christian, S.; Bock, H.; Ruhe, J.; Frank, C. W.; Knoll, W. On the Glass Transition in Ultrathin Polymer Films of Different Molecular Architecture. *Macromol. Chem. Phys.* **1998**, *199*, 1435–1444.

(49) Mundra, M. K.; Ellison, C. J.; Behling, R. E.; Torkelson, J. M. Confinement, Composition, and Spin-Coating Effects on the Glass Transition and Stress Relaxation of Thin Films of Polystyrene and Styrene-Containing Random Copolymers: Sensing by Intrinsic Fluorescence. *Polymer (Guildf).* **2006**, *47*, 7747–7759.

(50) Jiang, X.; Zheng, C.; Tanaka, K.; Takahara, A. Effect of Chain End Group on Surface Glass Transition Temperature of Thin Polymer Film. *Phys. Lett. A* **2001**, *281*, 363–367.

(51) Böhmer, T. R.; de Pablo, J. J. Evidence for Size-Dependent Mechanical Properties from Simulations of Nanoscopic Polymeric Structures. *J. Chem. Phys.* **2002**, *116*, 9939–9951.

(52) Cao, H. B.; Nealey, P. F.; Domke, W.-D. Comparison of Resist Collapse Properties for Deep Ultraviolet and 193 Nm Resist Platforms. *J. Vac. Sci. Technol. B* **2000**, *18*, 3303–3307.

(53) Stoykovich, M. P.; Cao, H. B.; Yoshimoto, K.; Ocola, L. E.; Nealey, P. F. Deformation of Nanoscopic Polymer Structures in Response to Well-Defined Capillary Forces. *Adv. Mater.* **2003**, *15*, 1180–1184.

(54) Workum, K. Van; de Pablo, J. J. Computer Simulation of the Mechanical Nanostructures. *Nano Lett.* **2003**, *3*, 1405–1410.

(55) Forrest, J. A. A Decade of Dynamics in Thin Films of Polystyrene: Where Are We Now? *Eur. Phys. J E* **2002**, *8*, 261–266.

(56) Roth, C. B.; Dutcher, J. R. Glass Transition and Chain Mobility in Thin Polymer Films. *J. Electroanal. Chem.* **2005**, *584*, 13–22.

(57) Tanaka, K.; Tateishi, Y.; Okada, Y.; Nagamura, T.; Doi, M.; Morita, H. Interfacial Mobility of Polymers on Inorganic Solids. *J. Phys. Chem. B* **2009**, *113*, 4571–4577.

(58) Wu, W.; Zanten, J. H. Van; William, J. O. Film Thickness Dependent Thermal Expansion in Ultrathin Poly(methyl Methacrylate) Films on Silicon. *Macromolecules* **1995**, *28*, 771–774.

(59) Park, C. H.; Kim, J. H.; Ree, M.; Sohn, B.-H.; Jung, J. C.; Zin, W.-C. Thickness and Composition Dependence of the Glass Transition Temperature in Thin Random Copolymer Films. *Polymer (Guildf).* **2004**, *45*, 4507–4513.

(60) Zanten, J. H. Van; Wallace, W. E.; Wu, W. Favorable Substrate Interactions. *Phys. Rev. E* **1996**, *53*, 2053–2056.

(61) Chai, Y.; Salez, T.; McGraw, J. D.; Benzaquen, M.; Dalnoki-Veress, K.; Raphaël, E.; Forrest, J. A. A Direct Quantitative Measure of Surface Mobility in a Glassy Polymer. *Science* **2014**, *343*, 994–999.

(62) Kajiyama, T.; Tanaka, K.; Takahara, A. Surface Molecular Motion of the Monodisperse Polystyrene Films. *Macromolecules* **1997**, *30*, 280–285.

(63) Priestley, R. D.; Ellison, C. J.; Broadbelt, L. J.; Torkelson, J. M. Structural Relaxation of Polymer Glasses at Surfaces, Interfaces, and in Between. *Science* **2005**, *309*, 456–459.

(64) Kim, S.; Torkelson, J. M. Distribution of Glass Transition Temperatures in Free-Standing, Nanoconfined Polystyrene Films: A Test of de Gennes' Sliding Motion Mechanism. *Macromolecules* **2011**, *44*, 4546–4553.

(65) Oba, T.; Vacha, M. Relaxation in Thin Polymer Films Mapped across the Film Thickness by Astigmatic Single-Molecule Imaging. *ACS Macro Lett.* **2012**, *1*, 784–788.

(66) Paeng, K.; Richert, R.; Ediger, M. D. Molecular Mobility in Supported Thin Films of Polystyrene, Poly(methyl Methacrylate), and poly(2-Vinyl Pyridine) Probed by Dye Reorientation. *Soft Matter* **2012**, *8*, 819.

(67) Paeng, K.; Swallen, S. F.; Ediger, M. D. Direct Measurement of Molecular Motion in Freestanding Polystyrene Thin Films. *J. Am. Chem. Soc.* **2011**, *133*, 8444–8447.

(68) Priestley, R.; Broadbelt, L.; Torkelson, J.; Fukao, K. Glass Transition and A-Relaxation Dynamics of Thin Films of Labeled Polystyrene. *Phys. Rev. E* **2007**, *75*, 061806.

(69) Dhinojwala, A.; Wong, G. K.; Torkelson, J. M. Rotational Reorientation Dynamics of Disperse Red 1 in Polystyrene: A -Relaxation Dynamics Probed by Second Harmonic Generation and Dielectric Relaxation. *J. Chem. Phys.* **1994**, *100*, 6046–6053.

(70) Yang, Z.; Fujii, Y.; Lee, F. K.; Lam, C.-H.; Tsui, O. K. C. Glass Transition Dynamics and Surface Layer Mobility in Unentangled Polystyrene Films. *Science* **2010**, *328*, 1676–1679.

(71) Oba, T.; Vacha, M. Relaxation in Thin Polymer Films Mapped across the Film Thickness by Astigmatic Single-Molecule Imaging. *ACS Macro Lett.* **2012**, *1*, 784–788.

(72) Flier, B. M. I.; Baier, M. C.; Huber, J.; Müllen, K.; Mecking, S.; Zumbusch, A.; Wöll, D. Heterogeneous Diffusion in Thin Polymer Films as Observed by High-Temperature Single-Molecule Fluorescence Microscopy. *J. Am. Chem. Soc.* **2012**, *134*, 480–488.

(73) Zheng, Z.; Li, D.; Yang, J.; Zhao, J. Segmental Dynamics near the Chain End of Polystyrene in Its Ultrathin Films: A Study by Single-Molecule Fluorescence de-Focus Microscopy. *Sci. China Chem.* **2014**, *57*, 389–396.

(74) Zondervan, R.; Xia, T.; van der Meer, H.; Storm, C.; Kulzer, F.; van Saarloos, W.; Orrit, M. Soft Glassy Rheology of Supercooled Molecular Liquids. *Proc. Natl. Acad. Sci. U. S. A.* **2008**, *105*, 4993–4998.

(75) Xia, T.; Xiao, L.; Orrit, M. Micron-Sized Structure in a Thin Glycerol Film Revealed by Fluorescent Probes. *J. Phys. Chem. B* **2009**, *113*, 15724–15729.

(76) Cicerone, M. T.; Ediger, M. D. Enhanced Translation of Probe Molecules in Supercooled O-Terphenyl: Signature of Spatially Heterogeneous Dynamics? *J. Chem. Phys.* **1996**, *104*, 7210–7218.

(77) Cicerone, M. T.; Blackburn, F. R.; Ediger, M. D. How Do Molecules Move near Tg? Molecular Rotation of Six Probes in O-Terphenyl across 14 Decades in Time. *J. Chem. Phys.* **1995**, *102*, 471–479.

(78) Heuberger, G.; Sillescu, H. Size Dependence of Tracer Diffusion in Supercooled Liquids. *J. Phys. Chem.* **1996**, *100*, 15255–15260.

(79) Kowert, B. A.; Sobush, K. T.; Fuqua, C. F.; Mapes, C. L.; Jones, J. B.; Zahm, J. A. Size-Dependent Diffusion in the N -Alkanes. *J. Phys. Chem. A.* **2003**, *107*, 4790–4795.

(80) Cicerone, M. T.; Ediger, M. D. Relaxation of Spatially Heterogeneous Dynamic Domains in Supercooled Ortho-Terphenyl. *J. Chem. Phys.* **1995**, *103*, 5684–5692.

(81) Blackburn, F. R.; Wang, C.; Ediger, M. D. Translational and Rotational Motion of Probes in Supercooled 1,3,5-Tris (Naphthyl) Benzene. *J. Phys. Chem.* **1996**, *100*, 18249–18257.

(82) Blackburn, F. R.; Cicerone, M. T.; Hietpas, G.; Wagner, P. a.; Ediger, M. D. Cooperative Motion in Fragile Liquids near the Glass Transition: Probe Reorientation in O-Terphenyl and Polystyrene. *J. Non. Cryst. Solids* **1994**, *172-174*, 256–264.

(83) Rajian, J. R.; Quitevis, E. L. Translational Diffusion in Sucrose Benzoate near the Glass Transition : Probe Size Dependence in the Breakdown of the Stokes-Einstein Equation. *J. Chem. Phys.* **2007**, *126*, 224506.

(84) Qi, F.; El Goresy, T.; Böhmer, T. R.; Döß, A.; Diezemann, G.; Hinze, G.; Sillescu, H.; Blochowicz, T.; Gainaru, C.; Rössler, E.; et al. Nuclear Magnetic Resonance and Dielectric Spectroscopy of a Simple Supercooled Liquid: 2-Methyl Tetrahydrofuran. *J. Chem. Phys.* **2003**, *118*, 7431–7438.

(85) Chang, I.; Sillescu, H. Heterogeneity at the Glass Transition: Translational and Rotational Self-Diffusion. *J. Phys. Chem. B* **1997**, *101*, 8794–8801.

(86) Wang, L.-M.; Richert, R. Exponential Probe Rotation in Glass-Forming Liquids. *J. Chem. Phys.* **2004**, *120*, 11082–11089.

(87) Huang, W.; Richert, R. Dielectric Study of Probe Rotation in Viscous Liquids. *Philos. Mag.* **2007**, *87*, 371–382.

(88) Gelin, M. F.; Kosov, D. S. What Can Be Learned about Molecular Reorientation from Single Molecule Polarization Microscopy? *J. Chem. Phys.* **2006**, *125*, 054708.

(89) Hinze, G.; Diezemann, G.; Basché, T. Rotational Correlation Functions of Single Molecules. *Phys. Rev. Lett.* **2004**, *93*, 203001.

(90) Wei, C. J.; Lu, C.; Kim, Y. H.; Bout, D. A. Vanden. Determining If a System Is Heterogeneous: The Analysis of Single Molecule Rotational Correlation Functions and Their Limitations. *J. Fluoresc.* **2007**, *17*, 797–804.

(91) Bingemann, D. Analysis of "blinking" or "hopping" Single Molecule Signals with a Limited Number of Transitions. *Chem. Phys. Lett.* **2006**, *433*, 234–238.

(92) Robbins, M. S.; Member, S.; Hadwen, B. J. The Noise Performance of Electron Multiplying Charge-Coupled Devices. *IEEE Trans. Electron Devices* **2003**, *50*, 1227–1232.

(93) Dries, T.; Fujara, F.; Kiebel, M.; Rössler, E.; Sillescu, H. 2H-NMR Study of the Glass Transition in Supercooled Ortho-Terphenyl. *J. Chem. Phys.* **1988**, *88*, 2139–2147.

(94) Stillinger, F. H.; Hodgdon, J. A. Translation-Rotation Paradox for Diffusion in Fragile Glass-Forming Liquids. *Phys. Rev. E* **1994**, *50*, 2064–2068.

(95) Stickel, F.; Fischer, E. W.; Richert, R. Dynamics of Glass-Forming Liquids. II. Detailed Comparison of Dielectric Relaxation, Dc-Conductivity, and Viscosity Data. *J. Chem. Phys.* **1996**, *104*, 2043–2055.

(96) Chemie, O.; Miinchen, U. Cyclic Carboxylic Imide Structures as Structure Elements of High Stability. Novel Developments in Perylene Dye Chemistry. *Heterocycles* **1995**, *40*, 477–500.

(97) Rademacher, A.; Langhals, S. M. H.; I, A. R.; Markle, S. Losliche Perylen-Fluoreszenzfarbstoffe Rnit Hoher Photostabilitiit. *Chem. Ber.* **1982**, *115*, 2927–2934.

(98) Langhals, H. Spectroscopic Studies of Fluorescent Perylene Dyes. *Spectrochim. Acta* **1991**, *4*, 857–861.

(99) Schröter, K.; Donth, E. Viscosity and Shear Response at the Dynamic Glass Transition of Glycerol. *J. Chem. Phys.* **2000**, *113*, 9101–9108.

(100) Hall, D. B.; Hamilton, K. E.; Miller, R. D.; Torkelson, J. M. Translational and Rotational Diffusion of Probe Molecules in Polymer Films near. *Macromolecules* **1999**, *32*, 8052–8058.

(101) Wu, L.; Nagel, S. R. Secondary Relaxation in O-Terphenyl Glass. *Phys. Rev. B* **1992**, *46*, 198–200.

(102) Montroll, E. W.; Shlesinger, M. F. On 1/f Noise and Other Distributions with Long Tails. *Proc. Natl. Acad. Sci. U. S. A.* **1982**, *79*, 3380–3383.

(103) Provencher, S. W. CONTIN: A General Purpose Constrained Regularization Program for Inverting Noisy Linear Algebraic and Integral Equations. *Comput. Phys. Commun.* **1982**, *27*, 229–242.

(104) Alvarez, F.; Alegra, A.; Colmenero, J. Relationship between the Time-Domain Kohlrausch-Williams-Watts and Frequency-Domain Havriliak-Negami Relaxation Functions. *Phys. Rev. B.* **1991**, *44*, 7306–7312.

(105) Schob, A.; Cichos, F.; Schuster, J.; Von Borczyskowski, C. Reorientation and Translation of Individual Dye Molecules in a Polymer Matrix. *Eur. Polym. J.* **2004**, *40*, 1019–1026.

(106) Jung, Y.; Garrahan, J. P.; Chandler, D. Dynamical Exchanges in Facilitated Models of Supercooled Liquids. *J. Chem. Phys.* **2005**, *123*, 084509.

(107) Möbius, M. E.; Xia, T.; van Saarloos, W.; Orrit, M.; van Hecke, M. Aging and Solidification of Supercooled Glycerol. *J. Phys. Chem. B* **2010**, *114*, 7439–7444.

(108) Leone, L. M.; Kaufman, L. J. Single Molecule Probe Reports of Dynamic Heterogeneity in Supercooled Ortho-Terphenyl. *J. Chem. Phys.* **2013**, *138*, 12A524.

(109) Herman, T. K.; Mackowiak, S. A.; Kaufman, L. J. High Power Light Emitting Diode Based Setup for Photobleaching Fluorescent Impurities. *Rev. Sci. Instrum.* **2009**, *80*, 016107.

(110) Laughlin, W. T.; Uhlmann, D. R. Flow in Simple Organic Liquids. *J. Phys. Chem.* **1972**, *78*, 2317–2325.

(111) Richert, R. On the Dielectric Susceptibility Spectra of Supercooled O-Terphenyl. *J. Chem. Phys.* **2005**, *123*, 154502.

(112) Olsen, N.; Christensen, T.; Dyre, J. Time-Temperature Superposition in Viscous Liquids. *Phys. Rev. Lett.* **2001**, *86*, 1271–1274.

(113) Reinsberg, S. A.; Heuer, A.; Doliwa, B.; Zimmermann, H.; Spiess, H. W. Comparative Study of the NMR Length Scale of Dynamic Heterogeneities of Three Different Glass Formers. *J. Non. Cryst. Solids* **2002**, *307-310*, 208–214.

(114) Schiener, B.; Chamberlin, R. V.; Diezemann, G.; Böhmer, R. Nonresonant Dielectric Hole Burning Spectroscopy of Supercooled Liquids. *J. Chem. Phys.* **1997**, *107*, 7746–7761.

(115) Ashtekar, S.; Lyding, J.; Gruebele, M. Temperature-Dependent Two-State Dynamics of Individual Cooperatively Rearranging Regions on a Glass Surface. *Phys. Rev. Lett.* **2012**, *109*, 166103.

(116) Richert, R. On the Dielectric Susceptibility Spectra of Supercooled O-Terphenyl. *J. Chem. Phys.* **2005**, *123*, 154502.

(117) Matter, P. B.; Fujara, F.; Geip, B.; Sillescu, H.; Fleischer, G. Condensed Translational and Rotational Diffusion in Supercooled Orthoterphenyl close to the Glass Transition. *Z. Phys. B Condens. Matter* **1992**, *204*, 195–204.

(118) Mapes, M. K.; Swallen, S. F.; Ediger, M. D. Self-Diffusion of Supercooled O-Terphenyl near the Glass Transition Temperature. *J. Phys. Chem. B* **2006**, *110*, 507–511.

(119) Grebenkin, S. Y.; Bol'shakov, B. V. Rotational Mobility of Guest Molecules in O-Terphenyl below T(g). *J. Phys. Chem. B* **2006**, *110*, 8582–8586.

(120) Wöll, D.; Braeken, E.; Deres, A.; De Schryver, F. C.; Uji-i, H.; Hofkens, J. Polymers and Single Molecule Fluorescence Spectroscopy, What Can We Learn? *Chem. Soc. Rev.* **2009**, *38*, 313–328.

(121) Kulzer, F.; Xia, T.; Orrit, M. Single Molecules as Optical Nanoprobes for Soft and Complex Matter. *Angew. Chem. Int. Ed. Engl.* **2010**, *49*, 854–866.

(122) Vacha, M.; Habuchi, S. Conformation and Physics of Polymer Chains: A Single-Molecule Perspective. *NPG Asia Mater.* **2010**, *2*, 134–142.

(123) Huang, B.; Wang, W.; Bates, M.; Zhuang, X. Three-Dimensional Super-Resolution Imaging by Stochastic Optical Reconstruction Microscopy. *Science* **2008**, *319*, 810–813.

(124) Uji-I, H.; Melnikov, S. M.; Deres, A.; Bergamini, G.; De Schryver, F.; Herrmann, A.; Mullen, K.; Enderlein, J.; Hofkens, J. Visualizing Spatial and Temporal Heterogeneity of Single Molecule Rotational Diffusion in a Glassy Polymer by Defocused Wide-Field Imaging. *Polymer (Guildf).* **2006**, *47*, 2511–2518.

(125) Deres, A.; Floudas, G. a.; Müllen, K.; Van der Auweraer, M.; De Schryver, F.; Enderlein, J.; Uji-i, H.; Hofkens, J. The Origin of Heterogeneity of Polymer Dynamics near the Glass Temperature As Probed by Defocused Imaging. *Macromolecules* **2011**, *44*, 9703–9709.

(126) Hinze, G.; Basché, T.; Vallée, R. a L. Single Molecule Probing of Dynamics in Supercooled Polymers. *Phys. Chem. Chem. Phys.* **2011**, *13*, 1813–1818.

(127) Zheng, F.; Zuo, B.; Zhu, Y.; Yang, J.; Wang, X. Probing Substrate Effects on Relaxation Dynamics of Ultrathin Poly(vinyl Acetate) Films by Dynamic Wetting of Water Droplets on Their Surfaces. *Soft Matter* **2013**, *9*, 11680.

(128) Habuchi, S.; Satoh, N.; Yamamoto, T.; Tezuka, Y.; Vacha, M. Multimode Diffusion of Ring Polymer Molecules Revealed by a Single-Molecule Study. *Angew. Chem. Int. Ed. Engl.* **2010**, *49*, 1418–1421.

(129) Tomczak, N.; Vallée, R. a L.; van Dijk, E. M. H. P.; Kuipers, L.; van Hulst, N. F.; Vancso, G. J. Segment Dynamics in Thin Polystyrene Films Probed by Single-Molecule Optics. *J. Am. Chem. Soc.* **2004**, *126*, 4748–4749.

(130) Braeken, E.; De Cremer, G.; Marsal, P.; Pèpe, G.; Müllen, K.; Vallée, R. a L. Single Molecule Probing of the Local Segmental Relaxation Dynamics in Polymer above the Glass Transition Temperature. *J. Am. Chem. Soc.* **2009**, *131*, 12201–12210.

(131) Biju, V. P.; Ye, J. Y.; Ishikawa, M. Spatial Heterogeneity in a Polymer Thin Film Probed by Single Molecules. *J. Phys. Chem. B* **2003**, *107*, 10729–10735.

(132) Ye, J. Y.; Ishikawa, M.; Yogi, O.; Okada, T.; Maruyama, Y. Bimodal Site Distribution of a Polymer Film Revealed by Flexible Single-Molecule Probes. *Chem. Phys. Lett.* **1998**, *288*, 885–890.

(133) Vallée, R. Molecular Fluorescence Lifetime Fluctuations: On the Possible Role of Conformational Effects. *Chem. Phys. Lett.* **2003**, *372*, 282–287.

(134) Vallée, R.; Cotlet, M.; Hofkens, J.; De Schryver, F. C.; Müllen, K. Spatially Heterogeneous Dynamics in Polymer Glasses at Room Temperature Probed by Single Molecule Lifetime Fluctuations. *Macromolecules* **2003**, *36*, 7752–7758.

(135) Vallée, R.; Tomczak, N.; Kuipers, L.; Vancso, G.; van Hulst, N. Single Molecule Lifetime Fluctuations Reveal Segmental Dynamics in Polymers. *Phys. Rev. Lett.* **2003**, *91*, 038301.

(136) Vallée, R.; Tomczak, N.; Kuipers, L.; Vancso, G.; van Hulst, N. Effect of Solvent on Nanoscale Polymer Heterogeneity and Mobility Probed by Single Molecule Lifetime Fluctuations. *Chem. Phys. Lett.* **2004**, *384*, 5–8.

(137) Vallée, R.; Cotlet, M.; Van der Auweraer, M.; Hofkens, J.; Müllen, K.; De Schryver, F. C. Single-Molecule Conformations Probe Free Volume in Polymers. *J. Am. Chem. Soc.* **2004**, *126*, 2296–2297.

(138) Tomczak, N.; Vallée, R. A. L.; van Dijk, E. M. H. P.; García-Parajó, M.; Kuipers, L.; van Hulst, N. F.; Julius Vancso, G. Probing Polymers with Single Fluorescent Molecules. *Eur. Polym. J.* **2004**, *40*, 1001–1011.

(139) Vallée, R.; Marsal, P.; Braeken, E.; Habuchi, S.; De Schryver, F. C.; Van der Auweraer, M.; Beljonne, D.; Hofkens, J. Single Molecule Spectroscopy as a Probe for Dye-Polymer Interactions. *J. Am. Chem. Soc.* **2005**, *127*, 12011–12020.

(140) Vallée, R.; Van der Auweraer, M.; Paul, W.; Binder, K. Fluorescence Lifetime of a Single Molecule as an Observable of Meta-Basin Dynamics in Fluids Near the Glass Transition. *Phys. Rev. Lett.* **2006**, *97*, 217801.

(141) Vallée, R.; Baruah, M.; Hofkens, J.; De Schryver, F. C.; Boens, N.; Van der Auweraer, M.; Beljonne, D. Fluorescence Lifetime Fluctuations of Single Molecules Probe the Local Environment of Oligomers around the Glass Transition Temperature. *J. Chem. Phys.* **2007**, *126*, 184902.

(142) Flier, B. M. I.; Baier, M. C.; Huber, J.; Müllen, K.; Mecking, S.; Zumbusch, A.; Wöll, D. Heterogeneous Diffusion in Thin Polymer Films as Observed by High-Temperature Single-Molecule Fluorescence Microscopy. *J. Am. Chem. Soc.* **2012**, *134*, 480–488.

(143) Paeng, K.; Swallen, S. F.; Ediger, M. D. Direct Measurement of Molecular Motion in Freestanding Polystyrene Thin Films. *J. Am. Chem. Soc.* **2011**, *133*, 8444–8447.

(144) Zheng, Z.; Kuang, F.; Zhao, J. Direct Observation of Rotational Motion of Fluorophores Chemically Attached to Polystyrene in Its Thin Films. *Macromolecules* **2010**, *43*, 3165–3168.

(145) Paeng, K.; Richert, R.; Ediger, M. D. Molecular Mobility in Supported Thin Films of Polystyrene, Poly(methyl Methacrylate), and poly(2-Vinyl Pyridine) Probed by Dye Reorientation. *Soft Matter* **2012**, *8*, 819–826.

(146) Roland, C. M.; Casalini, R. Temperature Dependence of Local Segmental Motion in Polystyrene and Its Variation with Molecular Weight. *J. Chem. Phys.* **2003**, *119*, 1838–1842.

(147) Kaufman, L.; Hoang, D.; Paeng, K.; Park, H.; Leone, L. Extraction of Rotational Correlation Times from Non-Ideal Single-Molecule Trajectories. *Anal. Chem.*

(148) A GUI Developed in House Is Used to Track Translating Features in a Dark Background and Utilizes a Particle Tracking Suite Developed by John Crocker and Eric Weeks.

(149) Tsakalakos, L. Strong Broadband Optical Absorption in Silicon Nanowire Films. *J. Nanophotonics* **2007**, *1*, 013552.

(150) Richert, R.; Angell, C. a. Dynamics of Glass-Forming Liquids. V. On the Link between Molecular Dynamics and Configurational Entropy. *J. Chem. Phys.* **1998**, *108*, 9016–9026.

(151) Elmatad, Y. S.; Chandler, D.; Garrahan, J. P.; Uni, V.; Ng, N. Corresponding States of Structural Glass Formers. *J. Phys. Chem. B* **2009**, *113*, 5563–5567.

Appendix A. Heating Correction

For all measurements collected using the wide-field fluorescence microscope setup during this thesis work, sample temperature regulation and heating from the laser were carefully controlled. Sample stage temperature is measured using a 100 Ω platinum resistive temperature device (Pt RTD) mounted directly on the sample stage with the vacuum grease (Apiezon N for low temperature glycerol and ortho-terphenyl (OTP) measurements) or no grease (high temperature polystyrene measurements). The temperature of the sample stage is controlled using a temperature controller (Lakeshore 331S). Sample stage temperature is stable within 50 mK of the set-point, with an absolute accuracy set by the Pt RTD calibration (estimated to be better than 200 mK). Sample temperature can be somewhat higher than Pt sensor temperature due to absorption of laser light by the Silicon wafer, which is ≈ 50% absorptive in the visible range.[149] To test for power dependence and potentially correct for it in the glycerol and OTP samples measured, power series are performed. Data is taken at multiple laser powers at multiple

temperatures since only a small range of powers allows for sufficiently long trajectories and sufficient signal to noise for accurate analysis at a given temperature. Such power series must be performed on each sample, as thermal contact and thus heat dissipation varies from sample to sample because of differences in the thickness of the vacuum grease used to affix the sample to the cryostat.

Because the absorption of laser light changes the temperature of the sample, we first describe correcting the set temperature to the actual temperature while not adjusting the measured rotational relaxation times of the probes, as these values are accurate for the corrected temperature. To make the heating correction in the manner described below, one must assume the temperature dependence of the rotational relaxation time of the fluorophore follows the temperature dependence of the viscosity of glycerol. The temperature dependence of glycerol's viscosity is known to vary with temperature according to the Vogel-Fulcher-Tammann-Hesse (VFTH) law,

$$\log \eta = \log \eta_0 + \frac{B}{T - T_0}, \qquad \text{(A.1)}$$

with η the viscosity, T the temperature in Kelvin, and B, η_0, and T_0 fit parameters. The VFTH parameters for glycerol in the temperature range investigated here as determined by rheology are $B = 1260$, $\eta_0 = 7.9 \times 10^{-8}$, and $T_0 = 118$.[99]

Calculation of actual temperature from set temperature and measured rotational correlation times of the probes requires use of the DSE equation (Eqn. 2.5). However, neither T nor V_h are known *a priori*; thus, the actual temperature and V_h are obtained simultaneously using a self-consistent approach. As an initial guess for V_h, the low temperature rotational correlation

time values are fit using the DSE equation and the temperature of the sample stage as reported by the Pt sensor. At low temperatures, very low laser powers are typically used and little heating is expected. The obtained hydrodynamic volume and the DSE equation are then used to numerically calculate corrected temperatures of the sample, which should be higher than the sample stage temperatures due to the laser heating. Based on the obtained temperatures for $<\tau_c>$ values (where $<\tau_c>$ refers to the median relaxation time obtained from all single molecules in a given movie) at each of the set temperatures, an average heating effect in terms of K/mW is calculated. This heating effect is then used to calculate a new actual temperature for each $<\tau_c>$ value. Using this new temperature and the experimental $<\tau_c>$ values, a new best-fit V_h can be obtained using the DSE equation. Comparing the experimental $<\tau_c>$ values at the corrected temperatures with the $<\tau_c>$ values predicted from the DSE equation and best-fit hydrodynamic volume provides a measure with which to evaluate the correction. If the difference in the resulting best-fit V_h between iterations is greater than 1%, the temperature correction is repeated using the last obtained V_h. In each iteration, a new V_h and new corrected temperatures are obtained by fitting the $<\tau_c>$ values and their temperature dependence to the DSE equation. The calculation is repeated until the difference between calculated V_h in two subsequent iterations is $< 1\%$.

Actual temperature at which data is collected can be ascertained as described above. However, it is often desirable to combine data from different movies and/or different samples. While each of these data sets may be collected at the same set temperature, they may not be collected at identical actual temperature. To attain sufficient data at a given temperature, correcting the values for the relaxation times of the probes to the set temperature rather than correcting the set temperature to an actual temperature is necessary. Doing this assumes that

time-temperature superposition holds over the temperature range between the set and actual temperatures of the combined data. Given that this range is less than 2K at the highest temperatures investigated and less than 0.2K at the lowest temperatures considered, this is expected to be a good assumption.

Combining Equation A.1 with the DSE equation gives the following relationship:

$$\tau_1 = \tau_2 * \frac{T_2}{T_1} * 10^{(\frac{B}{T_1 - T_0}) - (\frac{B}{T_2 - T_0})} \quad \text{(A.2)}$$

where τ_2 is the measured rotational relaxation time, T_2 is the actual temperature taking the heating effect into account, B and T_0 are the VFTH parameters, T_1 is the set temperature of the sample stage, and τ_1 is the corrected relaxation time for the sample stage temperature T_1. Thus, when the actual temperature T_2 is known, the τ_2 values can be corrected to the sample stage temperature T_1 by multiplying these values by the ratio τ_1/τ_2.

Fig. A.1 shows (a) raw data, (b) temperature corrected data, and (c) relaxation time corrected data on the dpPDI data set also shown (after relaxation time correction) in Figs. 3 and 4 in the manuscript. Fig. A.1a shows the experimental data and the eventual best-fit DSE line, corresponding to a hydrodynamic volume of 2.02 nm^3. The best-fit V_h for the uncorrected data, the starting point of the iterative process, is 1.94 nm^3. At low temperature, where low laser powers are employed, the points are close to the DSE line. At higher temperature, a deviation is apparent, which is due to more substantial heating at the higher laser powers used at these temperatures. As described above, the actual temperatures corresponding to the measured $<\tau_c>$ values are first found (Fig. A.1b), and then the $<\tau_c>$ values are corrected to those expected at the sample stage temperatures (Fig. A.1c). As expected, following the correction, correlation

between $<\tau_c>$ values and laser power is no longer present and all points are near the best-fit DSE line, which yields a final hydrodynamic volume of 2.02 nm^3.

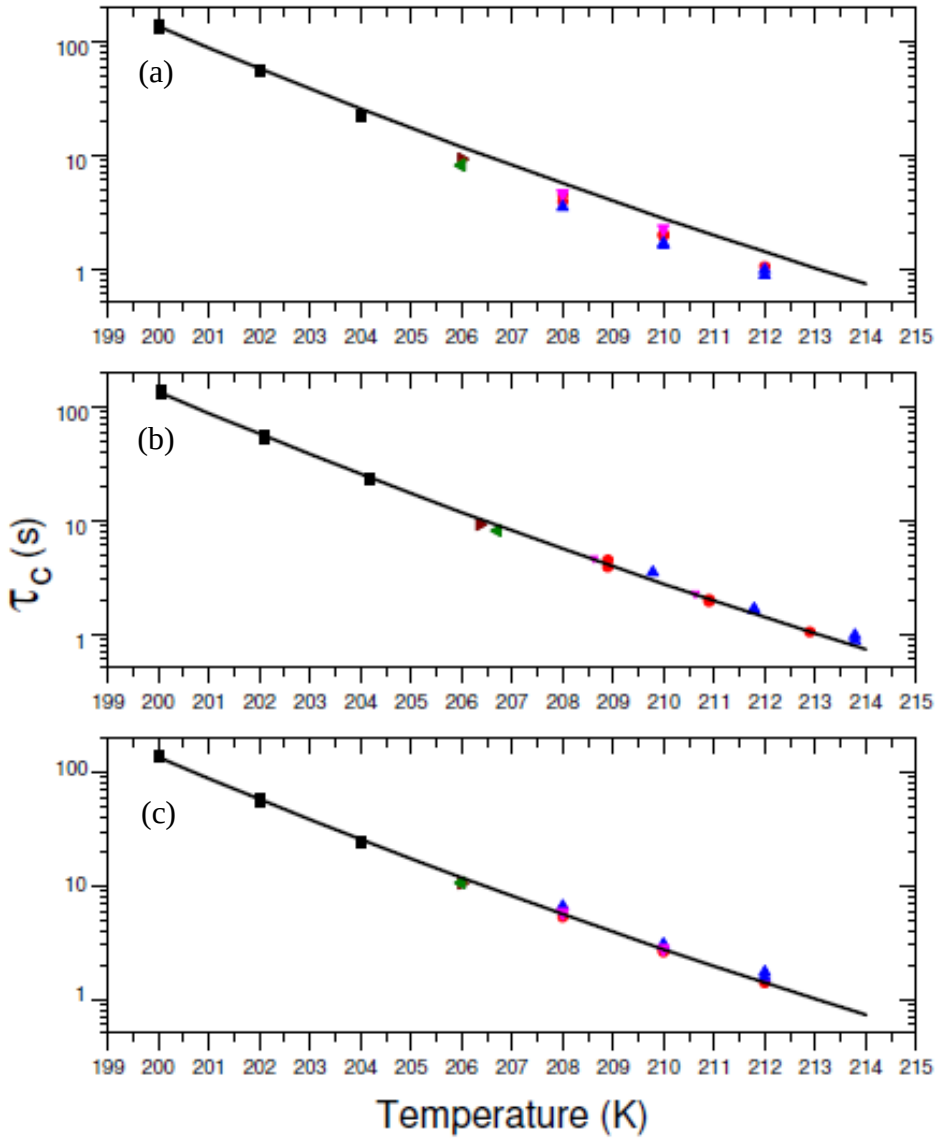

Figure A.1 Median τ_c values for each of 23 movies of dpPDI before and after heating correction with eventual best-fit DSE line corresponding to V_h = 2.02 nm^3. The different symbols represent different laser powers - blue upright triangle: 20mW, red circle: 10mW, magenta downright triangle: 7mW, olive left triangle: 8mW, wine right triangle: 4mW, black square: 0.5mW - 2mW. (a) Uncorrected experimental data. (b) Uncorrected median τ_c values with

corresponding actual temperature. (c) Corrected median τ_c values for sample stage set temperature, as also shown in Fig. 2.3.

The same procedure applied to SM data collected in glycerol is used for SM data in OTP to find both true temperature of the sample for each movie or, alternately, heat corrected τ_c values for each data point. The temperature dependent viscosity data for OTP used to perform the heating correction is given in Reference 111. A nearly identical heating correction is performed to obtain relative time scales of probe and host relaxation dynamics as characterized by probe rotational correlation time and host structural relaxation time, τ_c/τ_α. If the published temperature dependence of viscosity[110] and structural relaxation[116,150] of OTP were identical, a single τ_c/τ_α for each probe could be extracted from the heating correction procedure based on viscosity. However, because these curves are not identical using this approach results in somewhat temperature-dependent τ_c/τ_α values. To avoid this, we perform a second heating correction that yields τ_c/τ_α. As for the viscosity-based heating correction, the set temperature is first corrected to an actual temperature for each movie collected. Here, it is assumed the temperature dependence of probe τ_c follows the temperature dependence of the structural relaxation of OTP as given by,

$$\log\left(\frac{\tau}{\tau_0}\right) = \left(\frac{J}{T_0}\right)^2 \left(\frac{T_0}{T} - 1\right)^2 \qquad \text{(A.3)}$$

where τ is the structural relaxation time, T is temperature in Kelvin, and τ_0, J and T_0 are fit parameters. The parabolic fit parameters for OTP in the temperature range investigated here as determined by dielectric spectroscopy are $\log(\tau_0)$ = -9.8 s, J = 2898.5 K and T_0 = 341 K. [116,151]

Using probe rotational correlation times, τ_c, and set temperatures as τ and T in Equation A.3, respectively, the data is plot and a best-fit line to the data is chosen using the three lowest temperature data points, where low laser powers are used and little heating is expected. This initial guess line is used to calculate corrected temperatures for the sample. The difference in the corrected temperature value and the set recorded temperature is calculated for individual $\tau_{c,med}$ values and from this data, an average heating in terms of K/mW is obtained. This average value is then used to correct the set temperature to a new corrected temperature for each $\tau_{c,med}$ point. Using the new temperatures and the original τ_c values, a new best-fit line is found. The slope of this line is then artificially increased by 2% and the procedure is repeated. This procedure continues until the calculated best-fit line slope is 1 ± 0.01. At that point, the value of the line at T = T_g relative to the value of the host structural relaxation at T_g yields τ_c/τ_α. Maximum difference between a set temperature and corrected temperature is 1.9K for the data presented in this manuscript.

To attain sufficient data at a given temperature, correcting the values for the relaxation times of the probes to the set temperature rather than correcting the set temperature to an actual temperature is helpful. Doing this assumes that time-temperature superposition holds over the temperature range between the set and actual temperatures of the combined data. With this assumption and known actual temperature, heat-corrected τ_c values can be corrected to the sample stage temperature via:

$$\tau_1 = \tau_2 * 10^{\left(\frac{J}{T_0}\right)^2\left[\left(\frac{T_0}{T_1}-1\right)^2-\left(\frac{T_0}{T_2}-1\right)\right]^2} \qquad \text{(A.4)}$$

where J and T_0 are the parabolic fit parameters, τ_2 is the measured rotational relaxation time, T_2 is the actual temperature, T_1 is the set temperature of the sample stage, and τ_1 is the corrected relaxation time for the sample stage set temperature.

This process allows determination of τ_c/τ_α; however, this value depends sensitively on the structural relaxation data, and in cases where multiple sets of data and fits are available, the newest published data has been used[4]. A second procedure to determine τ_c/τ_α does not depend on any particular data set but instead relies on probe measurements, a defined T_g, and a definition of τ_α as 100s at T_g. Using heat-corrected SM data and extrapolating probe τ_c to T_g = 243K yields very similar τ_c/τ_α values to those obtained via the procedure described above for all probe:host pairs interrogated.